

DEVELOPMENT OF NEAR IR HEPTAMETHINE CYANINE DYES FOR  
TARGETED CANCER THERAPY



A Thesis Submitted in Partial Fulfillment of the Requirements for the Degree of  
Master of Science in Cellular and Molecular Science for Biomedical Applications

Suranaree University of Technology

Academic Year 2021

การพัฒนาสารเรืองแสงในช่วงอินฟราเรดช่วงคลื่นสั้นจำพวกเฮปตะเมรีน  
ไชนานีนสำหรับการรักษามะเร็งแบบมุ่งเป้า

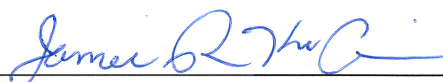


วิทยานิพนธ์นี้เป็นส่วนหนึ่งของการศึกษาตามหลักสูตรปริญญาวิทยาศาสตรมหาบัณฑิต  
สาขาวิชาวิทยาศาสตร์ระดับเซลล์และโมเลกุลสำหรับการประยุกต์ทางชีวการแพทย์  
มหาวิทยาลัยเทคโนโลยีสุรนารี  
ปีการศึกษา 2564

DEVELOPMENT OF NEAR IR HEPTAMETHINE CYANINE DYES FOR  
TARGETED CANCER THERAPY

Suranaree University of Technology has approved this thesis submitted in  
partial fulfillment of the requirements for a Master's degree

Thesis Examining Committee



---

(Prof. Dr. James R. Ketudat-Cairns)

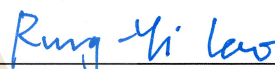
Chairperson



---

(Asst. Prof. Dr. Anyanee Kamkaew)

Member (Thesis Advisor)



---

(Dr. Rung Yi Lai)

Member



---

(Asst. Prof. Dr. Oratai Weeranantanapan)

Member



---

(Assoc. Prof. Dr. Apiwat Chompoosor)

Member



---

(Assoc. Prof. Dr. Chatchai Jothityangkoon) (Prof. Dr. Santi Maensiri)

Vice Rector for Academic Affairs



---

Dean of Institute of Science

and Quality Assurance

สิริวิไล สิริวิบูลย์ : การพัฒนาสารเรืองแสงในช่วงอินฟราเรดช่วงคลื่นสั้นจำพวกเฮปตะเมธีนไซยานีนสำหรับการรักษามะเร็งแบบมุ่งเป้า (DEVELOPMENT OF NEAR IR HEPTAMETHINE CYANINE DYES FOR TARGETED CANCER THERAPY) อาจารย์ที่ปรึกษา :  
ผู้ช่วยศาสตราจารย์ ดร.อัญญาณี คำแก้ว, 75 หน้า

คำสำคัญ: เฮปตะเมธีนไซยานีน; การบำบัดด้วยการกระตุ้นด้วยแสง; สภาพแวดล้อมของเซลล์มะเร็ง; การจับเซลล์มะเร็ง; ไฮโคลออกซีจีเนส2; สารเรืองแสงในช่วงอินฟราเรดช่วงคลื่นสั้น; Cy820

ในงานนี้ได้ทำการออกแบบตัวตรวจสอบที่เป็นสารเรืองแสงจำพวกอะมิโนเฮปตะเมธีนไซยานีน ( $I_2$ -IR783-Mpip) เพื่อจับเซลล์มะเร็งโดยมุ่งเป้าไปที่สิ่งแวดล้อมของเซลล์มะเร็ง สารเรืองแสงกลุ่มนี้ สามารถถูกกระตุ้นโดยแสงในช่วงอินฟราเรดช่วงคลื่นสั้นและขึ้นอยู่กับค่าพีเอช โดยในสารละลายที่เป็นกรด  $I_2$ -IR783-Mpip ดูดกลืนแสงในช่วงอินฟราเรดช่วงคลื่นสั้น (820–950 นาโนเมตร) และสามารถผลิต singlet oxygen ได้สูงเมื่อถูกกระตุ้นด้วยแสงช่วงคลื่นสั้น (850 นาโนเมตร) การเพิ่มโปรตอนให้กับ  $I_2$ -IR783-Mpip ในสารละลายที่เป็นกรด ทำให้ช่องว่างของพลังงานออร์บิทัลโมเลกุลลดลงและทำให้การเคลื่อนย้ายประจุระหว่างโมเลกุลเพิ่มขึ้น ภายใต้สภาพแวดล้อมที่เป็นกลางและกรด  $I_2$ -IR783-Mpip สามารถทำลายเซลล์มะเร็งได้เมื่อถูกกระตุ้นด้วยแสงได้อย่างมีประสิทธิภาพ ในทางตรงกันข้ามเซลล์ปกติยังคงมีสุขภาพดี การผลิต singlet oxygen ในเซลล์ถูกพบในเซลล์ที่มี  $I_2$ -IR783-Mpip ในสภาพแวดล้อมที่เป็นกรด ซึ่งแสดงให้เห็นว่า  $I_2$ -IR783-Mpip มีพลังงานแสงบำบัดที่มีประสิทธิภาพในสภาพแวดล้อมที่เป็นกรดนอกเหนือจากนี้ เมื่อถูกกระตุ้นด้วยแสง  $I_2$ -IR783-Mpip ทำลายเซลล์ที่อยู่ในระดับลึกได้อย่างมีประสิทธิภาพ ดังนั้นพวกเราเชื่อว่า  $I_2$ -IR783-Mpip เป็นตัวตรวจสอบตัวแรกที่สามารถจับและทำลายเซลล์มะเร็งในสภาพแวดล้อมที่เป็นกรดโดยกระตุ้นด้วยแสง 850 นาโนเมตร

เพื่อในการจดจำเซลล์มะเร็งมีความจำเพาะมากขึ้น สารเรืองแสงจำพวกเฮปตะเมธีนไซยานีน ได้ถูกสังเคราะห์ขึ้นเพื่อจับเอนไซม์ไฮโคลออกซีจีเนส2 ที่แสดงออกมากในเซลล์มะเร็ง ในงานนี้จึงมีการตรวจสอบความสามารถของสารเรืองแสงกลุ่มนี้ในการจับเซลล์มะเร็งและทำลายเซลล์มะเร็งเมื่อถูกกระตุ้นด้วยแสงโดยมีโปรตีนขนส่ง OATPs สามารถพาสารเรืองแสงจำพวกเฮปตะเมธีนไซยานีนบางส่วนเข้าเซลล์มะเร็งได้ ในงานนี้พวกเราได้นำอินโดเมทาซิน (indomethacin) ซึ่งเป็นยาต้านอักเสบชนิดไม่ใช้สเตียรอยด์มาต่อกับ Cy820 เพื่อสังเคราะห์ Cy820-IMC ซึ่งจำเพาะกับเอนไซม์ไฮโคลออกซีจีเนส โดยจากการทดลองพบว่า Cy820-IMC สามารถเข้าเซลล์มะเร็งได้เร็วกว่า Cy820 เนื่องจากมีอินโดเมทาซินเป็นตัวจับเซลล์มะเร็งเพิ่มขึ้นมา ความเป็นพิษกับเซลล์มะเร็งเมื่อถูกกระตุ้น

ด้วยแสงของ Cy820-IMC พบว่าสูงกว่า Cy820 อย่างไรก็ตาม อัตราส่วนความเป็นพิษในเซลล์ปกติ ต่อเซลล์มะเร็งของ Cy820 ค่อนข้างสูงกว่าของ Cy820-IMC ดังนั้นโดยรวมความสามารถในการจับ เซลล์มะเร็งและทำลายเซลล์มะเร็งเมื่อถูกกระตุ้นด้วยแสงของ Cy820-IMC เหนือกว่า Cy820

โดยสรุป วิทยานิพนธ์นี้ เป็นการศึกษาความสามารถในการจดจำเซลล์มะเร็งของสารเรืองแสง จำพวกเฮปตะเมธีนไซยานีน โดยวิธีการศึกษาที่สนใจคือ การมุ่งเป้าไปที่ความเป็นกรดของสิ่งแวดล้อม มะเร็ง และการเพิ่มหมู่ที่จำเพาะกับเอนไซม์ที่พบมากในเซลล์มะเร็ง ซึ่งจากการทดลองพบว่า การใช้ สองวิธีนี้จะช่วยให้สารเรืองแสงกลุ่มนี้มุ่งเป้าไปที่เซลล์มะเร็งมากขึ้น ส่งผลให้การรักษามะเร็งผ่านการ ฉายแสงมีประสิทธิภาพมากขึ้น



สาขาวิชาเคมี  
ปีการศึกษา 2564

ลายชื่อนักศึกษา  
ลายชื่ออาจารย์ที่ปรึกษา  
ลายชื่ออาจารย์ที่ปรึกษาร่วม

สิริวัลล์ สิทธิวัลย์

*(Signature)*

กับตงอว

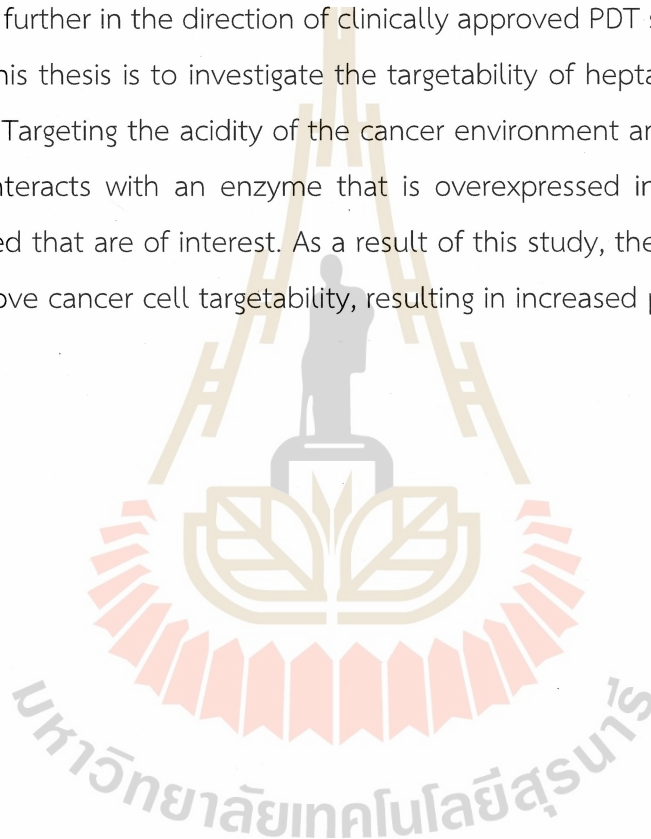
SIRIWALEE SIRIWIBOOL : DEVELOPMENT OF NEAR IR HEPTAMETHINE CYANINE DYES FOR TARGETED CANCER THERAPY. THESIS ADVISOR : ASST. PROF. ANYANEE KAMKAEW, Ph.D., 75 PP.

Keywords: heptamethine cyanine; photodynamic therapy; tumor environment; cancer targeting; COX-2; NIR photosensitizer; Cy820

To target the tumor environment, this work synthesized an amino heptamethine cyanine-based theranostic sensor (**I<sub>2</sub>-IR783-Mpip**) that is triggered by near-infrared light and is pH-dependent. In acidic conditions, **I<sub>2</sub>-IR783-Mpip** showed a broad, intense NIR absorbance peak (820–950 nm) with substantial singlet oxygen production when exposed to NIR light (~850 nm). Protonation of the probe in an acidic environment reduced molecular orbital energy gaps and boosted intramolecular charge transfer efficiency, according to theoretical simulations. Under normal and slightly acidic environments, **I<sub>2</sub>-IR783-Mpip** showed good photodynamic efficiency against liver hepatocellular cancer cells, whereas normal human embryonic kidney cells or normal cells remained alive. After NIR light exposure, intracellular reactive oxygen species (ROS) were detected in cells treated with **I<sub>2</sub>-IR783-Mpip**, confirming the effectiveness of PDT of the probe effectiveness in an acidic environment. In addition, **I<sub>2</sub>-IR783-Mpip** showed effective phototoxicity in a deep-seated tumor cell system. We believe that it is the first PDT agent with intrinsic tumor binding that preferentially eradicates tumors in an acidic environment using an 850 nm NIR lamp.

To target the cyclooxygenase-2 enzyme that is overexpressed in cancer cells, the potential of near-IR fluorescence sensitizers based on heptamethine cyanine (**Cy820** and **Cy820-IMC**) to target and eliminate tumor cells using photodynamic treatment (PDT) was investigated. Organic anion transporter proteins (OATPs) have been known to transfer heptamethine cyanine dyes into cancer cells. In this study, we conjugated **Cy820** with indomethacin, a non-steroidal anti-inflammatory medicine (NSAID), to form **Cy820-IMC** to target the cyclooxygenase-2 (COX-2) enzyme, which is overexpressed in cancer cells. The study indicated that **Cy820-IMC** was internalized

cancer cells faster than **Cy820** due to an extra targeting ligand, indomethacin. The cytotoxicity profiles of **Cy820** and **Cy820-IMC**, as determined by PDT tests, are remarkable. The photocytotoxicity index with HepG2 cells of **Cy820-IMC** is  $>7.13$  higher than that of **Cy820**, with values of 4.90, showing that **Cy820-IMC** has stronger PDT properties than **Cy820**. However, the normal-to-cancer cell toxicity ratio of **Cy820** is slightly higher than that of **Cy820-IMC**, at 6.58 and 3.63, respectively. Overall, the cancer targetability and phototoxicity of **Cy820-IMC** are superior. These features can be improved further in the direction of clinically approved PDT sensitizers. In brief, the purpose of this thesis is to investigate the targetability of heptamethine cyanine with cancer cells. Targeting the acidity of the cancer environment and adding a group that selectively interacts with an enzyme that is overexpressed in cancer cells are the strategies used that are of interest. As a result of this study, these strategies could be able to improve cancer cell targetability, resulting in increased photodynamic therapy efficiency.



School of Chemistry

Academic Year 2021

Student's Signature

Siriwalee Siriwibool

Advisor's Signature

Co-advisor's Signature

Kantapant

## ACKNOWLEDGEMENTS

This thesis can be completed because I received help, advice, and support from my advisor, Asst. Prof. Anyanee Kamkaew, and my collaborators. I would like to thank my advisor for providing me with a wealth of research ideas and information. She is the person who continues to encourage and assist me in a variety of ways. She always has time for her students to discuss problems and results. Without her, I would not have been able to succeed. I would like to thank my friends and everyone in the AK lab for giving me discussion, help, and creating a positive atmosphere in the lab.

I would like to thank my co-advisor, Dr. Kantapat Chansaenpak, at the National Nanotechnology Center (Nanotec), a research institute under the National Science and Technology Development Agency (NSTDA), Thailand for advice, teaching about the tools, and supporting me about this thesis. I would like to thank Assoc. Prof. Dr. Parinya Noisa and all CBAI members for allowing me to use the tools for doing *in vitro* experiments and teaching me about the *in vitro* technique. I would like to thank all lecturers in the School of Chemistry and Cellular and Molecular Science for Biomedical Application for teaching me about study and life.

I would like to thank NSTDA-TGIST Thailand Graduate Institute of Science and Technology under grant no. SCA-CO-2562-9812-TH for covering tuition, living costs, and travel grants, among other things.

Finally, I would like to thank my family who shaped me into the person I am today for always supporting and loving me.

Siriwalee Siriwibool



# CONTENTS

	Page
ABSTRACT IN THAI.....	I
ABSTRACT IN ENGLISH.....	III
ACKNOWLEDGEMENTS .....	V
CONTENTS .....	VI
LIST OF TABLES .....	IX
LIST OF FIGURES .....	X
LIST OF ABBREVIATIONS .....	XII
<b>CHAPTER</b>	
<b>I INTRODUCTION.....</b>	<b>1</b>
1.1 Research objectives .....	4
1.2 Scope .....	4
<b>II LITERATURE REVIEW.....</b>	<b>5</b>
2.1 Extracellular tumor pH.....	5
2.2 Piperazine for pH-sensitive compound.....	6
2.3 Cyanine dyes.....	8
2.4 Cyanine sensors based on intramolecular charge transfer (ICT) .....	9
2.5 Cyanine sensors based on photoinduced electron transfer (PET).....	10
2.6 Modification of Cyanine dye for PDT applications .....	11
2.7 Photodynamic therapy.....	11
2.8 Cyclooxygenase 2 and Cancer.....	12
2.9 Indomethacin for COX-2 targeting .....	14
<b>III RESEARCH METHODOLOGY.....</b>	<b>17</b>
3.1 Target: Tumor environment.....	17
3.1.1 Synthesis of I <sub>2</sub> -IR783-Mpip.....	17
3.1.2 General details for Vis-NIR and fluorescence measurements.....	17

## CONTENTS (Continued)

	Page
3.1.3 Singlet oxygen generation.....	18
3.1.4 Singlet oxygen quantum yield determination.....	18
3.1.5 Stability test.....	19
3.1.6 Cell culture.....	19
3.1.7 Cell survival assay of HepG2 cells in media 5.0.....	19
3.1.8 Live cell imaging.....	20
3.1.9 Localization study with lysotracker and mitotracker.....	20
3.1.10 Flow cytometry.....	20
3.1.11 Light induced cytotoxicity.....	21
3.1.12 Cellular reactive oxygen production.....	22
3.1.13 Statistical analysis.....	23
3.2 Target: Cyclooxygenase enzyme that overexpressed on tumor cells.....	23
3.2.1 Synthesis of <b>Cy820</b> and <b>Cy820-IMC</b> .....	23
3.2.1.1 Synthesis of <b>Cy820</b> .....	23
3.2.1.2 Synthesis of Indomethacin linker (B).....	24
3.2.1.3 Synthesis of <b>Cy820-IMC</b> .....	24
3.2.2 Photophysical properties of <b>Cy820-IMC</b> and <b>Cy820</b> .....	25
3.2.3 Singlet oxygen quantum yield of <b>Cy820-IMC</b> and <b>Cy820</b> .....	25
3.2.4 Cell culture.....	26
3.2.5 Cell imaging.....	26
3.2.6 Photodynamic therapy.....	27
3.2.7 LIVE/DEAD staining.....	27
3.2.8 Intracellular singlet oxygen generation.....	27
3.2.9 Cyclooxygenase-2 inhibition experiment.....	28
3.2.10 OATPs inhibition experiment.....	28
3.2.11 Colocalization experiment.....	28
3.2.12 Flow cytometry.....	28

## CONTENTS (Continued)

	Page
IV RESULTS AND DISCUSSION.....	30
4.1 Target: Tumor environment.....	30
4.1.1 Photophysical properties.....	30
4.1.2 Cell internalization of I <sub>2</sub> -IR783-Mpip.....	37
4.1.3 Photodynamic therapy.....	42
4.2 Target: Cyclooxygenase enzyme that overexpressed on tumor cells.....	47
4.2.1 Photophysical properties.....	47
4.2.2 Molecular interaction of Cy820-IMC with COX-2 protein.....	48
4.2.3 Time-dependent intracellular internalization.....	49
4.2.4 Mechanism of cell internalization.....	51
4.2.5 Intracellular localization.....	53
4.2.6 Photocytotoxicity.....	54
4.2.7 Intracellular singlet oxygen generation.....	56
V CONCLUSION .....	59
REFERENCES .....	60
APPENDICES.....	69
APPENDIX A SUPPORTING INFORMATION.....	70
APPENDIX B THESIS OUTPUT.....	74
CURRICULUM VITAE.....	75

## LIST OF TABLES

Table	Page
4.1	Photophysical properties of <b>Cy820-IMC</b> and <b>Cy820</b> .....48
4.2	IC50 and photocytotoxicity index of <b>Cy820</b> and <b>Cy820-IMC</b> .....56



## LIST OF FIGURES

Figure	Page
1.1	Compound structures proposed in this thesis..... 3
2.1	Extracellular pH levels of different cancers are compared to normal tissues... 6
2.2	Structures of near-infrared fluorescent probes and their emission spectra ..... 7
2.3	Classic cyanine structures are depicted schematically ..... 8
2.4	Molecule structure of IR2 and IR-780..... 9
2.5	Molecular structure of pH Probe 3 and its sensing mode toward H <sup>+</sup> ..... 10
2.6	Schematic showing the process of a-PET and d-PET..... 11
2.7	Type I and type II reactions in a photodynamic treatment ..... 12
2.8	COX-1 and COX-2 active sites..... 13
2.9	Molecular structure of indomethacin ..... 14
2.10	Molecular structure of NANQ-IMC6..... 15
2.11	Molecular structure of Nibblue-C6-IMC..... 15
3.1	Synthesis scheme of <b>Cy820</b> and <b>Cy820-IMC</b> ..... 23
4.1	Vis-NIR spectra and Equilibrium structures of <b>I<sub>2</sub>-IR783-Mpip</b> ..... 31
4.2	The relative total energy of possible structures of <b>I<sub>2</sub>-IR783-Mpip</b> ..... 33
4.3	<b>I<sub>2</sub>-IR783-Mpip</b> optical characteristics..... 35
4.4	Singlet oxygen formation based on a change in DPBF absorbance ..... 36
4.5	Relative cell viability of HepG2 cells after 0-36 hours of exposure to DMEM medium pH 5.0..... 37
4.6	Colocalization of <b>I<sub>2</sub>-IR783-Mpip</b> with LysoTracker green and flow cytometry of HepG2 cells incubated with 15 μM of <b>I<sub>2</sub>-IR783-Mpip</b> ..... 39
4.7	Analysis organelle colocalization of <b>I<sub>2</sub>-IR783-Mpip</b> ..... 40
4.8	Time-dependent cellular uptake of <b>I<sub>2</sub>-IR783-Mpip</b> in both pH 5.0 and pH 7.4..... 41
4.9	Photodynamic therapy effect of <b>I<sub>2</sub>-IR783-Mpip</b> ..... 43

## LIST OF FIGURES (Continued)

Figure	Page
4.10 Relative cell viabilities of HEK-293 cells after incubation with <b>I<sub>2</sub>-IR783-Mpip</b> .....	44
4.11 Fluorescence pictures of calcein AM and PI of HepG2 cells treated with <b>I<sub>2</sub>-IR783-Mpip</b> .....	45
4.12 The DCFDA cellular ROS detection assay produced by <b>I<sub>2</sub>-IR783-Mpip</b> .....	46
4.13 DCF relative fluorescence signal in HepG2 cells of incubation with <b>I<sub>2</sub>-IR783-Mpip</b> .....	46
4.14 Optical characteristics of <b>Cy820-IMC</b> and <b>Cy820</b> .....	47
4.15 3D representation of docked <b>Cy820-IMC</b> .....	49
4.16 Time-dependent cellular uptake and mean fluorescence intensity of <b>Cy820-IMC</b> and <b>Cy820</b> in HepG2 cells and HEK-293.....	50
4.17 Confocal imaging of HepG2 cells pre-treated with BSP and flow cytometry of <b>Cy820-IMC</b> and <b>Cy820</b> in HepG2 cells.....	52
4.18 Confocal images of COX-2 inhibition.....	53
4.19 Colocalization of <b>Cy820-IMC</b> with NBD-C6-ceramide, MitoTracker Green, and LysoTracker green.....	54
4.20 Photodynamic therapy effect of <b>Cy820-IMC</b> and <b>Cy820</b> in HepG2 and HEK293 cells.....	55
4.21 Fluorescence pictures of calcein AM and PI of HEK293 cells after treatment with <b>Cy820</b> and <b>Cy820-IMC</b> .....	57
4.22 Fluorescence pictures of calcein AM and PI of HepG2 cells after treatment with <b>Cy820</b> and <b>Cy820-IMC</b> .....	57
4.23 DCF relative fluorescence signal in HepG2 cells of incubated with <b>Cy820-IMC</b> .....	58

## LIST OF ABBREVIATIONS

BSP	Bromosulfophthalein
COX-2	Cyclooxygenase-2
DMF	Dimethylformamide
DMSO	Dimethyl sulfoxide
DPBF	1,3-diphenylisobenzofuran
F	Absorption correction factor
grad	Slope of the best linear fit
HEK-293	Human embryonic kidney 293
HepG2	Human hepatoma cancer cells
ISC	intersystem crossover
ICT	Intramolecular charge transfer
NMR	Nuclear Magnetic Resonance
nm	Nanometer
MFI	Mean fluorescence intensity
OATPs	Organic anion-transporting polypeptides
PDT	Photodynamic Therapy
PET	Photoinduced electron transfer
PS	Photosensitizer
SOSG	Singlet oxygen sensor green
$\Phi_{st}$	Quantum yield of the standard
$\Phi_x$	Quantum yield of the unknown
$\Phi_{\Delta}$	Singlet oxygen quantum yield
$\lambda$	Wavelength

## CHAPTER I

### INTRODUCTION

Cancer is still a leading cause of death and illness around the world. Radiation therapy, surgery, and chemotherapy are the most common cancer treatments in clinical practice. Those treatments, however, have some serious negative effects (WHO, 2017; Goldsmith, 1969) such as hair loss, nausea, and vomiting. Photodynamic therapy (PDT) is a non-invasive cancer treatment approach. PDT consists of two steps: (1) a PDT agent is delivered to a cancer cell, and (2) cancer areas are irradiated with particular light that activates a PDT agent, followed by the production of reactive oxygen species (ROS), which stimulate cancer cell death (Dolmans, Fukumura, and Jain, 2003). In general, cancer cells behave differently from normal cells. For example, a shortage of oxygen in cancer cells causes severe hypoxia, which leads to the increasing production of lactic acid, to decrease the extracellular pH level in the tumor environment (pH 6.2–6.7) (Hao, Xu, and Li, 2018; Persi et al., 2018). Furthermore, the pH of the lysosome in cancer cells ( $\text{pH}_{\text{lys}}$  3.8–4.7) is lower than in normal cells ( $\text{pH}_{\text{lys}}$  4.5 - 6.0) (Kroemer and Jaattela, 2005).

Because of the lower background fluorescence from endogenous molecules in the 700–1000 nm range, near-infrared fluorescent dyes are useful for tumor detection at millimeter depth (Luo, Zhang, Su, Cheng, and Shi, 2011; Weissleder, 2001). Because of heptamethine cyanines (Hcyanines) have high fluorescence quantum yields, great photodynamic effect, and good biocompatibility, they have been used as cancer imaging reagents (Shi, Wu, and Pan, 2016; Sun, Guo, Hu, Fan, and Peng, 2016). Furthermore, Hcyanines have been shown to be internalized to cancer cells via organic anion-transporting polypeptides (OATPs), a class of cell membrane-bound solute carriers. (Buxhofer-Ausch et al., 2013; Liu, and Li, 2014; Tan et al., 2012). OATPs mediate the cellular transport of drug and exogenous materials (Thakkar, Lockhart, and Lee, 2015). Hcyanine uptake in cancer cells is known to link to hypoxia and activation of HIF1 $\alpha$ /OATPs signaling, resulting in increased uptake dye, but little or no dye



uptake is observed in normal cells due to low OATPs expression (Usama, Lin, and Burgess, 2018).

Some Hcyanines compounds have recently been found to target an acidic tumor environment and show therapeutic effects (Feng, L. Z. et al., 2018; Xue, F. et al., 2017). Only a few Hcyanines have been described as stand-alone small pH-sensitive compounds that create heat (photothermal effect) or produce the PDT effect after activation. By altering the intramolecular charge transfer (ICT) efficiency using the dimethylamine group, IR2 was reported as a pH switchable NIR fluorescence and photothermal agent (Zhang et al., 2016). IR2 (Figure 2.4) demonstrated its ability to specifically detect and kill cancer cells in this manner (Zhang et al., 2016). In another study, Rhodamine was conjugated with Hcyanine via a disulfide bond (Meng et al., 2017), to form RhoSSCy was found to be dual-responsive to both thiols and pH *in vitro* and *in vivo* based on NIRF/PA dual-modal imaging and NIR-sensitizing PDT activities. As all result, clinical translations benefit from the development of theranostic probes for precisely detecting and eradicating tumors.

In addition to tumor environment targeting, we are also particularly interested in small molecule ligand-dye conjugates. These strategies have been demonstrated to be effective in cancer imaging and treatment (Myochin et al., 2011). Therefore, in this study, we propose two types of Hcyanine targeting probes; 1) Tumor environment targeting probe: **I<sub>2</sub>-IR783-Mpip** for NIR fluorescent imaging and PDT that target cancer cells via OATPs and acidic tumor environment; and 2) enzyme targeting probes: **Cy820-IMC**, the conjugation between indomethacin, a non-selective COX-2 inhibitor, and cyanine dye and **Cy820** is a cyanine dye without indomethacin. They were used to investigate selectivity (Figure 1.1).

Cyclooxygenase (COX), a prostaglandin-endoperoxide synthase, is an enzyme involving for the synthesis of prostanoids (Fitzpatrick, 2004). COX-2 is overexpressed in all stages of cancer, from the earliest premalignant phase to metastasis (Subbaramaiah, and Dannenberg, 2003) according to the clinical data. High levels of COX-2 have been found to be upregulated in a variety of cancers, including pancreas, colon, gastric, stomach, breast, head/neck carcinoma, and inflammatory lesions (Echizen, Hirose,

Maeda, and Oshima, 2016; Edelman et al., 2012; Kim et al., 2018). Therefore, COX-2 is considered to be an excellent cancer target (Kim et al., 2018).

The COX-2 targeting probes with fluorescence have been developed in recent decades (Bhardwaj et al., 2014; Pewklang et al., 2019). However, the development of COX-2 specific cancer biomarkers is still required for clinical usage. Moreover, COX-2 inhibitors were discovered to boost the PDT impact when used in conjunction with other therapies (Mao, Wang, Xu, and Han, 2018).

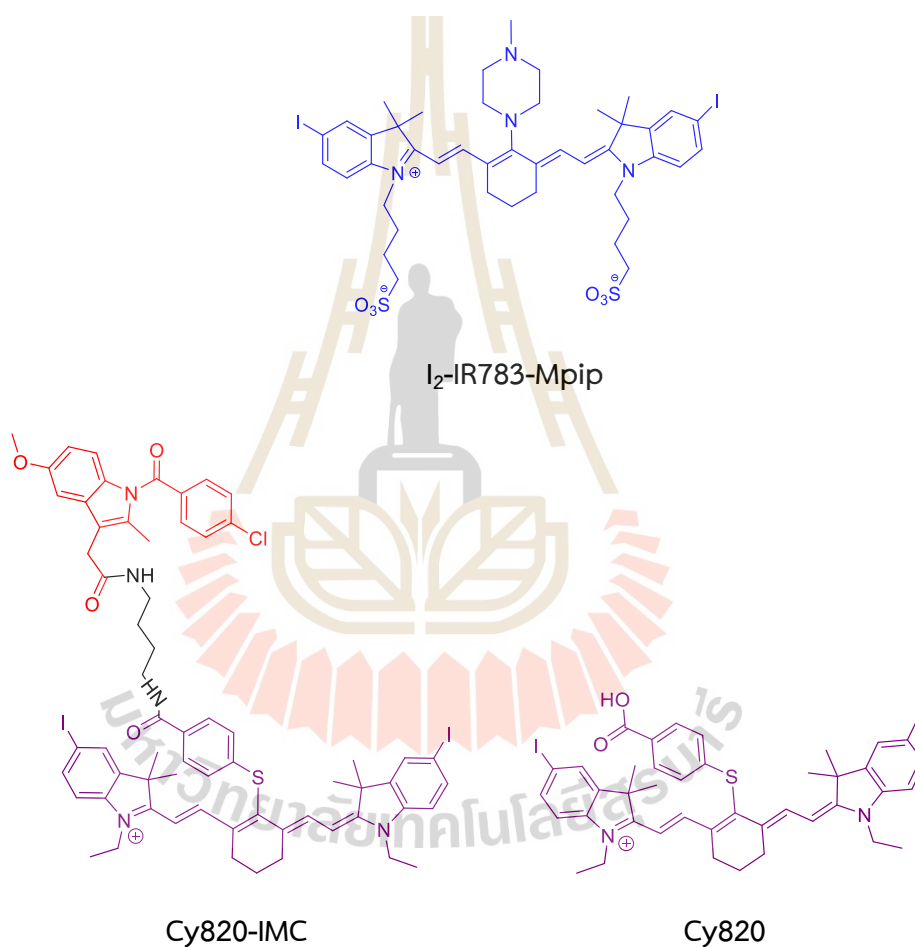


Figure 1.1 Compound structures proposed in this thesis.

## 1.1 Research objective

The ultimate goal of this study is to develop effective tumor-targeted PDT probes that enhance cancer therapy *in vitro*. Although there are various ways to target cancer cells, this thesis only focuses on targeting tumor environment and cyclooxygenase-2 enzyme overexpressed on tumor cells as the followings:

### Target: Tumor environment

- 1) To synthesize and characterize the **I<sub>2</sub>-IR783-Mpip** probe.
- 2) To apply the **I<sub>2</sub>-IR783-Mpip** probe for photodynamic therapy in cancer cells.
- 3) To demonstrate the better selectivity of the probe to tumor cells than healthy cells.

### Target: Cyclooxygenase-2 enzyme overexpressed on tumor cells

- 1) To synthesize and characterize **Cy820** and **Cy820-IMC** probes.
- 2) To apply the **Cy820-IMC** probes for photodynamic therapy in cancer cells.
- 3) To demonstrate the better selectivity of the probe to tumor cells that overexpress the COX-2 enzyme.
- 4) To compare COX-2 selectivity between indomethacin conjugates or Cy820-IMC and Cy820 to tumor cells overexpress the COX-2 enzyme.

## 1.2 Scope

The scope of this thesis was only for *in vitro* study of **I<sub>2</sub>-IR783-Mpip**, **Cy820-IMC**, and **Cy820**.

## CHAPTER II

### LITERATURE REVIEW

#### 2.1 Extracellular tumor pH

To create successful treatments, researchers must first understand the pathogenesis and characteristics of cancer. The pH of the tumor microenvironment has been linked to the development and therapy of cancer. Tumors had an acidic extracellular pH compared to normal cells (Hao, Xu, and Li, 2018). The extracellular pH of the normal cell is typically in the range of 7.2–7.5. The extracellular pH of tumor cells, on the other hand, is gently acidic in the range of 6.4–7.0 (Figure 2.1). Tumor cells prefer anaerobic glycolysis to oxidative phosphorylation for energy, which is thought to be the primary cause of extracellular acidity in tumor tissues (Warburg, Wind, and Negelein, 1927). Lactate dehydrogenase converts two pyruvate molecules into two lactate molecules during anaerobic glycolysis. In comparison to normal tissue, tumor growth necessitates a considerable quantity of energy, resulting in the production of more lactate ions in the tumor. Because the generated lactic acid is discharged into the extracellular space of cancer cells, the extracellular pH of tumors is lower than that of normal cells (Hao, Xu, and Li, 2018).

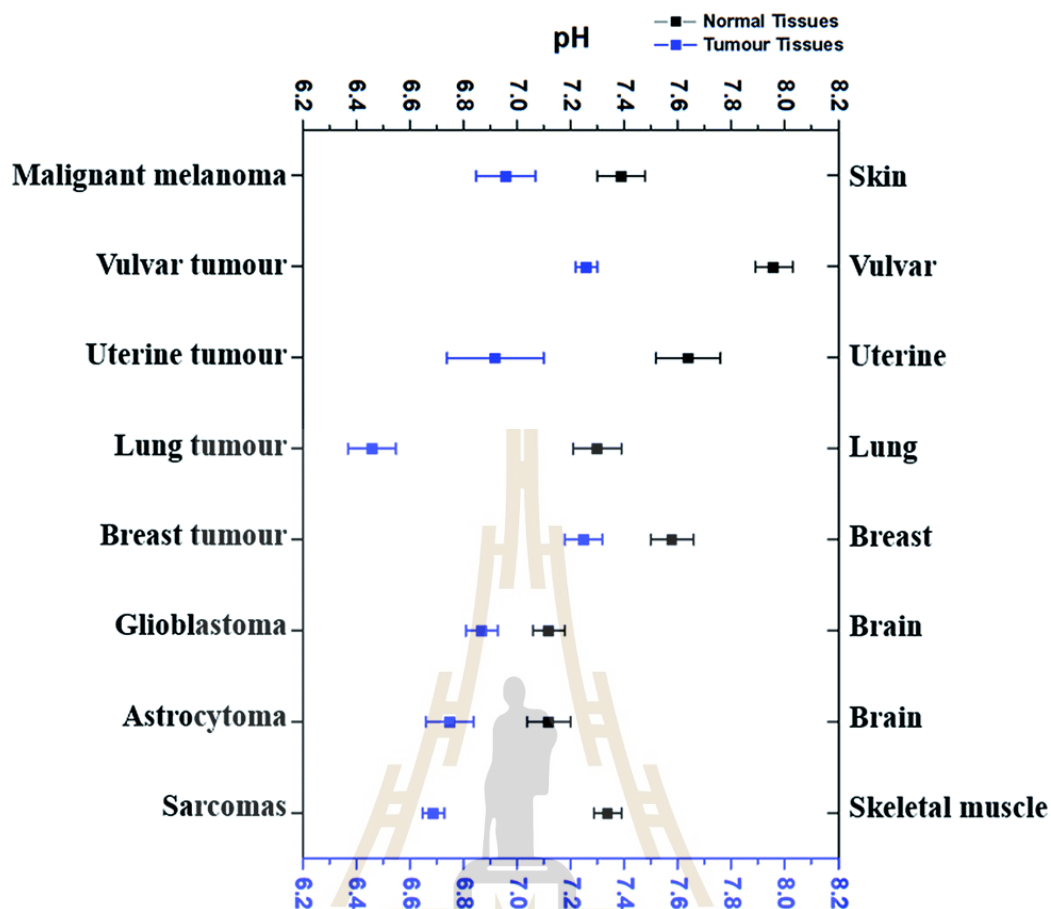
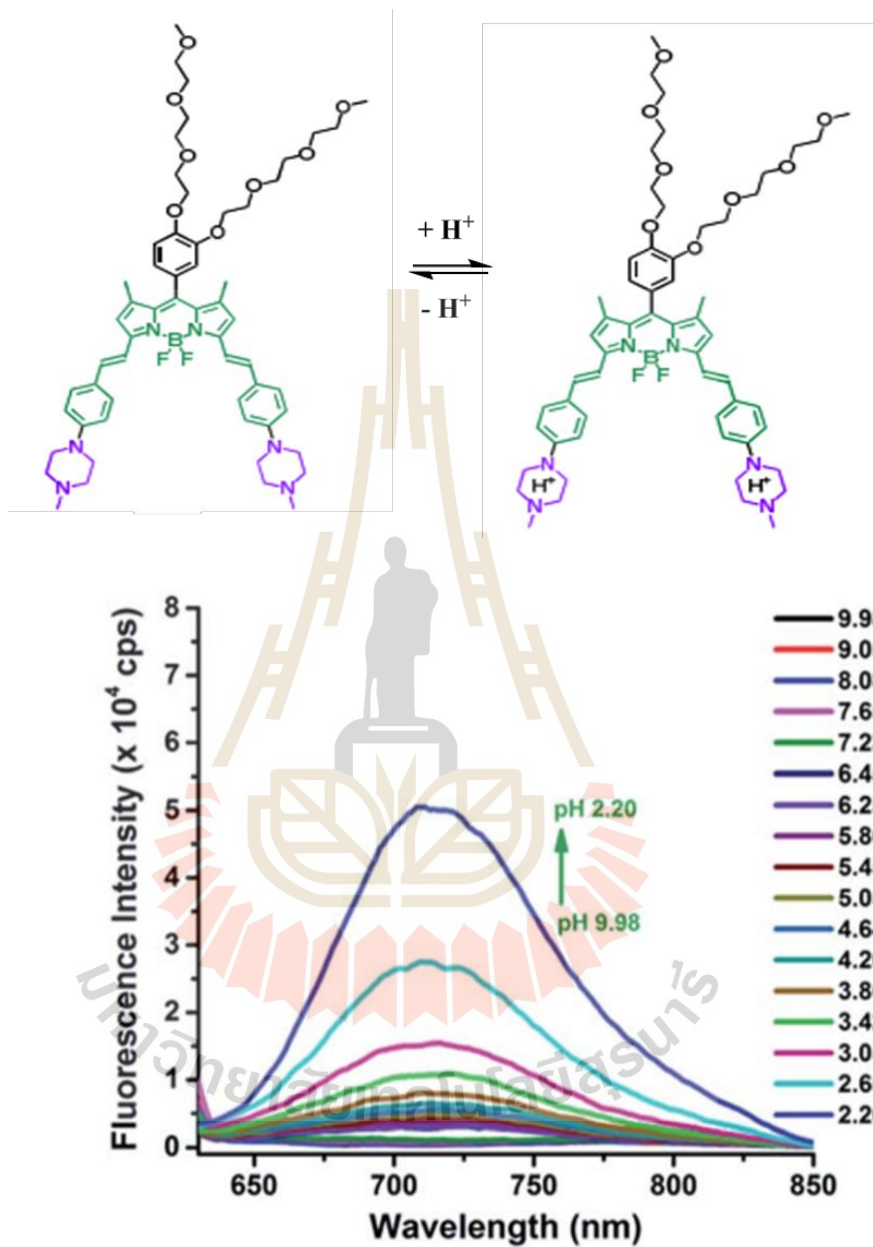


Figure 2.1 Extracellular pH levels of different cancers are compared to normal tissues. (Hao, Xu, and Li, 2018). Copyright © 2018 RSC Advances.

## 2.2 Piperazine for pH-sensitive compound

Piperazine residue was utilized to adjust the fluorescent responses of the probes to pH by modulating the intramolecular charge transfer (ICT) effect and potential photoinduced electron transfer (PET) of piperazine molecules at 3, 5, and 7 positions to BODIPY cores at various pH values. The protonation of piperazine residues at acidic pH reduces the ICT effect of piperazine residues on BODIPY cores, and the potential PET effect on probe fluorescence intensity by the result showed that fluorescence intensity increases significantly when pH decreases (Figure 2.2), and probes have selective NIR imaging of lysosomal pH in living cells (Zhang et al., 2015). Therefore, in this study that focuses on the tumor environment, we have focused on

1-methylpiperazine to be a part of the probe (cyanine dye) for pH responses in the tumor environment.



**Figure 2.2** Structures of near-infrared fluorescent probes and their emission spectra (5  $\mu$ M) in buffer solution at various pH levels. (Zhang et al., 2015). Copyright © The Royal Society of Chemistry 2015.

## 2.3 Cyanine dyes

Cyanine dyes have two nitrogen centers in heterocycles (Figure 2.3), one of which is positively charged and conjugated to the second nitrogen center by a chain of an odd number of carbon atoms.

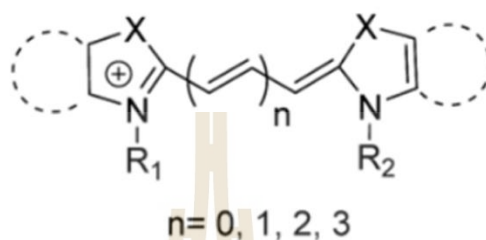


**Figure 2.3** Classic cyanine structures are depicted schematically (Zhou, Lee, Xu and Yoon, 2015) Copyright © 2015 American Chemical Society.

Monomethine (Cy1), trimethine (Cy3), pentamethine (Cy5), and heptamethine (Cy7) cyanines can be divided into four types based on the number of carbon atoms in the chain. The absorption of these dyes and emission spectra are adjustable depending on the length of the conjugated polymethine chain utilized. For example, traditional Cy3 fluorescence is greenish yellow ( $\lambda_{\text{ex}} = 550 \text{ nm}$ ;  $\lambda_{\text{em}} = 570 \text{ nm}$ ), whereas Cy5 and Cy7 fluorescence is in the near-infrared ( $\lambda_{\text{ex}} = 650 \text{ nm}$ ;  $\lambda_{\text{em}} = 670 \text{ nm}$  for Cy5 and  $\lambda_{\text{ex}} = 750 \text{ nm}$ ;  $\lambda_{\text{em}} = 770 \text{ nm}$  for Cy7). Because the absorption and emission maximum of Cy5 and Cy7 are well into the NIR region, these two dyes are better for constructing cancer cell sensors, because they are less phototoxic and have a lower fluorescence background (Zhou, Lee, Xu and Yoon, 2015).

The wavelength of light affects how well it penetrates tissues. The shorter wavelength lights absorb the tissue's surface. Longer wavelength lights penetrate deeper into tissue and are employed for *In vivo* imaging. Hemoglobin and water are two major components of human tissue; hemoglobin substantially absorbs light at wavelengths less than 650 nm, whereas water absorbs light at wavelengths greater than 900 nm. For *in vivo* imaging, the optimal wavelength is between 650 and 900 nm (Weissleder, 2001).

Heptamethine cyanine (Cy7) dyes have been studied extensively as a photodynamic agent throughout the last decade (Shi, Wu, and Pan, 2016). Intracellular uptake of Hcyanine-based theranostic probes (IR2) in HepG2 cells increased proportionately within the first 12 hours of incubation, according to one study. Furthermore, after being exposed to IR2 and 750 nm laser irradiation, 82.8 percent of HepG2 and 84.8 percent of Hela cells died, whereas the viability of HL 7702 (normal cells) remained above 80.0 percent (Zhang et al., 2016). Another study found that IR 780 has a preference for tumor accumulation in *in vivo* imaging. In numerous tumor xenografts as well as chemically produced lung tumors in mice, IR-780 has been discovered to be selectively retain in the mitochondria of tumor cells. With 20  $\mu$ M IR-780 treatments, ROS generation in A549/DR cancer cells increased dramatically. After incubation with 20  $\mu$ M IR-780 for 24 hours, more than 60% of the cells were induced to apoptosis, compared to just 7% in the control group, demonstrating that IR-780 can significantly induce apoptosis in A549/DR cancer cells. IR-780 accumulated in the mitochondria of drug-resistant lung cancer cells, causing an increase in ROS generation and death (Wang et al., 2014).

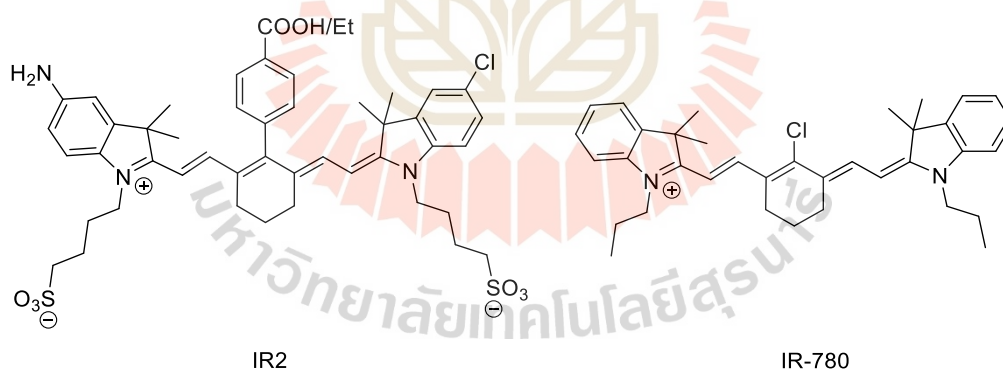


**Figure 2.4** Molecule structure of IR2 (Zhang et al., 2016) and IR-780 (Wang et al., 2014).

## 2.4 Cyanine sensors based on intramolecular charge transfer (ICT)

Intramolecular charge transfer (ICT) is a mechanism in chemosensors that produces a ratiometric characteristic. Modifying the electron-donating ability of the donor in a cyanine structure by substituting amino, ether, or thioether groups at the meso-



position, results in an absorption and/or fluorescence spectrum change. The protonation/deprotonation of the diamine substituent is used to modulate the amine moiety's electron-donating ability, which is used to build a pH sensor (Figure 2.5) (Sun, Guo, Hu, Fan, and Peng, 2016). The sensor had a particular color response to pH probe 3 (Myochin et al., 2011): when the pH dropped from 12.3 to 2.5, the sensor's absorption shifted from 670 to 750 nm, and the color of the sensor changed from blue to green.

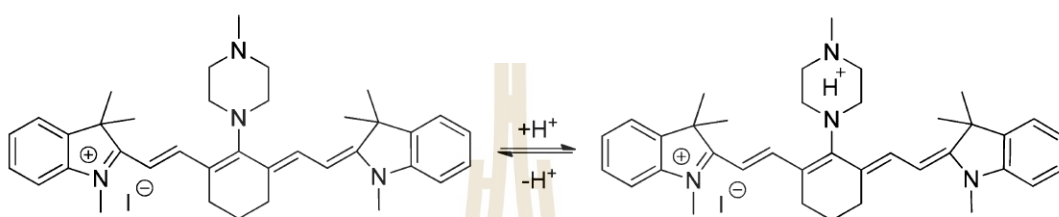


**Figure 2.5** Molecular structure of pH Probe 3 (Myochin et al., 2011). and its sensing mode toward  $H^+$  (Sun, Guo, Hu, Fan, and Peng, 2016). Copyright © 2016 American Chemical Society.

## 2.5 Cyanine sensors based on photoinduced electron transfer (PET)

The cyanine fluorophore, spacer, and recognition site are the three main components of these fluorescent cyanine sensors. Recognition sites act as electron donors or acceptors. When the oxidation potential of the recognition site is less than that of the cyanine fluorophore, electrons transfer from the recognition site to the cyanine group, causing the fluorescence of the sensor to be quenched. This process is called “a-PET”, as the cyanine fluorophore acts as the electron acceptor. In another way, the term “d-PET” is used, if the excited state of the cyanine fluorophore can donate electrons to the lowest unoccupied molecular orbital (LUMO) of the recognition site that causes fluorescence to be inhibited (Sun, Guo, Hu, Fan, and Peng, 2016).

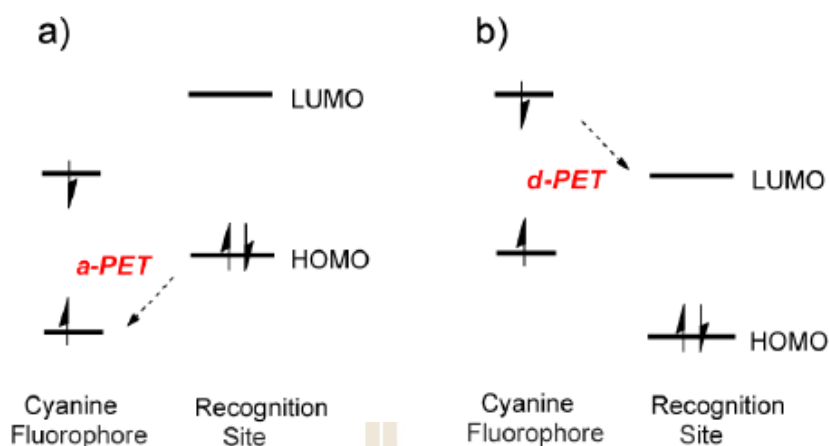


**Figure 2.6** Schematic showing the process of (a) a-PET and (b) d-PET (Sun, Guo, Hu, Fan, and Peng, 2016). Copyright © 2016 American Chemical Society.

## 2.6 Modification of Cyanine dye for PDT applications

The addition of heavy atoms to a conjugated aromatic structure is known to promote singlet oxygen formation by increasing the intersystem crossover (ISC) process. The modified structure produced more  $^1\text{O}_2$  than the unmodified structure, while the NIR fluorescence was still preserved by the fluorescence emission of the modified structure, which was reduced more than the fluorescence emission of the original structure (Atchison et al., 2017). As a result, this study focuses on the tumor environment and focuses on targeting the cyclooxygenase-2 enzyme that is overexpressed on tumor cells, and we designed heavy atoms (iodine) to be part of a probe (cyanine dye) for photodynamic treatment to destroy cancer cells.

## 2.7 Photodynamic therapy

Although light's therapeutic capabilities have been known for thousands of years, photodynamic therapy (PDT) was only established in the last century. Photodynamic therapy (PDT) is a treatment that involves the use of medications known as a photosensitizer (PS) or photosensitizing agent, as well as a specific type of light. When a specific wavelength of light excites the photodynamic agent. Its interactions with the environment in the cell are referred to as type I and type II reactions.

Photodynamic agent reacts with biomolecules in type I reactions. It produces free radicals, which subsequently react with oxygen to produce reactive oxygen species. When a photodynamic agent reacts with oxygen, it is referred to be type II. It produces highly reactive singlet oxygen, which is cytotoxic (Figure 2.7) (Calixto et al., 2016). When photosensitizing is injected into the bloodstream, according to the purpose of PDT in cancer treatment. The PDT agent should be able to target cancer cells with higher effects than normal cells.

When the majority of the agent has left normal cells but remains in cancer cells, the cancer cells are exposed to light, causing PS to produce singlet oxygen, which kills adjacent cells (Dougherty et al., 1998; Dolmans, Fukumura, and Jain, 2003).

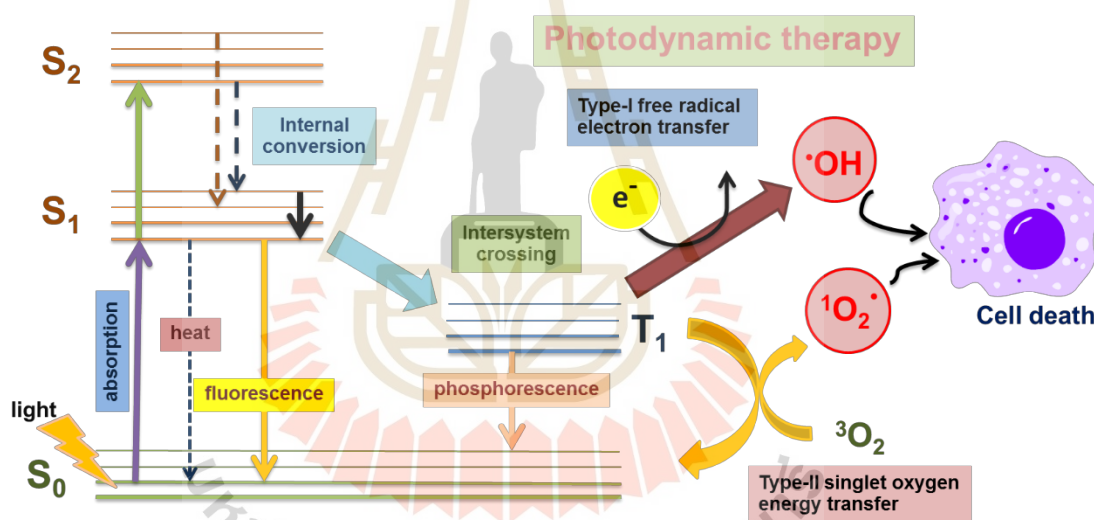
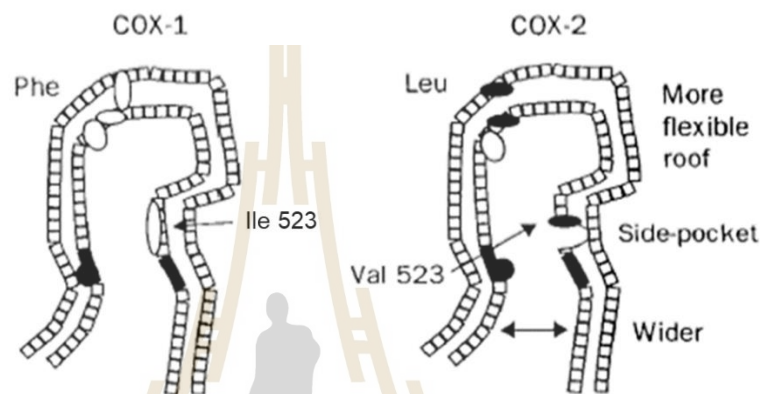


Figure 2.7 Type I and type II reactions are depicted in a photodynamic treatment (PDT) schematic.

## 2.8 Cyclooxygenase 2 and Cancer

Cyclooxygenase (COX) is a crucial enzyme in the conversion of arachidonic acid (AA) to intermediate prostaglandins (PG-G<sub>2</sub>) (Castellone, Teramoto, and Gutkind, 2006). COX has two isoenzymes, COX-1 and COX-2 (Figure 2.8), with COX-2 playing a key role in prostaglandin production during the inflammatory response (Smith, Wade, Lewis, and Qi, 2012). COX-2 is overexpressed in all phases of cancer, from early premalignant

to metastasis, according to clinical data (Kim et al., 2018). In addition, COX-2 expression is linked to tumor features such as transformation, cell proliferation and apoptosis, tumor angiogenesis, and immune response modulation (Trifan, and Hla, 2003). COX-2 levels were discovered to be elevated in pancreas, colon, gastric, stomach, breast, and inflammatory lesions, among other malignancies (Wang and Dubois, 2010). As a result, COX-2 may be a promising molecular target for cancer detection and treatment.



**Figure 2.8** COX-1 and COX-2 active sites are depicted in these structures. (Mengle-Gaw, and Schwartz, 2002). Copyright © Mediators of Inflammation 2002.

Cyclooxygenase was found at the luminal side of the endoplasmic reticulum (Blanke, 2004; Vane and Botting, 1998) and nuclear membrane (Blanke, 2004). COX-1 is found in almost every cell type and is involved in tissue homeostasis (Blanke, 2004; Sobolewski et al., 2010). COX-2 levels in normal cells are extremely low (Prusakiewicz et al., 2004; Wang et al., 2015), but they can be increased by inflammatory stimuli, cytokines, and tumor growth factors (Blanke, 2004; Vane and Botting, 1998).

The Golgi apparatus is a critical organelle for transporting and secreting several essential enzymes that are overexpressed in cancer cells (H. Zhang et al., 2013). When the stress signaling threshold is exceeded, the Golgi apparatus is reported to be actively involved in the initiation and execution of apoptotic processes, resulting in COX-2 accumulation in the Golgi apparatus (Wang et al., 2015; H. Zhang et al., 2013).

## 2.9 Indomethacin for COX-2 targeting

Cyclooxygenase 2 can be the target of several compounds for anticancer. In the past, NSAIDs were used to treat inflammation. Indomethacin (Figure 2.9) is NSAID that is a non-selective COX-2 inhibitor. This is because indomethacin may interfere with COX-1-mediated homeostatic function (Sobolewski et al., 2010). Indomethacin binds to COX-2 through a reversible competitive inhibition. Kurumbail and co-worker (Kurumbail et al., 1996) found that the 2'-methyl group on indomethacin's indole ring inserts into the hydrophobic pocket of COX-2 active site, which includes Val349, Ala527, Ser530, and Leu531 (Kurumbail et al., 1996; Prusakiewicz et al., 2004). Although Indomethacin is non-selective for COX-2, indomethacin becomes more selective for COX-2 when it is conjugated with a fluorescent dye (Kim, Sharma, Ren, et al., 2018; Pewklang, Chansaenpak, Lai, Noisa, & Kamkaew, 2019; Kim, Park, Ren, et al., 2018).

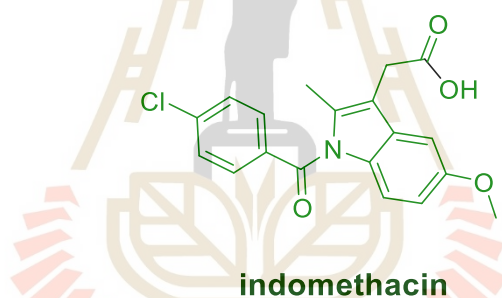


**Figure 2.9** Molecular structure of indomethacin.

For example, Jiang and co-workers (Zhang et al., 2014) reported indomethacin was bound to BT DAN dye utilizing a hexanediamine linker (BT DAN-COX2). The fluorescence of the probe is activated in COX-2-containing solutions, cells, and tissues. Peng and co-workers (Hua Zhang et al., 2013; H. Zhang et al., 2013) reported indomethacin was linked with ANQ and intro-acenaphthenequinone (NANQ) dye with a hexanediamine linker (ANQ-IMC-6 and NANQ-IMC6). Where COX-2 was expressed, the fluorescence of probes was turned on. In the Golgi apparatus of cancer cells, ANQ-IMC-6 can bind to COX-2. NANQ-IMC6 (Figure 2.10) can thereby exploit the difference between normal cells and tissues and cancer cells and tissues. A rhodamine-iridium (III) complex with indomethacin moiety was reported by Li and co-workers (Liu, Xiang, Xiang, and Li, 2021). Indomethacin can improve uptake of the probe to cancer cells.

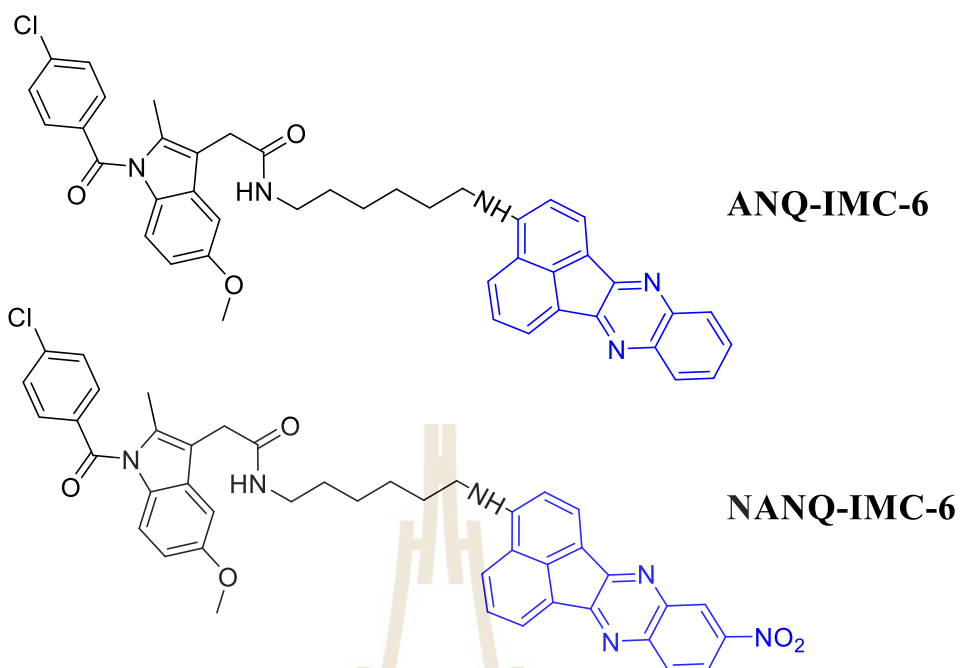


**Figure 2.10** Molecular structure of NANQ-IMC6 (H. Zhang et al., 2013).

Indomethacin was conjugated with Nile Blue dye by using a hexanediamine linker as a NIR fluorescent imaging probe (Figure 2.11), which was localized to the Golgi in cancer cells that overexpressed COX-2. Additionally, this NIR probe identified tumors preferentially in vivo, implying that it may be used for imaging-guided surgery (Wang et al., 2015). Another study used a quinolinium-based compound conjugated to indomethacin by click chemistry, and the conjugation demonstrated outstanding targeted capacity towards cancer cells over normal cells, which was related to COX-2 levels (Kim, Sharma, Ren, et al., 2018).

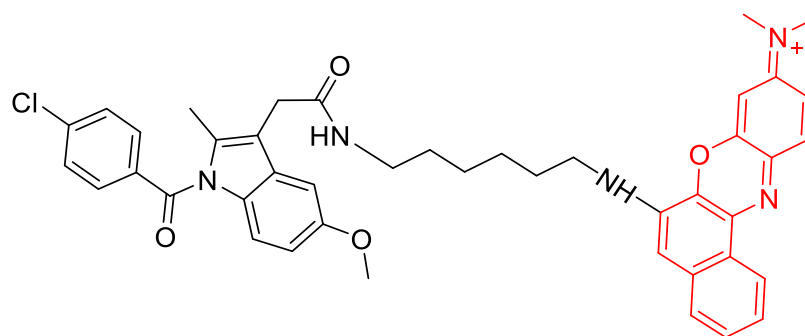


**Figure 2.11** Molecular structure of Niblue-C6-IMC or the probe conjugating generated by Nile Blue dye and Indomethacin (Wang et al., 2015).

Therefore, the main purpose of this study is to investigate indomethacin selectivity and PDT enhancement after conjugation with cyanine dye compared with the control probe.



## CHAPTER III

### METHODOLOGY

#### 3.1 Target: Tumor environment

##### 3.1.1 Synthesis of I<sub>2</sub>-IR783-Mpip

50 mg (0.1 mmol) of I<sub>2</sub>-IR783 was dissolved in 5 mL of anhydrous DMF. 40 mg (0.4 mmol) of N-methylpiperazine will be added to the solution. The mixture was stirred at 30 °C for 3 h under a nitrogen atmosphere. Thereafter, the solvent was removed under reduced pressure, and the crude product was purified by column chromatography using CH<sub>2</sub>Cl<sub>2</sub>:MeOH (gradient from ratio 9:1 to 7:3) to afford a blue solid (40.2 mg, 80.4%). <sup>1</sup>H NMR (500 MHz, DMSO-d<sub>6</sub>): δ 7.93 (s, 01 H, Ar-CH), 7.70 (dd, J = 8.5, 1.5, 1 H, Ar-CH), 7.60 (d, J = 12.0, 1 H, CH), 7.15 (d, J = 8.5, 1 H, Ar-CH), 5.98 (d, J=13.0, 1 H, CH), 4.04 (s, 2 H, N-CH<sub>2</sub>), 3.84 (s, 2 H, N-CH<sub>2</sub>), 2.69 (s, 2 H, N-CH<sub>2</sub>), 2.55 (s, 3 H, N-CH<sub>3</sub>), 2.40 (s, 2 H, N-CH<sub>2</sub>), 1.67–1.83 (m, 16 H). <sup>13</sup>C NMR (125 MHz, DMSO-d<sub>6</sub>): δ 171.4, 166.8, 148.3, 143.5, 142.7, 142.0, 140.5, 136.8, 130.8, 127.1, 124.1, 113.9, 95.8, 89.6, 60.6, 50.9, 49.0, 47.5, 45.8, 42.7, 31.9, 28.32, 28.2, 25.5, 22.6. HRMS-ESI (m/z): the calculated value (calcd) for C<sub>43</sub>H<sub>55</sub>I<sub>2</sub>N<sub>4</sub>Na<sub>2</sub>O<sub>6</sub>S<sub>2</sub><sup>+</sup> [M+H]<sup>+</sup>: 1087.1442, found 1087.1449.

##### 3.1.2 General details for Vis-NIR and fluorescence measurements

The stock solution of I<sub>2</sub>-IR783-Mpip was prepared by dissolving 2.2 mg of I<sub>2</sub>-IR783-Mpip with methanol in a 3 mL standard micro volumetric flask (6.7 × 10<sup>-4</sup> M). The UV-Vis-NIR and fluorescence measurements were performed by taking the appropriate amount of this stock solution.

Vis-NIR absorption measurement: The stock solution of I<sub>2</sub>-IR783-Mpip (20 μL) was added to 3 mL of buffer solutions at various pH (pH 3-12) in a 3.5 mL quartz cuvette with 1 cm light path (final concentration = 4.5 μM). The UV-Vis-NIR absorption



spectra were recorded by a Cary Series UV-Vis-NIR spectrophotometer (Agilent Tech, Santa Clara, CA, USA)

Fluorescence measurement: The stock solution of **I<sub>2</sub>-IR783-Mpip** (20  $\mu$ L) was added to 3 mL buffer solutions with various pH (pH 3–12) in a 3.5 mL quartz cuvette with 1 cm light path (final concentration = 4.5  $\mu$ M). The fluorescence spectra were recorded by PTI QuantaMaster 500 – Near Infra-Red Photoluminescence System (HORIBA Scientific), using the following parameters: the excitation wavelengths = 850 nm, the excitation slit widths = 10 nm, and the emission slit widths = 10 nm.

### 3.1.3 Singlet oxygen generation

10  $\mu$ L (0.5 mM) of singlet oxygen sensor green (SOSG) was added to the solutions of **I<sub>2</sub>-IR783-Mpip** (30  $\mu$ M) at pH 5.0, 7.0, and 9.0, respectively. Then, the solution was exposed to a NIR lamp (850 nm) at a light intensity of 30 mW cm<sup>-2</sup> for 5, 10, 20, 40, and 60 min. the buffers (pH 5.0, 7.0, and 9.0) without **I<sub>2</sub>-IR783-Mpip** were also carried out as the controls using the same method. Finally, fluorescent intensities of SOSG were measured at an excitation of 494 nm using a fluorescence microplate reader (Thermo scientific/VARIOSKAN LUX). Data was reported within error bars of three replicates experiments.

### 3.1.4 Singlet oxygen quantum yield determination

Singlet oxygen generation of **I<sub>2</sub>-IR783-Mpip** was determined using an 850 nm LED lamp. Sample solutions were prepared in phosphate buffer pH 5.0 and 7.4 at a concentration of 15  $\mu$ M on a 6-well plate. 1,3-Diphenylisobenzofuran (DPBF, 1 mM) was prepared in DMSO and diluted to 70  $\mu$ M in buffer solutions. The decrease in absorbance was measured at 418 nm every 1 min for 10 min by a BMG Labtech/SpreeTrostar Nano microplate reader. The rate of change of absorbance is plotted against irradiation time.

$$\Phi_x = \Phi_{st}(\text{grad}_x / \text{grad}_{st})(F_{st}/F_x)$$

$\Phi_{st}$  represents the quantum yield of the standard;  $\Phi_x$  represents the quantum yield of the unknown, and grad is the slope of the best linear fit. F stands for the

absorption correction factor ( $F = 1 - 10^{-abs}$ ; abs represents absorbance), and subscripts x and st denote the unknown and the standard, respectively.

### 3.1.5 Stability test

Solutions of **I<sub>2</sub>-IR783-Mpip** (15  $\mu$ M) in 5% FBS in DMEM cell culture media at pH 5.0 and pH 7.4 were incubated at 37 °C for up to 168 h or 7 days. Vis-NIR spectra of the solutions were measured at different time points including 0, 1, 3, 6, 12, 24, 48, 72, 96, 120, 144, and 168 h respectively.

### 3.1.6 Cell culture

Human hepatoma cancer cells (HepG2) and human embryonic kidney 293 (HEK-293) cells were cultured on 75 cm<sup>2</sup> culture flasks in Dulbecco's Modified Eagle Medium/High glucose (DMEM/HIGH GLUCOSE, GE Healthcare Life Sciences HyClone Laboratories) supplemented with 10% fetal bovine serum (FBS, Gibco) and 1% Penicillin Streptomycin Solution 100X (CORNING). All cells were cultured in a humidified incubator at 37 °C with 5% CO<sub>2</sub>.

### 3.1.7 Cell survival assay of HepG2 cells in media 5.0

For cell survival assay, HepG2 cells were seeded into 96-well cell culture plates at  $7 \times 10^3$ /well and incubated for 24 h at 37 °C under 5% CO<sub>2</sub>. After that, cell culture media was replaced with 5% FBS DMEM pH 5.0 at various incubation times (1, 3, 6, 12, 24, 36 h), and cells cultured in 5% FBS DMEM pH 7.4 was used as control. After incubation, the cell viabilities were measured using the previously reported MTT protocol (Pewklang, 2019). Briefly, the cells were washed with PBS (3 times) before being treated with methylthiazolyldiphenyl-tetrazolium bromide (20  $\mu$ L, 0.5 mg/mL, Sigma-Aldrich) for 2 h. Then, culture media was replaced with DMSO and the cell viabilities were determined through UV-vis absorption of the resulting formazan at wavelength 560 nm using a microplate reader (BMG Labtech/SPECTROstar Nano).

### 3.1.8 Live cell imaging

HepG2 cells were seeded at a density of  $7 \times 10^3$  cells per well in 8-well Chambered Coverglass with non-removable wells (Nunc Lab-Tek II Chamber Slide) and were incubated for 24 h at 37 °C under 5% CO<sub>2</sub>. After that, cell culture media was removed and solutions of **I<sub>2</sub>-IR783-Mpip** in DMEM with 5% FBS at pH 5.0 and pH 7.4 with final concentrations of 30 μM were added. After 1, 3, 6, 12, and 24 h incubation, the cells were washed three times with PBS to remove the non-uptake dye. Thereafter, the cells were stained with 1.0 μM Hoechst 33342 (Thermo Fisher Scientific) for 10 min. All cells were brought to image under Laser Scanning Confocal Microscope (LSCM, Nikon A1Rsi). **I<sub>2</sub>-IR783-Mpip** was excited by 641 nm laser and Hoechst 33342 was excited by 405 nm laser. A 60 X oil immersion objective lens was used.

### 3.1.9 Localization study with lysotracker and mitotracker

After seeding the cells in an 8-well Chambered Coverglass and incubated for 24 h at 37 °C under 5% CO<sub>2</sub>, the cells were incubated with 30 μM of **I<sub>2</sub>-IR783-Mpip** in DMEM with 5% FBS at pH 5.0 and pH 7.4 for another 12 h, washed three times with PBS and incubated with Lysotracker Green DND 26, Mitotracker Green FM (Thermo Fisher Scientific) for 20 min. The cells were washed again before staining with Hoechst 33342 for 10 min. After that, cells were visualized under LSCM: **I<sub>2</sub>-IR783-Mpip** was excited by 641 nm laser; Lysotracker and Mitotracker were excited by 488 nm laser, and Hoechst 33342 was excited by 405 nm laser. A 60 X oil immersion objective lens was used. To quantify the colocalization of **I<sub>2</sub>-IR783-Mpip** and organelles trackers, we obtained the intensities of the red and green channels from each pixel of the confocal image, corresponding to the excitations from **I<sub>2</sub>-IR783-Mpip** and organelles trackers, respectively, and calculate the Pearson's correlation coefficient between the two intensities. The computation was carried out in Python, using a built-in function from the scipy statistical package.

### 3.1.10 Flow cytometry

HepG2 and HEK293 cells were seeded into 6-well cell culture plates density of  $2 \times 10^5$  cells/well and incubated for 48 h at 37 °C under 5% CO<sub>2</sub>. After that, cell

culture media was removed and solutions of **I<sub>2</sub>-IR783-Mpip** in DMEM with 5% FBS at pH 5.0 and pH 7.4 with final concentrations of 15  $\mu\text{M}$  were added. After 12 h incubation, culture media was removed, and the cells were thoroughly washed with PBS. Thereafter, the cells were harvested by trypsinization whose action was stopped with 10% FBS in DMEM cell-culture media. The cells were transferred into Eppendorf tubes and were washed three times with ice-cold PBS to remove the non-uptake dye by centrifugation at 800 g, 4 °C for 5 min and were resuspended in 1 mL of fresh ice-cold PBS. Then 20,000 events (cells) were analyzed by flow cytometry using an Attune NxT Flow Cytometer (Life Technologies) using red excitation laser 637 nm and emission filter 780/60 nm.

### 3.1.11 Light induced cytotoxicity

*In vitro* cell viability was measured using a standard methyl thiazolyltetrazolium (MTT) assay. HepG2 and HEK293 cells were seeded into 96-well cell culture plates at  $7 \times 10^3$  cells/well and were incubated for 24 h at 37 °C under 5% CO<sub>2</sub>. After that, cell culture media was removed and solutions of **I<sub>2</sub>-IR783-Mpip** in DMEM with 5% FBS at pH 5.0 and pH 7.4 with various concentrations (0, 10, 20, 40, 50  $\mu\text{M}$ ) were added and the cells were continued incubated for another 6 h. Thereafter, the cells were irradiated by an 850 nm lamp with a light intensity of 30 mW/cm<sup>2</sup> for 30 min before re-incubation for another 12 h. In the case of deep-tissue simulation, a piece of 5-mm pork slice (sterile with 95% alcohol) was placed on the top of a 96-well plate to insert between the cells and the lamp before irradiation. After incubation, the cell viabilities were measured using standard MTT protocol (Pewklang, 2019) and the absorption of formazan was measured at wavelength 560 nm using a microplate reader (BMG Labtech/SPECTROstar Nano).

For LIVE/DEAD viability/cytotoxicity assay, HepG2 cells were seeded into 6-well cell culture plates at a density of  $2 \times 10^5$  cells/well and were incubated for 24 h at 37 °C under 5% CO<sub>2</sub>. After that, cell culture media was removed and solutions of **I<sub>2</sub>-IR783-Mpip** in DMEM with 5% FBS at pH 5.0 and pH 7.4 with final concentrations of 20  $\mu\text{M}$ , 50  $\mu\text{M}$  were added. After 6 h incubation, the cells were irradiated by an 850 nm lamp with a light intensity of 30 mW/cm<sup>2</sup> for 30 min before re-incubation for

another 12 h. Thereafter, the cells were stained with 4  $\mu\text{M}$  calcein AM and propidium iodide (PI) (Thermo Fisher Scientific) for 5 min, and then were imaged by fluorescence microscope (BioRad/Zoe) using 490 nm excitation and 515 nm emission filters for calcein AM and 535 nm excitation and 615 nm emission filters for PI.

### 3.1.12 Cellular reactive oxygen production

HepG2 cells were seeded at a density of  $7 \times 10^3$  cells per well in 8-well Chambered Coverglass with non-removable wells and were incubated for 24 h at 37 °C under 5%  $\text{CO}_2$ . After that, cell culture media was removed and solutions of **I<sub>2</sub>-IR783-Mpip** (20  $\mu\text{M}$ ) in DMEM with 5% FBS at pH 5.0 and pH 7.4 were added. After 6 h incubation, the cells were washed three times with PBS to remove the non-uptake dye, and then 20  $\mu\text{M}$  of 2,7-dichloro-dihydro-fluorescein diacetate (DCFH-DA, Sigma-Aldrich) was added into the cells. After incubation for 1 h, the cells were washed three times with PBS to remove the non-uptake DCFH-DA dye before irradiation with an 850 nm lamp for 20 min. Before imaging, the cells were stained with 1.0  $\mu\text{M}$  Hoechst 33342 (Thermo Fisher Scientific) for 10 min then fluorescence of the resulting 2,7-dichloro-dihydro-fluorescein (DCF) was monitored using 488 nm excitation laser and Hoechst 33342 was excited at 405 nm under Laser Scanning Confocal Microscope (Nikon A1Rsi). A 60 X oil immersion objective lens was used.

For quantitative analysis, HepG2 cells were seeded into 96-well cell culture plates at  $7 \times 10^3$ /well and were incubated for 24 h at 37 °C under 5%  $\text{CO}_2$ . After that, cell culture media was removed and solutions of **I<sub>2</sub>-IR783-Mpip** (20  $\mu\text{M}$ ) in DMEM with 5% FBS at pH 5.0 and pH 7.4 with various concentrations (0, 10, 20, 40, 50  $\mu\text{M}$ ) were added. After 6 h incubation, the cells were washed three times with PBS before being irradiated by an 850 nm lamp for 20 min. Thereafter, 20  $\mu\text{M}$  of DCFH-DA was added to each well and the cells were continued incubated for another 45 min. The fluorescent end point of the DCF production was recorded at 495 nm excitation and 529 nm emission using a fluorescence microplate reader (Thermo Fisher Scientific/VARIOSKAN LUX).

### 3.1.13 Statistical analysis

Data are illustrative of three independent experiments and presented as the mean of four individual observations ( $n = 4$ ) with the standard deviation (mean  $\pm$  SD). The statistical analysis was performed using one-way ANOVA followed by Tukey's post-hoc analysis.  $P$  values  $< 0.05$  were considered to indicate significance (\* $P < 0.05$ , \*\* $P < 0.01$ , \*\*\* $P < 0.001$ ).

## 3.2 Target: Cyclooxygenase enzyme that overexpressed on tumor cells

### 3.2.1 Synthesis of Cy820 and Cy820-IMC

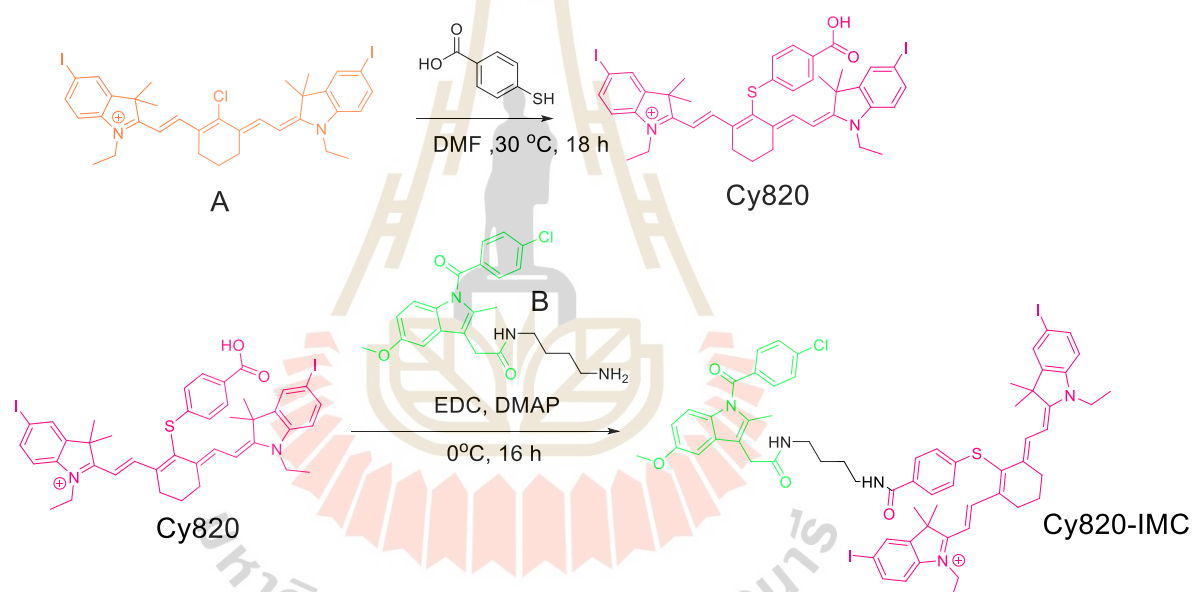


Figure 3.1 Synthesis scheme of Cy820 and Cy820-IMC.

#### 3.2.1.1 Synthesis of Cy820

0.0500 g (0.0655 mmol) of A and 0.0101g (0.0655 mmol) of 4-mercaptobenzoic acid were dissolved in 10 mL DMF. The mixture was stirred at room temperature for 18 h. After solvent removal, the crude material was purified by normal phase flash chromatography with methanol: dichloromethane (2:98 V/V). The **Cy820** was isolated as green solid (34.5%).  $^1\text{H}$  NMR (500 MHz,  $\text{DMSO-}d_6$ ):  $\delta$  8.34 (s, 2 H, CH), 7.87 (s, 2 H, Ar-CH), 7.84 (d,  $J = 10.0$ , 2 H, Ar-CH), 7.69 (d,  $J = 5.0$ , 2 H, Ar-CH), 7.33 (d,  $J$

=10.0, 2 H, Ar-CH), 7.16 (d,  $J = 5.0$ , 2 H, Ar-CH), 6.20 (s, 2 H, CH), 4.11 (s, 4 H, CH<sub>2</sub>), 2.77 (s, 4 H, CH<sub>2</sub>), 1.92 (s, 2 H, CH<sub>2</sub>), 1.36 (s, 12 H, CH<sub>3</sub>), 1.23 (s, 6 H, CH<sub>3</sub>). <sup>13</sup>C NMR (125 MHz, DMSO-*d*<sub>6</sub>):  $\delta$  171.4, 167.3, 148.2, 145.1, 144.1, 142.9, 141.9, 137.6, 134.3, 131.7, 130.9, 130.8, 126.6, 125.8, 113.9, 102.4, 89.9, 49.3, 27.3, 26.3, 20.7, 12.6. HRMS-ESI (*m/z*): the calculated value (calcd) for C<sub>41</sub>H<sub>43</sub>I<sub>2</sub>N<sub>2</sub>O<sub>2</sub>S<sup>+</sup> [M+H]<sup>+</sup>: 881.1129, found 881.1122.

### 3.2.1.2 Synthesis of Indomethacin linker (B)

1.0000 g (2.7949 mmol) of indomethacin and 1,1-carbonyldiimidazole (CDI) were dissolved in 15 mL of dry THF at 30 °C under an N<sub>2</sub> atmosphere. The mixture was stirred for 90 min. After that, the reaction was added over 20 min to a solution of 0.2464 (2.7949 mmol) of 1,4-diaminobutane in 5 mL of dry THF at 30 °C under an N<sub>2</sub> atmosphere. The reaction mixture was stirred for 26 h at 30 °C under an N<sub>2</sub> atmosphere. The mixture was diluted with H<sub>2</sub>O and extracted with ethyl acetate. The organic layer was washed with brine, dried Magnesium sulfate anhydrous, and ethyl acetate was then removed under reduced pressure. After solvent removal, the crude material was purified by normal phase flash chromatography with ethyl acetate: dichloromethane (1:1 V/V). The **Indomethacin linker** was isolated as a yellow liquid (11.5%). <sup>1</sup>H NMR (500 MHz, DMSO-*d*<sub>6</sub>):  $\delta$  6.94 (d,  $J = 10.0$ , 2 H, Ar-CH), 6.60 (d,  $J = 10.0$ , 2 H, Ar-CH), 6.26 (d,  $J = 10.0$ , 1 H, Ar-CH), 6.10 (d,  $J = 2.5$ , 1 H, Ar-CH), 5.78 (dd,  $J = 10.0$  and 2.5, 2 H, Ar-CH), 2.87 (s, 3 H, OCH<sub>3</sub>), 2.60 (s, 2 H, CH<sub>2</sub>), 2.42 (t,  $J = 10.0$ , 2 H, N-CH<sub>2</sub>), 2.27 (t,  $J = 10.0$ , 2 H, N-CH<sub>2</sub>), 1.47 (s, 3 H, CH<sub>3</sub>), 0.64 (m, 4 H, CH<sub>2</sub>). <sup>13</sup>C NMR (125 MHz, DMSO-*d*<sub>6</sub>):  $\delta$  171.6, 165.7, 152.9, 135.9, 133.4, 132.8, 129.9, 128.4, 127.8, 110.3, 109.3, 103.9, 99.6, 55.5, 31.1, 26.2, 25.9, 10.3. HRMS-ESI (*m/z*): the calculated value (calcd) for C<sub>23</sub>H<sub>26</sub>ClN<sub>3</sub>NaO<sub>3</sub><sup>+</sup> [M+H]<sup>+</sup>: 450.1555, found 450.1562.

### 3.2.1.3 Synthesis of Cy820-IMC

0.029 g (0.068 mmol) of **Indomethacin linker** was dissolved in 2 mL of anhydrous DCM. 0.0130 g (0.0680 mmol) of EDC and 0.0035 g (0.0284 mmol) of DMAP was added into solution. The mixture was stirred at 0 °C for 30 min and then 0.0500 (0.0567 mmol) of **Cy820** was added to the mixture. The mixture was continuously stirred for 12 h at 30 °C. The reaction was diluted with water and extracted with DCM.

The organic solvent was washed with brine, dried with magnesium sulfate anhydrous. After solvent removal, the crude material will be purified by normal phase flash chromatography with methanol: dichloromethane (2:98 V/V). The **Cy820-IMC** was isolated as green-yellow solid (46.4%).  $^1\text{H}$  NMR (500 MHz, DMSO- $d_6$ ):  $\delta$  10.86 (s, 2 H, NH), 8.54 (d,  $J = 15.0$ , 2 H, CH), 8.34 (t,  $J = 5.0$ , 1 H, Ar-CH), 7.92 (s, 2 H, Ar-CH), 7.74 (t,  $J = 10.0$ , 6 H, Ar-CH), 7.31 (d,  $J = 10.0$ , 2 H, Ar-CH), 7.23 (d,  $J = 10.0$ , 2 H, Ar-CH), 7.07 (d,  $J = 10.0$ , 2 H, Ar-CH), 6.94 (d,  $J = 2.5$ , 1 H, Ar-CH), 6.54 (dd,  $J = 10.0$ , 2.5, 1 H, Ar-CH), 6.33 (d,  $J = 15.0$ , 2 H, CH), 4.17 (d,  $J = 10$ , 4 H,  $\text{CH}_2$ ), 3.65 (s, 3 H,  $\text{OCH}_3$ ), 3.32 (s, 2 H,  $\text{CH}_2$ ), 3.17 (m, 2 H,  $\text{CH}_2$ ), 3.01 (m, 2 H,  $\text{CH}_2$ ), 2.78 (s, 4 H,  $\text{CH}_2$ ), 2.28 (s, 3 H,  $\text{CH}_3$ ), 1.93 (s, 2 H,  $\text{CH}_2$ ), 1.39 (s, 16 H,  $\text{CH}_2$ ,  $\text{CH}_3$ ), 1.24 (t,  $J = 10.0$ , 6 H,  $\text{CH}_3$ ).  $^{13}\text{C}$  NMR (125 MHz, DMSO- $d_6$ ):  $\delta$  171.4, 171.1, 165.7, 153.4, 148.8, 145.2, 144.1, 142.0, 140.8, 137.6, 134.3, 134.1, 132.4, 131.6, 130.6, 129.2, 128.8, 127.8, 125.7, 114.3, 113.9, 111.2, 109.9, 105.4, 102.3, 100.8, 89.9, 30.2, 55.8, 49.3, 38.8, 32.2, 27.4, 27.2, 27.0, 26.3, 20.8, 12.6, 12.0. HRMS-ESI (m/z): the calculated value (calcd) for  $\text{C}_{64}\text{H}_{67}\text{Cl}_2\text{N}_5\text{O}_4\text{S}^+$   $[\text{M}+\text{H}]^+$ : 1290.2686, found 1288.2771.

### 3.2.2 Photophysical properties of Cy820-IMC and Cy820

For Vis-NIR absorption and fluorescence studies: stock solutions of Cy820-IMC (310  $\mu\text{M}$ ) and Cy820 (596  $\mu\text{M}$ ) were prepared in DMSO. The UV-Vis-NIR absorption and fluorescence spectra were measured with quartz cuvette using a Cary Series UV-Vis-NIR spectrophotometer (Agilent Tech, Santa Clara, CA, USA) and PTI QuantaMaster 500 – Near Infra-Red Photoluminescence System (HORIBA Scientific), excitation wavelength = 780 nm, excitation slit widths = 10 nm, and emission slit widths = 10 nm, respectively.

### 3.2.3 Singlet oxygen quantum yield of Cy820-IMC and Cy820

1,3-diphenylisobenzofuran (DPBF, Sigma-Aldrich) was used as a singlet oxygen scavenger. 20  $\mu\text{M}$  of DPBF was added into solutions of **Cy820-IMC** and **Cy820** (2  $\mu\text{M}$ ) in DMSO and PBS buffer (3% tween) pH 7.4. After that, the solution was exposed to a 780 nm LED Lamp at 2.37  $\text{mW}/\text{cm}^2$  for 1, 2, 3, 5, 7, and 9 min. The absorbance of DPBF was measured at 408 nm by UV-vis spectrophotometer (T80+ UV/vis spectrometer PG



Instruments Ltd). Singlet oxygen quantum yield was calculated according to the equation below.

$$\Phi_x = \Phi_{st}(\text{grad}_x / \text{grad}_{st})(F_{st}/F_x)$$

$\Phi_{st}$  represents the quantum yield of the standard;  $\Phi_x$  represents the quantum yield of the unknown, and grad is the slope of the best linear fit. F stands for the absorption correction factor ( $F = 1 - 10^{-\text{abs}}$ ; abs represents absorbance), and subscripts x and st denote the unknown and the standard, respectively.

### 3.2.4 Cell culture

Human hepatoma cancer cells (HepG2) and human embryonic kidney 293 (HEK-293) cells were cultured on 75 cm<sup>2</sup> culture flasks in Dulbecco's Modified Eagle Medium/High glucose (DMEM/HIGH GLUCOSE, Cytiva HyClone Laboratories) supplemented with 10% fetal bovine serum (FBS, Gibco) and 1% Penicillin Streptomycin solution 100X (CORNING). All cells were cultured in a humidified incubator at 37 °C with 5% CO<sub>2</sub>.

### 3.2.5 Cell imaging

HepG2 cells were seeded at a density of  $1 \times 10^4$  cells per well in 8-well Chambered Coverglass with non-removable wells (Nunc Lab-Tek II Chamber Slide) and incubated for 24 h at 37 °C under 5% CO<sub>2</sub>. Then, media were removed and 5 μM of **Cy820-IMC** and **Cy820** in DMEM with 5% FBS were added at incremental incubation time intervals of 1, 3, 6, 12, and 24 h, the cells were washed 3 times with PBS to remove the non-uptake dye. Thereafter, the cells were stained with 1.0 μM Hoechst 33342 (Thermo Fisher Scientific) for 10 min to visualize the cell nucleus.

In all imaging experiments, unless stated otherwise, the cells were monitored by a Laser Scanning Confocal Microscope (LSCM, Nikon A1Rsi). **Cy820-IMC** and **Cy820** were excited with 641 nm laser and Hoechst 33342 was excited with 405 nm laser. A 60 X oil immersion objective lens was used.

### 3.2.6 Photodynamic therapy

HepG2 and HEK-293 cells were seeded into 96-well cell culture plates at  $2 \times 10^4$  cells/well and incubated for 24 h at 37 °C under 5% CO<sub>2</sub>. Then, media were removed and 5 μM of **Cy820-IMC** and **Cy820** in DMEM with 5% FBS were added at incremental concentrations 0, 1.25, 2.5, 5, 10, and 20 μM, and then the cells were incubated for 6 h. Thereafter, the cells were irradiated by a 780 nm lamp at 2.37 mW/cm<sup>2</sup> for 30 min and re-incubated for another 16 h. After incubation, the cell viabilities were measured using a standard methyl thiazolyltetrazolium (MTT) assay and absorption of formazan at 560 nm was detected by a microplate reader (BMG Labtech/SPECTROstar Nano).

### 3.2.7 LIVE/DEAD staining

HepG2 and HEK-293 cells were seeded into 96-well cell culture plates at  $3 \times 10^4$  cells/well and incubated for 24 h at 37 °C under 5% CO<sub>2</sub>. Then, the media were replaced with **Cy820-IMC** and **Cy820** in DMEM with 5% FBS at concentrations 0 and 5 μM, and the cells were incubated for 6 h. Thereafter, the cells were irradiated by a 780 nm lamp at 2.37 mW/cm<sup>2</sup> for 30 min and cells were re-incubated for another 16 h. After that, 4 μM calcein AM and propidium iodide (PI) (Thermo Fisher Scientific) were added to the tested cells for 5 min. Then all the cells were brought to image using a fluorescence microscope (BioRad/Zoe) with 490 nm excitation and 515 nm emission filter for calcein and 535 nm excitation and 615 nm emission filter for PI.

For the following set of experiments, HepG2 cells were seeded at a density of  $1 \times 10^4$  cells per well in 8-well Chambered Coverglass with non-removable wells (Nunc Lab-Tek II Chamber Slide) and incubated for 24 h at 37 °C under 5% CO<sub>2</sub> before treatments.

### 3.2.8 Intracellular singlet oxygen generation

Culture media were replaced with 5 μM of **Cy820-IMC** in DMEM with 5% FBS before incubation for 6 h. Thereafter, the cells were washed with PBS (3 times) and re-incubated with 20 μM of 2,7-dichloro-dihydro-fluorescein diacetate (DCFH-DA, Sigma-

Aldrich) for 1 h. Then the cells were washed with PBS (3 times) before being irradiated by a 780 nm lamp at 2.37 mW/cm<sup>2</sup> for 30 min and re-incubated for 10 min. After that, 1.0 µM Hoechst 33342 (Thermo Fisher Scientific) were added to the cells before being imaged with LSCM. The fluorescence product of DCFH-DA, 2,7-dichloro-dihydro-fluorescein (DCF), was detected by a 488 nm excitation laser and Hoechst 33342 was excited at 405 nm. A 60 X oil immersion objective lens was used.

### 3.2.9 Cyclooxygenase-2 inhibition experiment

The cells were pre-treated with 15 µM of celecoxib and aceclofenac for 2 h in fresh media. After that, the media were replaced with 5 µM of **Cy820-IMC** and **Cy820** in DMEM with 10% FBS, and the cells were incubated for 3 h. Thereafter, the cells were washed, stained with 1.0 µM Hoechst 33342, and imaged with LSCM.

#### 3.2.10 OATPs inhibition experiment

The cells were pre-treated with 250 µM of Sulfobromophthalein disodium salt hydrate (BSP, Sigma-Aldrich) for 10 min in serum-free media. After that, the cells were treated with 5 µM of **Cy820-IMC** and **Cy820** in serum-free media for 3 h. Before being imaged by LSCM, the cells were washed and stained with 1.0 µM Hoechst 33342.

#### 3.2.11 Colocalization experiment

The cells were treated with 5 µM of **Cy820-IMC** in fresh DMEM with 10% FBS and incubated for 6 h. Thereafter, the cells were washed with PBS (3 times) and incubated with 20 µM of LysoTracker Green DND 26, Mitotracker Green FM, and NBD-C6-ceramide (Thermo Fisher Scientific) for 20 min. Before being imaged with LSCM, the cells were washed with PBS (3 times) and stained with 1.0 µM Hoechst 33342 (Thermo Fisher Scientific) for 10 min. LysoTracker Green DND 26, Mitotracker Green FM, and NBD-C6-ceramide were excited at 488 nm.

#### 3.2.12 Flow cytometry

HepG2 and HEK-93 cells were seeded into 6-well cell culture plates at  $3 \times 10^5$  cells/well and incubated for 24 h at 37 °C under 5% CO<sub>2</sub>. Then, the media were

replaced with 5  $\mu\text{M}$  of **Cy820-IMC** and **Cy820** in DMEM with 10% FBS, and the cells were incubated for 3 h. After that, the cells were washed with PBS (3 times) to remove the non-uptake dye.

For the OATPs inhibition experiment, the cells were pre-treated with 250  $\mu\text{M}$  of BSP in serum-free DMEM for 10 min before being treated with 5  $\mu\text{M}$  of **Cy820-IMC** and **Cy820** in serum-free DMEM for another 3 h. After that, the cells were washed with PBS (3 times) to remove the non-uptake dye.

For the Cyclooxygenase-2 inhibition experiment, the cells were pre-treated with 15  $\mu\text{M}$  of celecoxib and aceclofenac for 2 h before being treated with 5  $\mu\text{M}$  of **Cy820-IMC** and **Cy820** in DMEM with 10% FBS and incubated for another 3 h. After that, the cells were washed with PBS (3 times) to remove the non-uptake dye.

All the cells were harvested by trypsinization and the action was stopped with 10% FBS DMEM. The cells were transferred into Eppendorf tubes and washed three times with ice-cold PBS by centrifugation at 800 g, 4  $^{\circ}\text{C}$  for 5 min and re-suspended in 1 mL of cold PBS containing trypan blue (to quench non-uptake dye). Then 10,000 events (cells) were measured by flow cytometry using an Attune NxT Flow Cytometer (Life Technologies) using red excitation laser 637 nm and emission filter 780/60 nm.

## CHAPTER IV

### RESULTS AND DISCUSSION

#### 4.1 Target: Tumor environment

##### 4.1.1 Photophysical properties

The optical properties of the dye were found to be affected by the pH of the solution. Under pH 6–7, **I<sub>2</sub>-IR783-Mpip** absorbed light from the visible to the near-infrared range (500–920 nm), peaking at 860 nm. The absorption spectra of **I<sub>2</sub>-IR783-Mpip** were red-shifted when two nitrogen atoms of the N-methylpiperazine moiety were protonated in acidic conditions (pH 3.0–5.0) (Figure 4.1A). The absorption spectra of **I<sub>2</sub>-IR783-Mpip** were blue-shifted when it was subjected to basic conditions (pH 8.0–12.0). In **I<sub>2</sub>-IR783-Mpip**, these phenomena could be the result of intramolecular charge transfer (ICT). Charge separation is achieved within the fluorophore because the **I<sub>2</sub>-IR783-Mpip** comprises both an electron donor (amine) and an acceptor (Hcyanine). The ability of a donor at the meso-position in a cyanine scaffold to donate electrons would cause absorption and/or fluorescence spectra to shift (Myochin et al., 2011). Furthermore, the molecular structures of **I<sub>2</sub>-IR783-Mpip** were postulated in three forms, **I<sub>2</sub>-IR783-Mpip<sup>-1</sup>**, **I<sub>2</sub>-IR783-Mpip<sup>0</sup>**, and **I<sub>2</sub>-IR783-Mpip<sup>+1</sup>** in solutions pH 8–12, 6–7 and 3–5, respectively (Figure 4.1A) based on the reported pKa values of sulfonic acid (pKa = -2.6) and N-methylpiperazine (pKa = 3.81 and 8.38) (Khalili, Henni, and East, 2009).

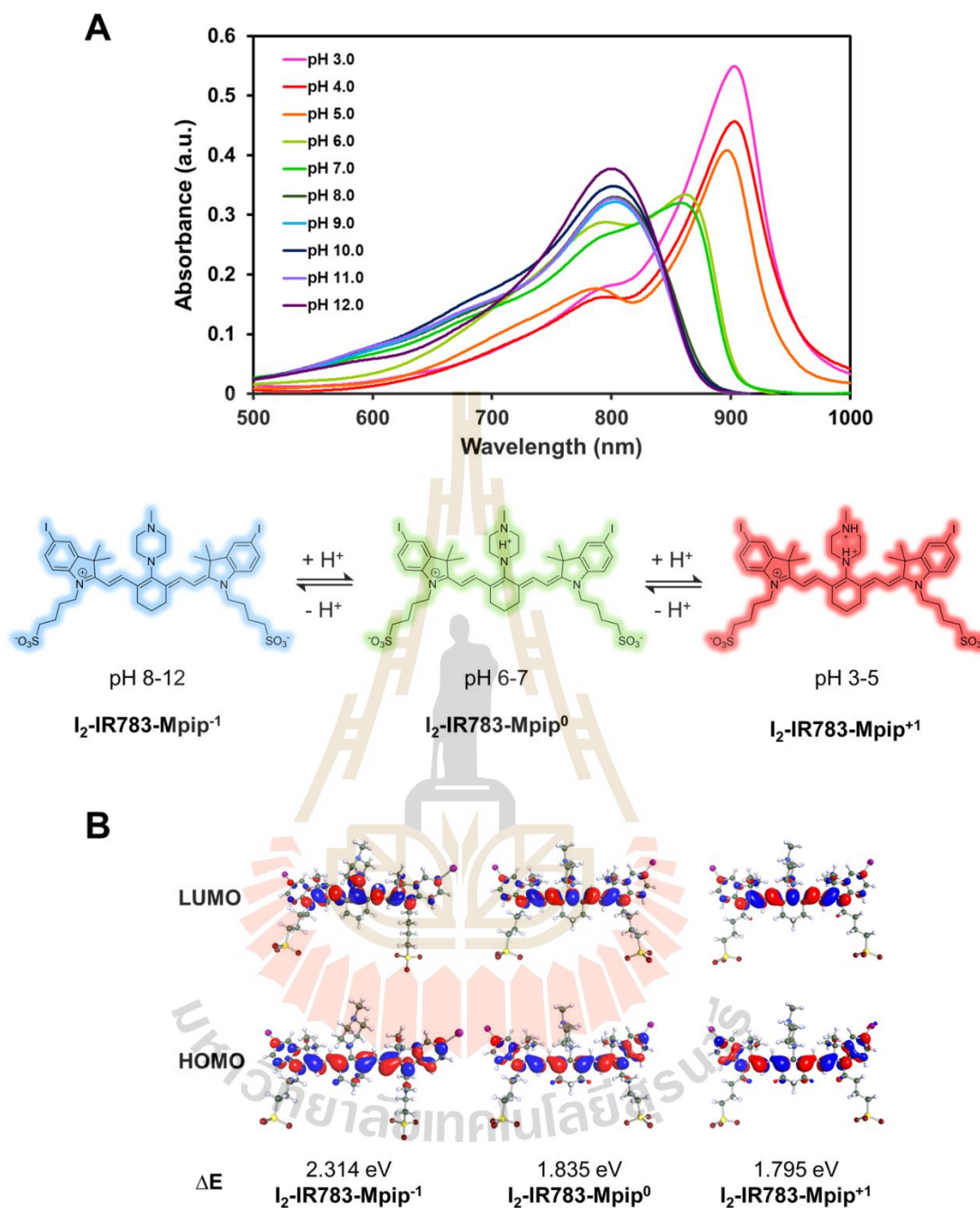


**Figure 4.1** (A) Vis-NIR spectra of  $\text{I}_2\text{-IR783-Mpip}$  and suggested structures in different pH ranges (3–12). (B) Equilibrium structures of  $\text{I}_2\text{-IR783-Mpip}^{-1}$ ,  $\text{I}_2\text{-IR783-Mpip}^0$ , and  $\text{I}_2\text{-IR783-Mpip}^{+1}$  were obtained from DFT/6-311 G geometry optimizations in the COSMO phase, dielectric environment 78. The values of the HOMO and LUMO isosurfaces are 0.025.

Quantum chemical calculations based on the density functional theory (DFT) approach were used in the COSMO phase, dielectric environment 78, to acquire essential information on the effect of pH and charge states of **I<sub>2</sub>-IR783-Mpip** on the absorption spectra in Figure 4.1A Figure 4.1B shows the electronic ground state equilibrium structures of the deprotonated and protonated forms of **I<sub>2</sub>-IR783-Mpip<sup>n</sup>** (n = 1, 0, and +1) using the TURBOMOLE software tool (Suwannakham, Chaiwongwattana, and Sagarik, 2018). The HOMO and LUMO molecular orbitals of **I<sub>2</sub>-IR783-Mpip<sup>1</sup>**, **I<sub>2</sub>-IR783-Mpip<sup>0</sup>**, and **I<sub>2</sub>-IR783-Mpip<sup>+1</sup>**, hypothetical species that existed in solutions with pH varying from 3–12, were shown in the DFT/6-311 G frontier molecular orbital. The HOMO and LUMO modifications in all three structures demonstrated that after excitation, electron density on iodinated-indole rings was dispersed to the IR783 backbone. Additionally, when the total structural charge increased, the localized electron on the iodinated-indole ring on the HOMO became more prominent, implying that there is a stronger charge transfer to the IR783 core in acidic conditions. As a result of the increased electron distribution from **I<sub>2</sub>-IR783-Mpip<sup>-1</sup>** to **I<sub>2</sub>-IR783-Mpip<sup>+1</sup>**, the energy gap between them shrinks to 0.519 eV, causing the absorption spectra in acidic solutions to red-shift. Additionally, a structure with a balanced charge, **I<sub>2</sub>-IR783-Mpip<sup>0</sup>**, was postulated as an existent form in solution pH 6–7, where the absorbance spectra were exhibited in the middle (Figure 4.1A), as confirmed by a reduced energy gap of 0.479 eV. In addition, the calculated energies of **I<sub>2</sub>-IR783-Mpip<sup>0</sup>** with different protonated sites of N-substituted piperazine suggested that proton could possibly add to either nitrogen atom in the piperazine ring, since the total energies of the two protonated forms are not significantly different (Figure 4.2).

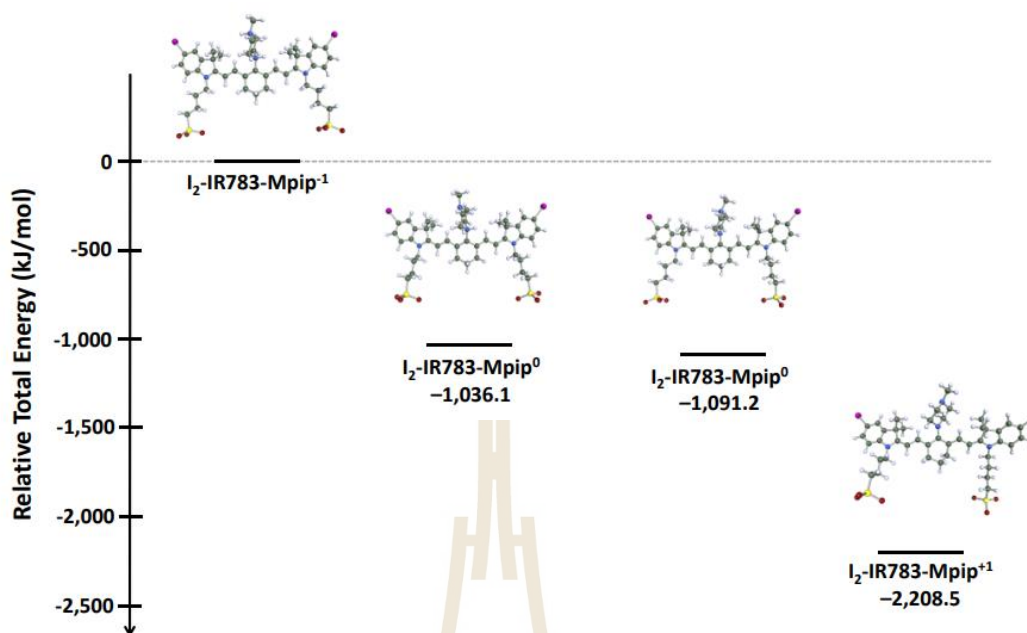


**Figure 4.2** The relative total energy of possible structures of  $I_2$ -IR783-Mpip<sup>0</sup> (2 forms) and  $I_2$ -IR783-Mpip<sup>+1</sup> compared to  $I_2$ -IR783-Mpip<sup>-1</sup> obtained from DFT/6-311G geometry optimizations in the COSMO phase, dielectric environment 78.

To activate the molecules in neutral and acidic environments,  $I_2$ -IR783-Mpip was excited at 850 nm, which has the lowest background signal (Sandell, and Zhu, 2011; Smith, Mancini, and Nie, 2009), to target the tumor microenvironment. Strong emission intensities were only shown from the solution with a pH of less than 7.0, as expected (Figure 4.3A). These results indicated that  $I_2$ -IR783-Mpip could be selectively detected at different pH. In basic conditions, the solutions turned blue, whereas, in acidic environments (pH 6.0), the solutions gradually turned green, with the color varying depending on the optical absorption peaks in the Vis-NIR absorbance spectra (Figure 4.3B). Furthermore, in both acidic and basic conditions, our probe exhibited reversible optical responses. When an aqueous solution of HCl was added to an alcoholic solution of  $I_2$ -IR783-Mpip, protonation occurred at the two nitrogen atoms of N-methylpiperazine, resulting in a reduction of the two nitrogen atoms' electron-donating ability, causing a redshift of the absorption spectra to around 900 nm, turning the solution green. A few drops of aqueous NaOH, on the other hand, caused the



protonated solution to revert to the blue color of the deprotonated form. These results suggest that **I<sub>2</sub>-IR783-Mpip** could be used as a color pH probe that is reversible.

Because spectra redshifted after protonation, <sup>1</sup>O<sub>2</sub> production of **I<sub>2</sub>-IR783-Mpip** when activated by a NIR LED lamp was examined under various conditions. The <sup>1</sup>O<sub>2</sub> created by the light-triggered reaction was detected using a singlet oxygen sensor green (SOSG). After 60 minutes of NIR light (850 nm, 30 mW/cm<sup>2</sup>) irradiation of **I<sub>2</sub>-IR783-Mpip** in buffer solutions pH 5.0, pH 7.0, and pH 9.0, SOSG emission intensities (at 510 nm) increased significantly in the acidic solution containing **I<sub>2</sub>-IR783-Mpip** (Figure 4.3D). The results revealed that when **I<sub>2</sub>-IR783-Mpip** was in an acidic environment (pH 5.0), <sup>1</sup>O<sub>2</sub> was produced over time, whereas in neutral and basic environments, significantly less <sup>1</sup>O<sub>2</sub> was produced. Furthermore, when compared to methylene blue, singlet oxygen quantum yield ( $\Phi_{\Delta}$ ) of **I<sub>2</sub>-IR783-Mpip** under 850-nm excitation was reported to be 0.12 and 0.10 in buffer pH 5.0 and 7.0, respectively (Figure 4.4). As a result, because tumor environs are typically acidic, our pH probe can be used to target cancer. Furthermore, by producing <sup>1</sup>O<sub>2</sub> only when exposed to NIR light at 850 nm, this probe could be harmful to tumor cells.



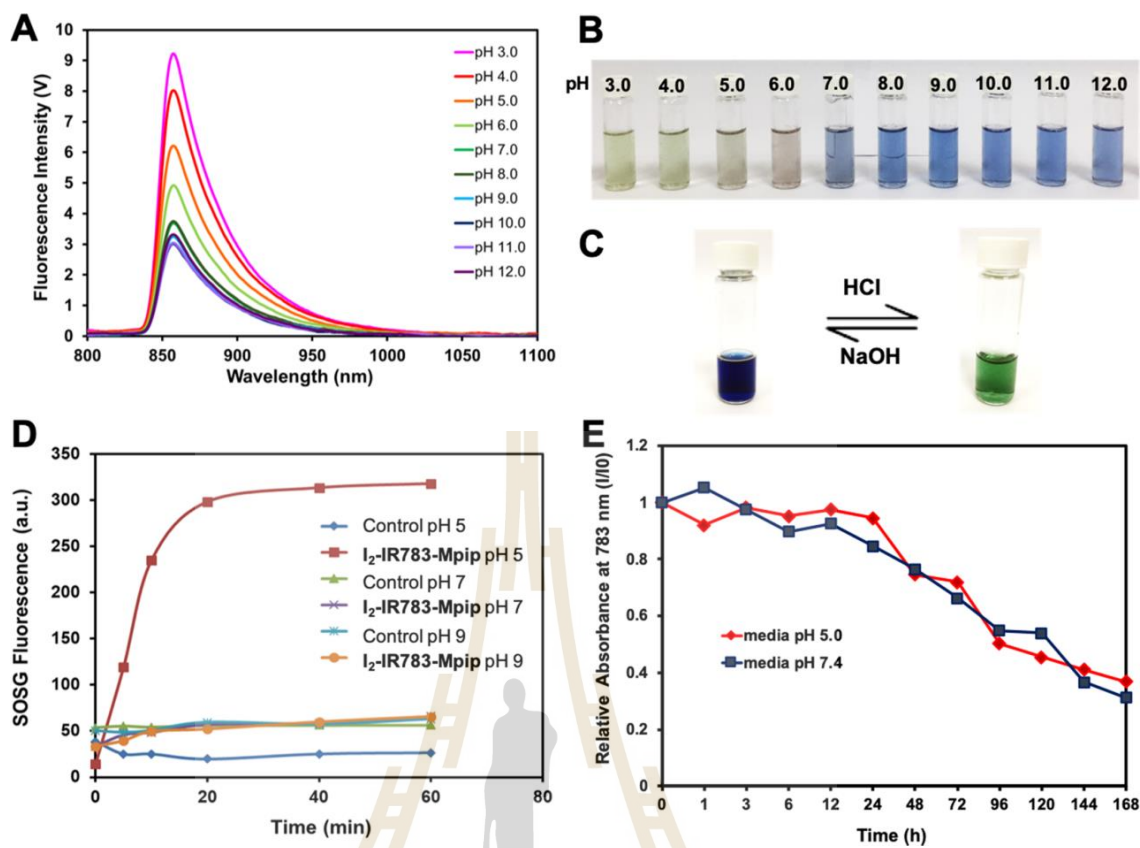
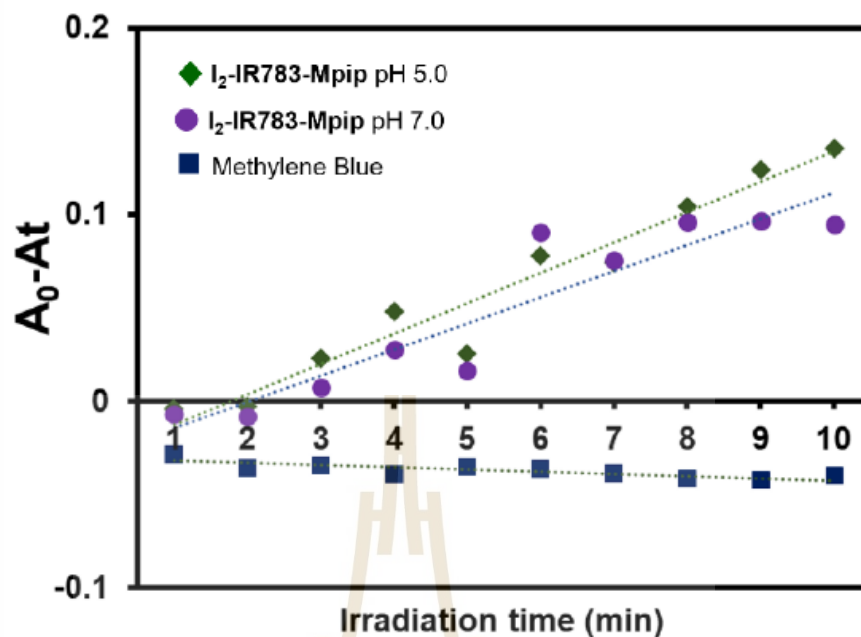


Figure 4.3  $I_2$ -IR783-Mpip optical characteristics. (A) Fluorescent spectra of  $I_2$ -IR783-Mpip in various pH (3.0–12.0) solutions under excitation at  $\lambda$  850 nm. (B) Solutions of  $I_2$ -IR783-Mpip at various pH (3.0–12.0). (C) Reversible color changes of  $I_2$ -IR783-Mpip in methanol solution. (D) Singlet oxygen generation of  $I_2$ -IR783-Mpip upon irradiation with 850 nm lamp up to 60 min. (E) Stability tests of  $I_2$ -IR783-Mpip in cell culture media pH 5.0 (red line) and pH 7.4 (blue line) at 37 °C for up to 7 days.

Before going on to *in vitro* investigations, the stability of  $I_2$ -IR783-Mpip was tested for up to 7 days in cell culture conditions with pH 5.0 and pH 7.4 at 37 °C (Figure 4.3E).  $I_2$ -IR783-Mpip was shown to be stable for 24 hours under these conditions, and the NIR absorptions steadily reduced from day 2 to day 7.



**Figure 4.4** Assay for singlet oxygen ( $^1O_2$ ) formation based on a change in DPBF (1,3-diphenylisobenzofuran; applied in situ) absorbance at 418 nm.

In both cell culture conditions,  $I_2$ -IR783-Mpip showed a similar stability profile. In addition, to confirm the influence of the pH of the cell culture media, a cell viability experiment of HepG2, a human liver cancer cell line, was performed. HepG2 cells were observed to sustain full viability after being exposed to media pH 5.0 for up to 12 h. After 24 to 36 h incubation with media pH 5.0, the cells remained at about 70% viability (Figure 4.5). This showed that prolonged exposure to pH 5.0 media had an impact on cell viability.

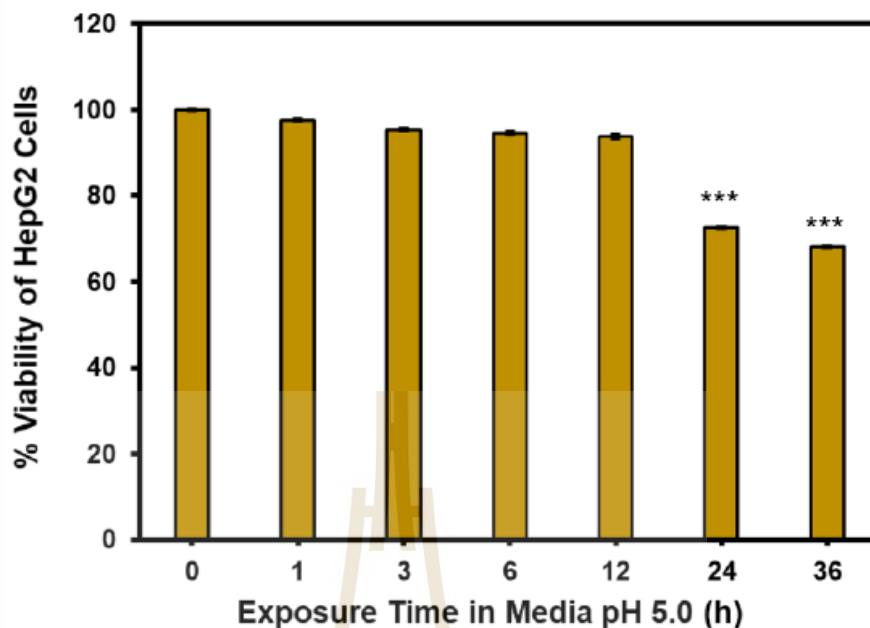


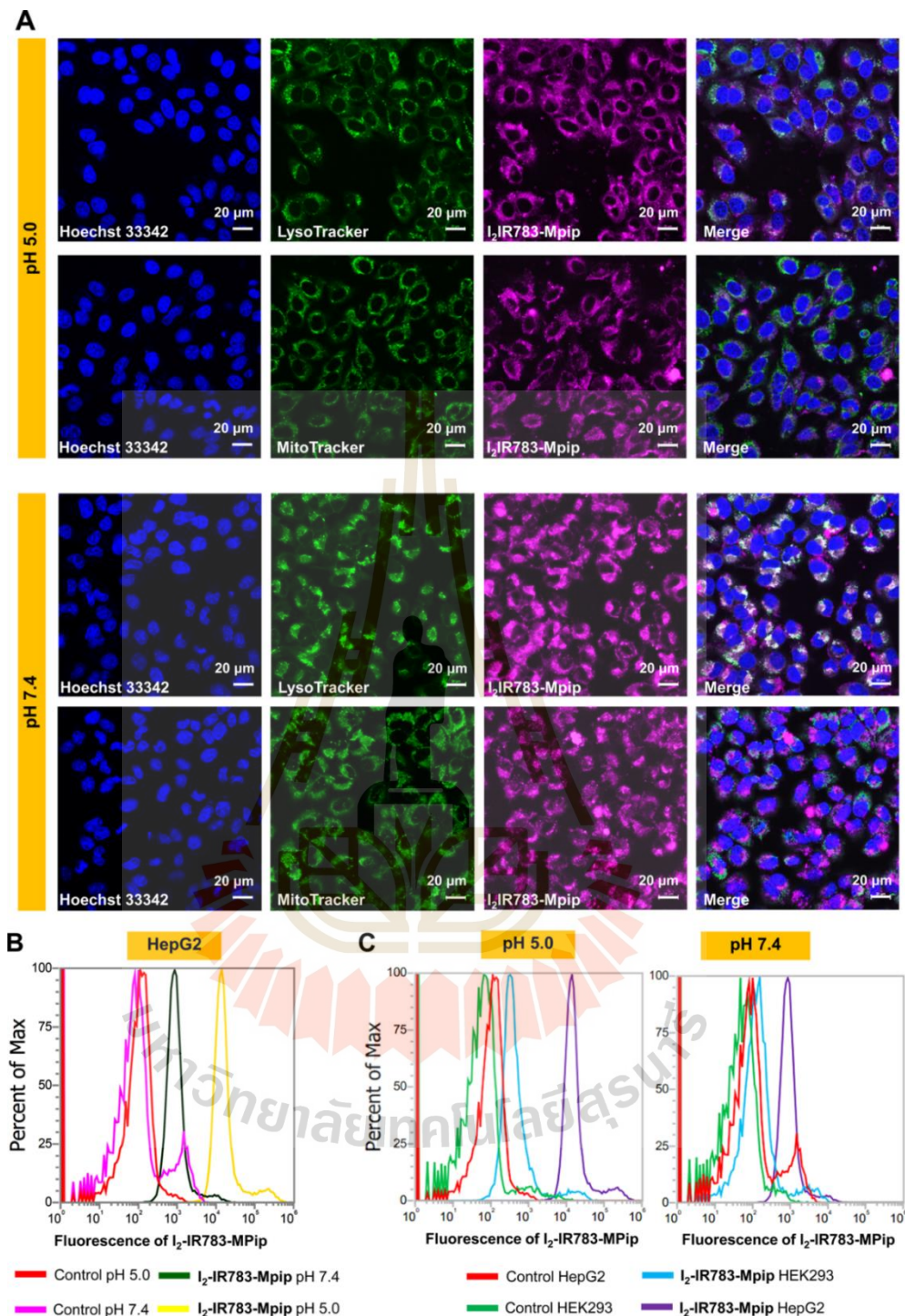
**Figure 4.5** Relative cell viability of HepG2 cells after 0-36 hours of exposure to DMEM medium pH 5.0 supplemented with 5% FBS. Statistical analysis are based on Student's t-test (\*P < 0.05, \*\*P < 0.01, \*\*\*P < 0.001).

#### 4.1.2 Cell internalization of I<sub>2</sub>-IR783-Mpip

To confirm the use of I<sub>2</sub>-IR783-Mpip in cancer cell treatment, *in vitro* tests were carried out. Internalization and colocalization tests in HepG2 cells were used to identify favored organelles for I<sub>2</sub>-IR783-Mpip accumulation. I<sub>2</sub>-IR783-Mpip was internalized into HepG2 and colocalized with MitoTracker Green to some extent (Pearson's R value = 0.31 in pH 5.0 and 0.45 in pH 7.4) and considerably more with LysoTracker green (Pearson's R value = 0.68 in pH 5.0 and 0.68 in pH 7.4, Figure 4.6A and 4.7). These results showed that the probe accumulated largely in lysosomes and less in mitochondria, which is advantageous for the photosensitizer that can be triggered at acidic pH, as the lysosomal pH<sub>lys</sub> in cancer cells is around 3.8–4.74. I<sub>2</sub>-IR783-Mpip could be transported by OATP membrane proteins at physiological pH (Thakkar, Lockhart, and Lee, 2015). However, in an acidic environment (pH 3–5), the molecular structure of I<sub>2</sub>-IR783-Mpip is displayed as positive charges (+1), suggesting that the dye's preferred absorption mechanism at pH 5.0 could be active transport, such as ATP-

driven transport, instead of OATPs. Furthermore, the absorption process of some cyanine derivatives, such as IR783, has been linked to micropinocytosis (Usama, Lin, and Burgess, 2018; Lin and Alexander-Katz, 2013).

Moreover, time-dependent internalization of **I<sub>2</sub>-IR783-Mpip** in cancer cells (HepG2) was tested in both pH 5.0 and 7.4 culture media. Within the first 12 hours of incubation in both culture media, confocal pictures demonstrated that **I<sub>2</sub>-IR783-Mpip** uptake in HepG2 cells increased significantly (Figure 4.8). Following that, flow cytometry was used to perform a quantitative cell internalization investigation of **I<sub>2</sub>-IR783-Mpip** in cancer cells and normal cells to investigate tumor selectivity. The absorption of **I<sub>2</sub>-IR783-Mpip** by HepG2 cells was significantly higher in media pH 5.0 than in media pH 7.4 at various pH (Figure 4.6B). In both medium conditions, the absorption of **I<sub>2</sub>-IR783-Mpip** in normal cells (Human embryonic kidney 293 cells, HEK293) was significantly lower than that in HepG2 cells at a concentration of 15  $\mu$ M and a 12 h incubation (pH 5.0 and pH 7.4, Figure 4.6C). As a result, **I<sub>2</sub>-IR783-Mpip** could be a cancer-targeted agent with the ability to selectively kill cancer cells via PDT.



cytometry of HepG2 and HEK293 cells incubated with 15  $\mu\text{M}$  of  $\text{I}_2\text{-IR783-Mpip}$  for 12 h in culture media pH 5.0 and 7.4. Scale bars = 20  $\mu\text{m}$ .

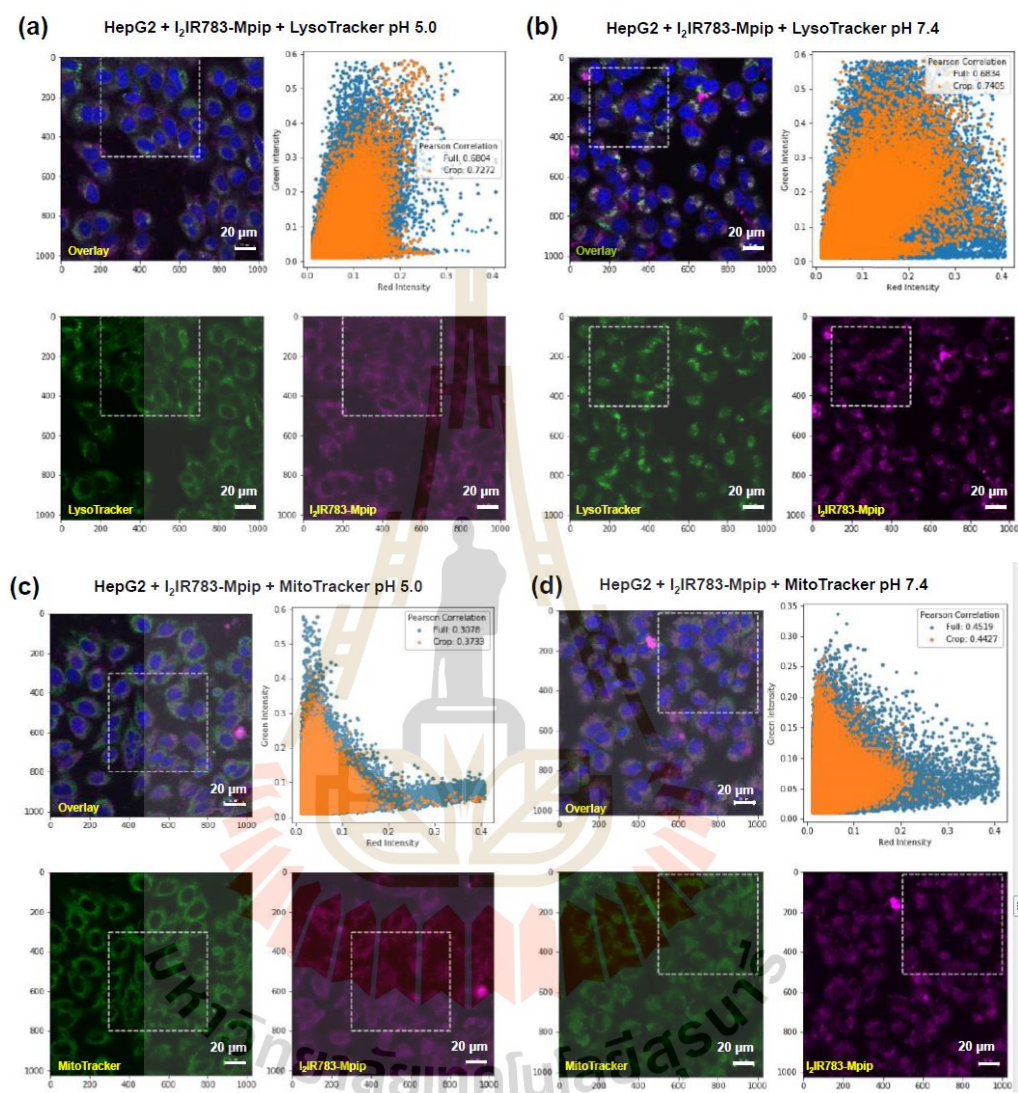
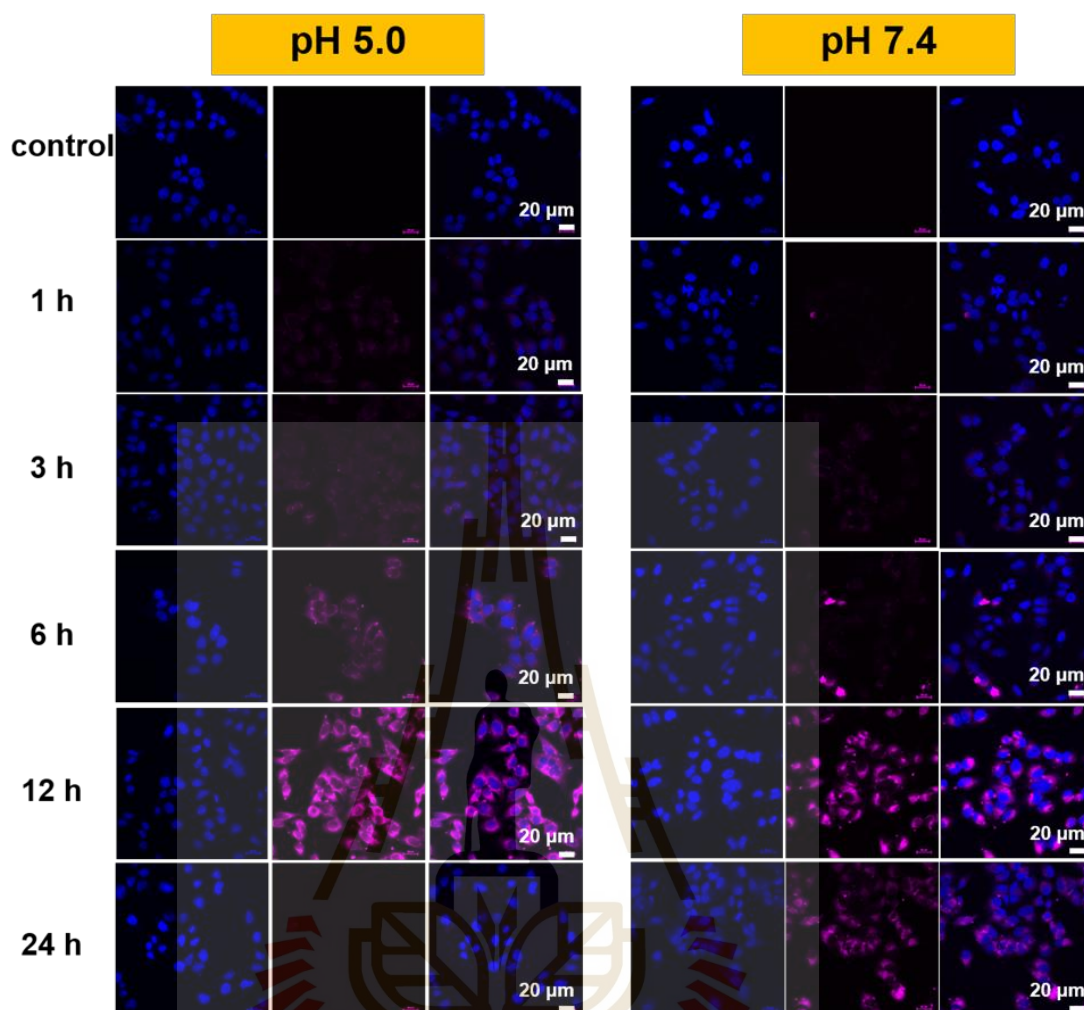


Figure 4.7 LysoTracker in media pH 5.0 (a) and pH 7.4 (b) and MitoTracker Green in media pH 5.0 (c) and pH 7.4 (d) were used to analyze organelle colocalization in  $\text{I}_2\text{-IR783-Mpip}$ .



**Figure 4.8** Cellular uptake was time-dependent in both pH 5.0 and pH 7.4 solutions. Confocal pictures of HepG2 cells after incubation with I<sub>2</sub>-IR783-Mpip (30 μM) at various time periods (1, 3, 6, 12, 24 h). The fluorescent signal of I<sub>2</sub>-IR783-Mpip is presented in purple, while the DAPI nucleus co-staining signal was shown in blue. Scale bars = 20 μm.



### 4.1.3 Photodynamic therapy

In general, PDT agents should be relatively innocuous in the dark, but highly harmful once exposed to specific light. HepG2 cells were incubated with various concentrations of **I<sub>2</sub>-IR783-Mpip** for 6 hours in both pH 5.0 and pH 7.4 media, exposed to 850 nm LED light (30 mW/cm<sup>2</sup>) for 30 minutes, and then re-incubated in the dark for an additional 12 h to investigate photocytotoxicity. In both culture media conditions, relative viabilities of cells when exposed to 850 nm light were shown to be inversely proportioned to **I<sub>2</sub>-IR783-Mpip** concentrations. Even at high concentrations up to 50 μM, no appreciable dark cytotoxicity of **I<sub>2</sub>-IR783-Mpip** was seen in both culture media in a cell viability assay (pH 5.0 and pH 7.4, Figure 4.9A and B). Normal cells HEK293 treated with **I<sub>2</sub>-IR783-Mpip**, on the other hand, maintained viability in both culture conditions after 850 nm light exposure for 30 minutes (Figure 4.10), showing that **I<sub>2</sub>-IR783-Mpip** was only hazardous to cancer cells after irradiation.

A piece of 5 mm pork tissue was inserted between the cells and the light source to investigate whether the NIR-absorbed **I<sub>2</sub>-IR783-Mpip** could be triggered in deep-seated tumor cells. HepG2 cell viability reduced in a dose-dependent pattern after exposure to light (Figure 4.9A and B), which was identical to the results obtained when the cells were not covered with pork tissue. When **I<sub>2</sub>-IR783-Mpip** was irradiated with 850 nm LED light for 30 minutes in both physiological and slightly acidic conditions, these findings strongly showed that it could selectively eliminate deep-seated cancer cells.

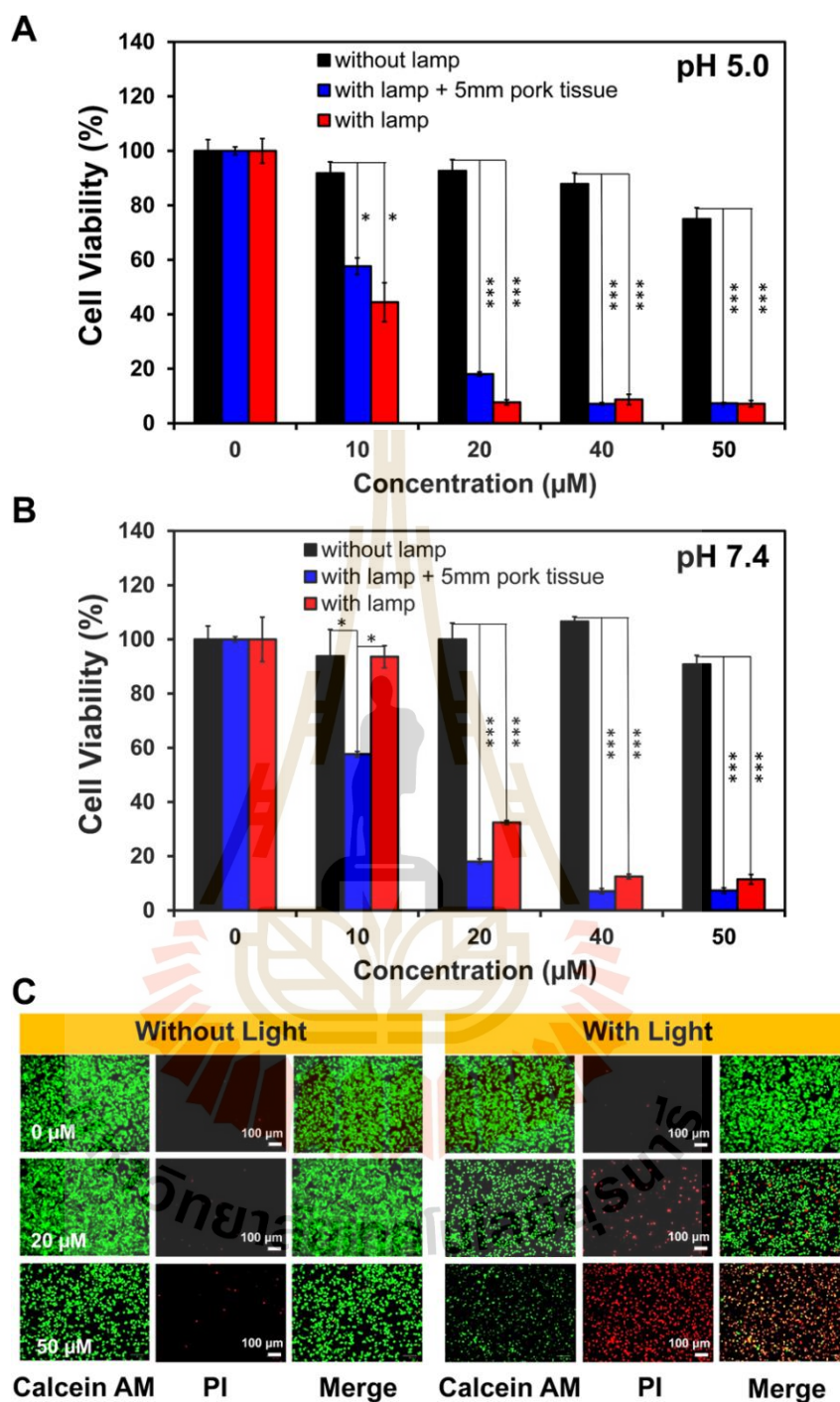


**Figure 4.9** Photodynamic therapy effect of  $I_2$ -IR783-Mpip. Relative viabilities of HepG2 cells in media (A) pH 5.0 and (B) pH 7.4; red bars represent cells irradiated with 850 lamp, blue bars represent cells covered by 5 mm pork tissue with 850 nm light irradiation and black bars represent cells without irradiation. (C) Fluorescence pictures of HepG2 cells after 6 h of incubation with  $I_2$ -IR783-Mpip at concentrations of 20 and 50  $\mu$ M in DMEM pH 5.0 with and without light (850nm). Calcein AM and PI were used

to stain live and dead cells, as shown in the photos in green and red, respectively. Scale bars = 100  $\mu\text{m}$ . One-way ANOVA is used in the statistical analysis, followed by Tukey's posthoc analysis (\* $P < 0.05$ , \*\* $P < 0.01$ , \*\*\* $P < 0.001$ ).

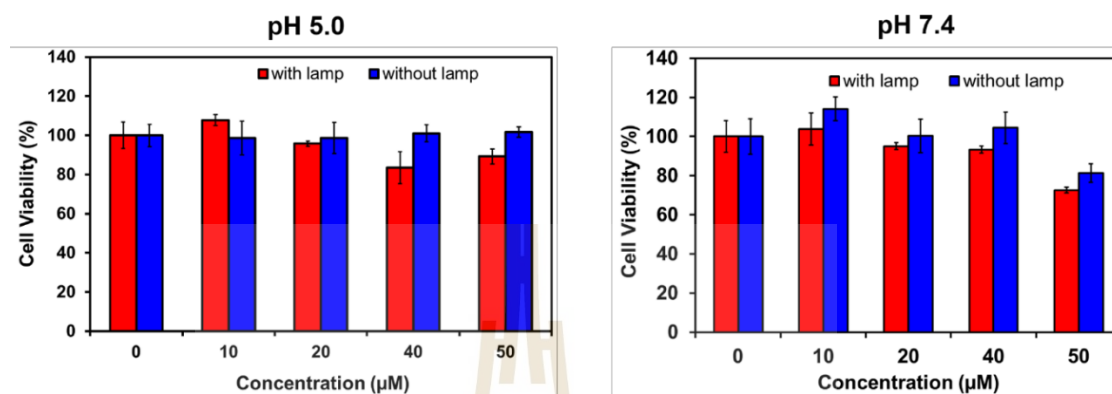


**Figure 4.10** Relative cell viabilities of HEK-293 cells after incubation with  $\text{I}_2\text{-IR783-Mpip}$  at various concentrations (0 – 50  $\mu\text{M}$ ) at pH 5.0 and pH 7.4 for 6 h and with and without being exposed to 850 nm lamp (light intensity 30  $\text{mW}/\text{cm}^2$ ) for 30 min.

A LIVE/DEAD viability/cytotoxicity assay was used to confirm the efficiency of  $\text{I}_2\text{-IR783-Mpip}$  in terminating cancer cells under light irradiation. HepG2 cells were seeded in a 6-well plate and incubated for 24 hours before adding  $\text{I}_2\text{-IR783-Mpip}$  at 20 and 50  $\mu\text{M}$  and re-incubating for another 6 h. The cells were then stained with calcein AM and propidium iodide (PI) after being exposed to 850 nm light for 30 minutes. Calcein AM can easily enter the live cells and emit a bright green fluorescence after being activated with a 495 nm laser, whereas PI can easily enter the dead cells, bind to DNA by intercalating between the bases, and emit a bright red fluorescence after being activated with a 535 nm laser. Increased red fluorescence was shown with an increasing proportion of  $\text{I}_2\text{-IR783-Mpip}$  incubated in cells following irradiation with 850 nm light using an inverted fluorescence microscope, showing that more dead cell populations appeared when the dose of  $\text{I}_2\text{-IR783-Mpip}$  was increased. The efficiency of photodynamic cancer cell ablation produced by  $\text{I}_2\text{-IR783-Mpip}$  in the medium at pH 5.0 (Figure 4.9C) and pH 7.4 (Figure 4.11) was validated by fluorescence from Calcein AM and PI co-stained cells.

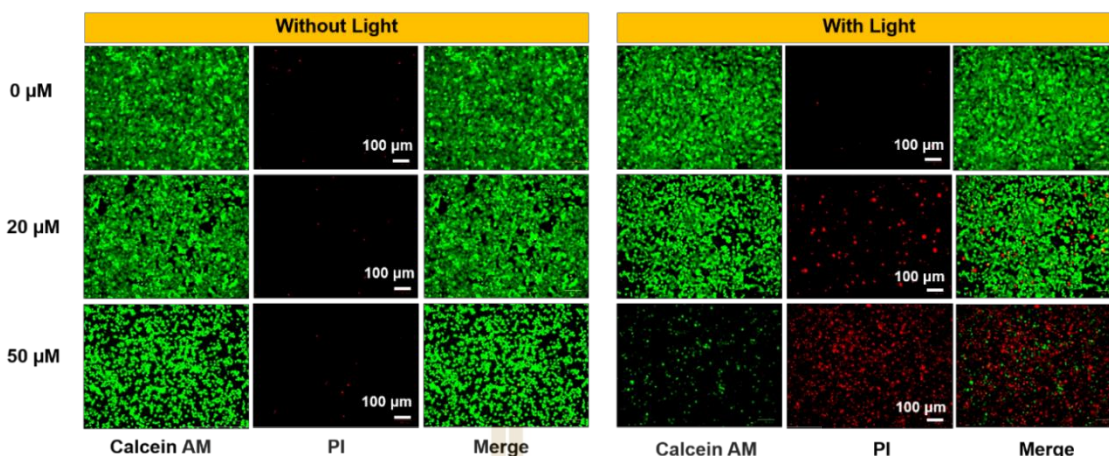


**Figure 4.11** Fluorescence pictures of HepG2 cells after 6 h of incubation with  $I_2$ -IR783-Mpip at concentrations of 20 and 50  $\mu\text{M}$  in DMEM pH 7.4 with and without light (850 nm). Calcein AM and PI were used to stain live and dead cells, as shown in the photos in green and red, respectively. Scale bars = 100  $\mu\text{m}$ .

After irradiation with 850 nm light, intracellular reactive oxygen species (ROS) production was observed in the cell culture carrying  $I_2$ -IR783-Mpip. In both media (pH 5.0 and 7.4), HepG2 cells were treated with  $I_2$ -IR783-Mpip for 6 h, stained with 2,7-dichloro-dihydro-fluorescein diacetate (DCFH-DA), and then exposed to 850 nm light for 20 min. Intracellular ROS can oxidize DCFH-DA to generate 2,7-dichloro-dihydro-fluorescein (DCF). Fluorescence confocal microscopy with 488 nm excitation produces a strong green fluorescence, which can be used to detect intracellular DCF. The generation of DCF was greatly increased in the presence of light exposure and  $I_2$ -IR783-Mpip in both culture media, but mostly in the pH 5.0 media than in the pH 7.4 media, according to the confocal pictures (Figure 4.12). Additionally, a more acidic condition could generate a higher amount of green fluorescence (Figure 4.13).

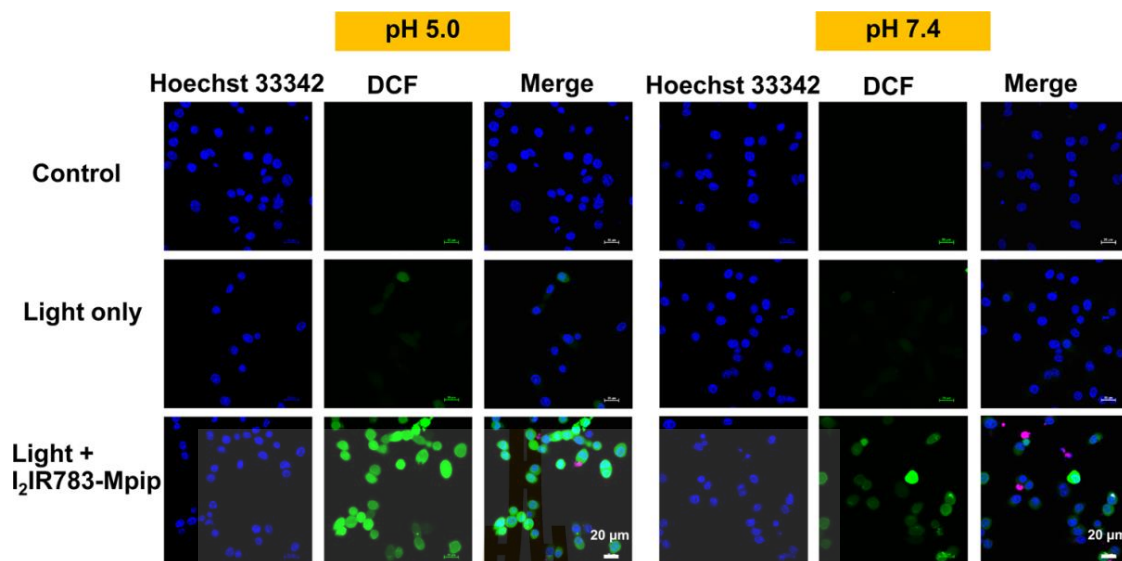


Figure 4.12 The DCFDA cellular ROS detection assay was used to detect intracellular reactive oxygen species produced by  $I_2$ -IR783-Mpip (20  $\mu$ M) in HepG2 cells at pH 5.0 and 7.4. Scale bars = 20  $\mu$ m.

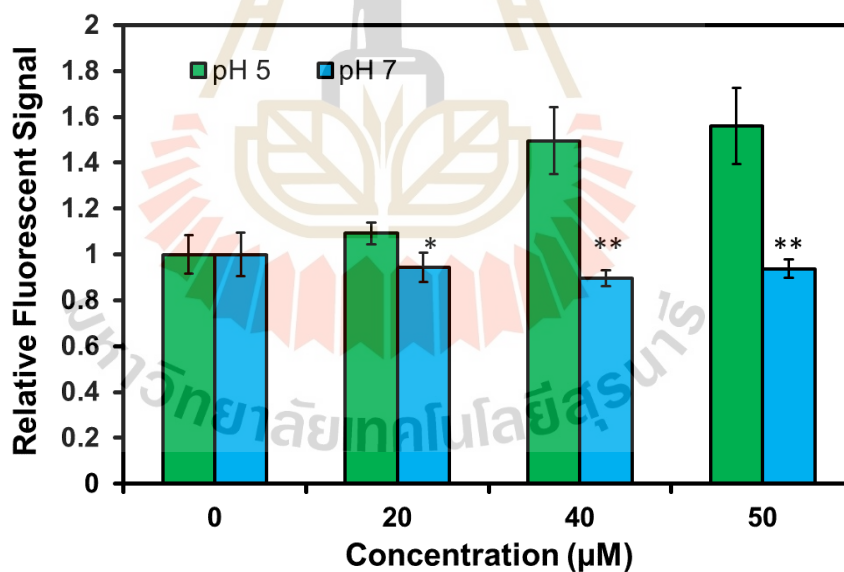


Figure 4.13 DCF relative fluorescence signal in HepG2 cells after 6 h of incubation with  $I_2$ -IR783-Mpip at various concentrations (0–50  $\mu$ M) at pH 5.0 and pH 7.4 and 30 min of exposure to an 850 nm lamp (light intensity 30 mW/cm<sup>2</sup>). The Student's two-tailed t-test was used for statistical analysis. (\*P < 0.05, \*\*P < 0.01, \*\*\*P < 0.001).

## 4.2 Target: Cyclooxygenase enzyme that overexpressed on tumor cells

### 4.2.1 Photophysical properties

The absorbance and fluorescence spectra of **Cy820** and **Cy820-IMC** are identical. (Figure 4.14A and Table 4.1). Both probes exhibit maximum absorption around 820 nm in DMSO and PBS, while emission spectra are more red-shifted in DMSO ( $\lambda_{\text{max}} \sim 860$  nm, with fluorescent quantum yield  $\sim 0.2$ ) than the solution in PBS ( $\lambda_{\text{max}} \sim 850$  nm, with fluorescent quantum yield  $\sim 0.1$ ). Moreover, the singlet oxygen generation efficiency of **Cy820** and **Cy820-IMC** was investigated for photodynamic therapy application. Singlet oxygen quantum yield was monitored through the decreasing of absorbance of 1,3-diphenylisobenzofuran (DPBF), a singlet oxygen ( $^1\text{O}_2$ ) scavenger. After **Cy820** and **Cy820-IMC** were exposed to 780 nm light,  $^1\text{O}_2$  was produced within a few minutes in an irradiation time-dependent manner as appeared in the declining of DPBF absorbance at 408 nm (Figure 4.14B). Additionally, **Cy820** and **Cy820-IMC** can generate  $^1\text{O}_2$  at a faster rate than that of indocyanine green (ICG, standard photosensitizer). The singlet oxygen quantum yield ( $\Phi_{\Delta}$ ) of **Cy820** and **Cy820-IMC** was calculated to be 0.20 and 0.12, respectively, relative to ICG.

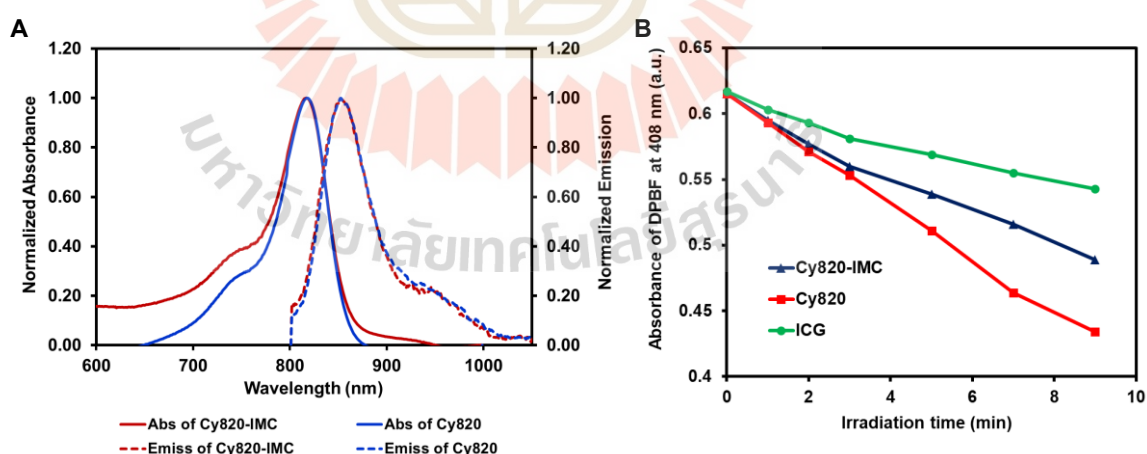


Figure 4.14 (A) UV-vis-NIR absorption and fluorescent spectra of **Cy820-IMC** and **Cy820** in PBS. (B) Singlet oxygen generation of **Cy820-IMC** and **Cy820** in PBS compared to standard (ICG).

**Table 4.1** Photophysical properties of **Cy820-IMC** and **Cy820**

Compound	Solvent	$\lambda_{\max}$ (nm)	$\epsilon$ ( $M^{-1}cm^{-1}$ )	$\lambda_{\text{emiss}}^a$ (nm)	$\Delta\lambda$ (nm)	$\Phi_f^b$	$\Phi^c$ ( $^1O_2$ )
<b>Cy820-IMC</b>	DMSO	822	307092	861	39	0.2	0.15
	PBS (3% tween 80)	819	369469	851	32	0.093	0.12
<b>Cy820</b>	DMSO	820	250911	861	41	0.21	0.17
	PBS (3% tween 80)	820	300227	852	32	0.123	0.20

<sup>a</sup> Samples were excited at 780 nm. <sup>b</sup>Relative to ICG in DMSO ( $\Phi_f = 0.13$ ). <sup>c</sup>Relative to ICG in DMSO ( $\Phi_{\Delta} = 0.077$ ). <sup>d</sup>PBS containing 3% tween 80.

#### 4.2.2 Molecular interaction of Cy820-IMC with COX-2 protein

Consequently, molecular docking was performed to study the binding interaction between the **Cy820-IMC** and COX-2 using Auto Dock 4.2 (Figure 4.15A). The cyanine moiety (Cy820 part) is well docked into the hydrophobic pocket surrounding important amino acids. It was found that the **Cy820-IMC** molecule made polar contacts with the COX-2 residues, such as Tyr355, Arg120, Ser119, Glu524, and Ser530, which stabilized the cyanine moiety by H-bond and  $\pi$ -cation interactions. Additionally, the crystal structure of the COX-2 in the complex with indomethacin-butylidiamine-dansyl conjugate (**L7M**, PDB:6bl3) was taken into compared with the docking model (Figure 4.15B). The phenyl ring of the indomethacin in both structures is oriented toward the central binding pocket whereas the dansyl and cyanine moieties are directed towards the proximal binding pocket close to the entrance cavity. This result suggested that **Cy820-IMC** might bind to COX-2 and provide the extra targeted ability to the system.

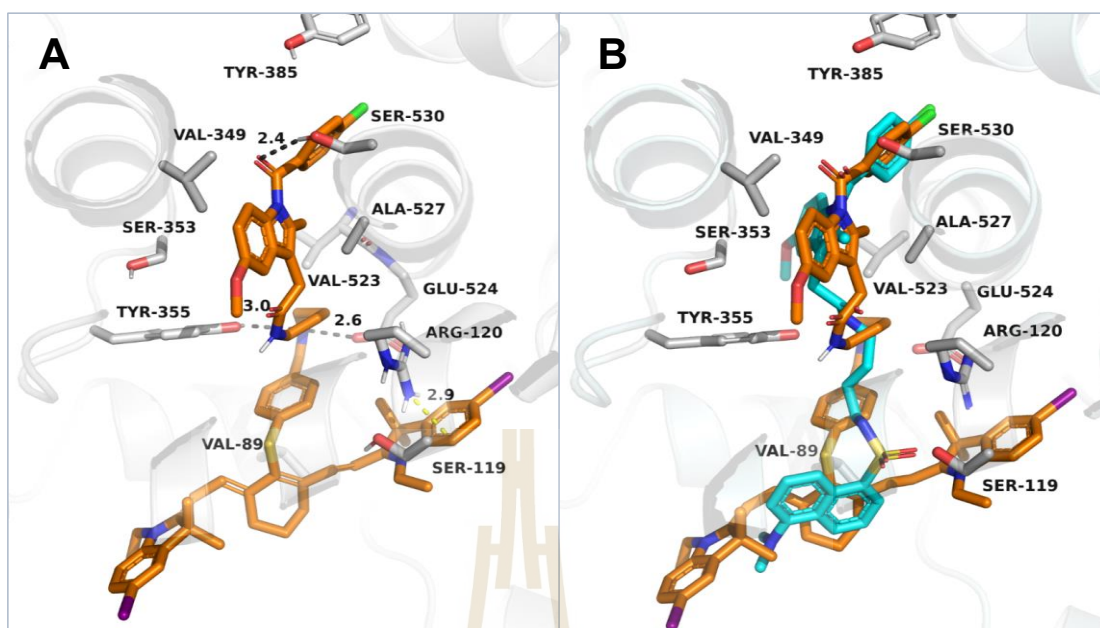


**Figure 4.15** 3D representation of docked **Cy820-IMC** in the robbly region of COX-2 (PDB:6bl3) simulated by AutoDock 4.2. A) The orange stick structure represents **Cy820-IMC**, while the gray sticks show the selected key residues of COX-2 in the binding pocket. The hydrogen bond is highlighted in the black dot. The yellow dotted line indicates  $\pi$ -cation interaction. B) Comparison of the co-crystallized ligand **L7M** (Xu et al., 2019) (cyan color) and the calculated pose for the **Cy820-IMC** (colored by orange) by the docking simulation. (For interpretation of the references to color in this figure legend, the reader is referred to the web version of this article.)

#### 4.2.3 Time-dependent intracellular internalization

We hypothesized that **Cy820** and **Cy820-IMC** could be internalized and accumulated in cancer cells differently due to an extra targeting ligand, indomethacin. Therefore, **Cy820** and **Cy820-IMC** were tested for specific uptake into tumor cells. To determine the best timing for light irradiation in PDT, a time-dependent cellular internalization study was done first. Cancer cells (HepG2) with high COX-2 (Wang et al., 2015) and OATPs levels (Kullak-Ublick, Beuers, and Paumgartner, 1996) and a normal cell (HEK-293) with a low COX-2 media (Pewklang, Chanseanpak, Lai, Noisa, and Kamkaew, 2019) and OATPs levels (Ahlin et al., 2009), were used to investigate the uptake via OATPs and COX-2. As shown in Figure 4.16A and B, after 3 h, NIR fluorescent



signals can be clearly observed from the cancer cells incubated with **Cy820** and **Cy820-IMC**, then the fluorescent signals rise in a time-dependent manner. In contrast, within the first 6 hours, the control cells have essentially non-detectable fluorescence. Quantitative analysis of the uptake at 3 h of **Cy820** and **Cy820-IMC** for both cell lines was performed via flow cytometry (Figure 4.16C). The results also confirm the tumor-specific uptake of these two dyes.

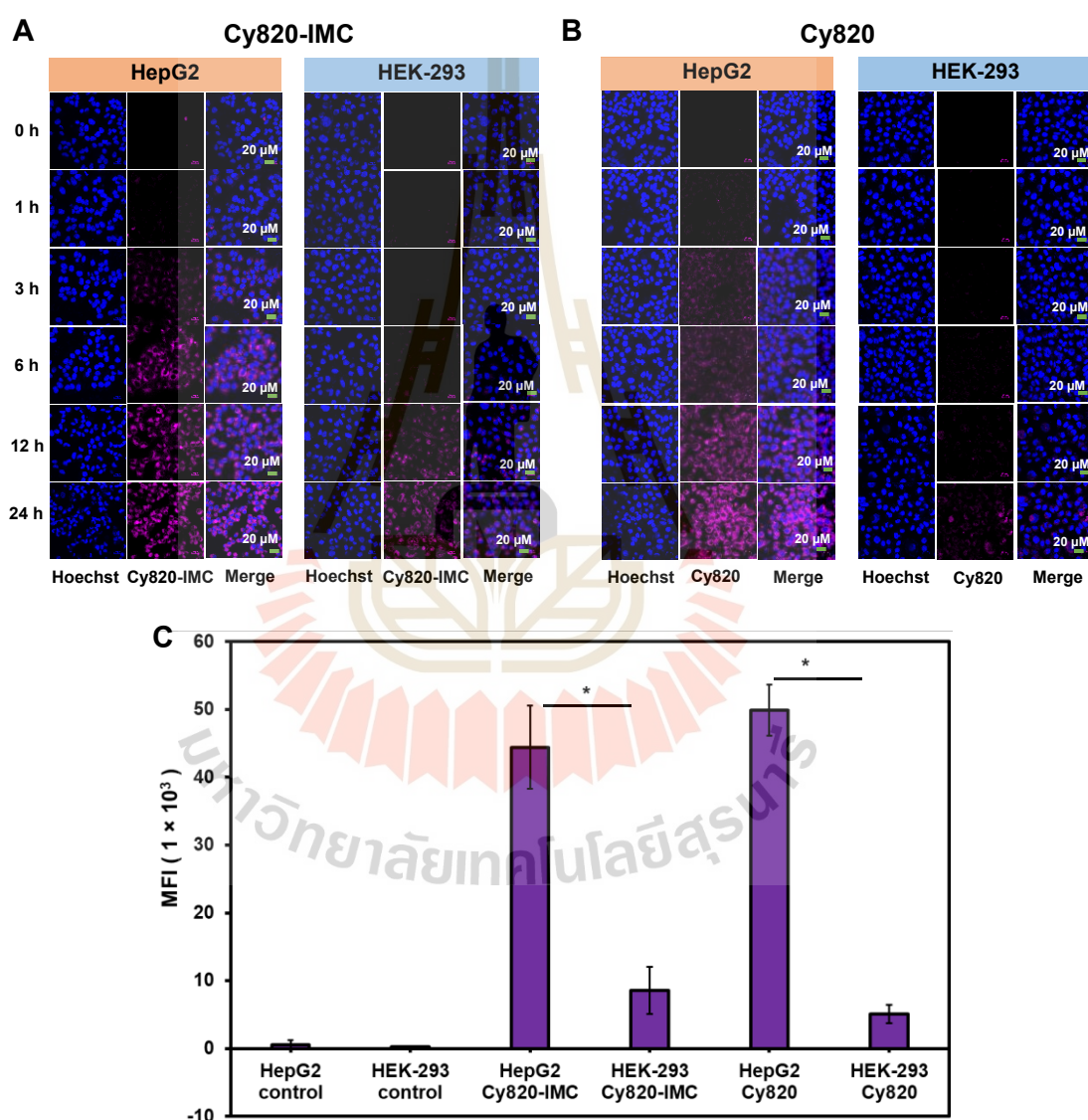


**Figure 4.16** Fluorescence imaging of HepG2 cells and HEK-293 were treated with 5 μM of **Cy820-IMC** (A) and **Cy820** (B) at 0, 1, 3, 6, 12, 24 h. and C) Mean fluorescence intensity (MFI) from flow cytometry of HepG2 cells and HEK-293 cells were treated

with 5  $\mu\text{M}$  of **Cy820-IMC** and **Cy820** for 3 h. data are showed as means  $\pm$  SD (n = 3), \*P < 0.05, \*\*P < 0.01, or \*\*\*P < 0.001 are determined on Student's T-test.

#### 4.2.4 Mechanism of cell internalization

As both dyes are tumor-specific, the uptake mechanism was then investigated. Figure 4.17A&B compare fluorescence uptake by HepG2 cells treated with **Cy820-IMC** and **Cy820** between without and with inhibitor. HepG2 cells were pre-treated with sulfobromophthalein (BSP), an OATPs inhibitor (Usama, Thavornpradit, and Burgess, 2018; Zhang et al., 2018) before treated with **Cy820-IMC** and **Cy820**. Imaging data from Figure 4.17A showed that **Cy820-IMC** and **Cy820** are less uptakes when OATPs was blocked. Moreover, the cell uptake was also quantified by FACS (Figure 4.17B) and the results support the data from confocal imaging. This information suggested that OATPs are the mediator for the internalization of these probes. In addition, the cellular uptake of **Cy820-IMC** and **Cy820** is proved to be energy-dependent as well. As shown in Figure 4.17C, the uptake of both probes is obviously decreased when the incubation temperature was reduced to 4 °C.

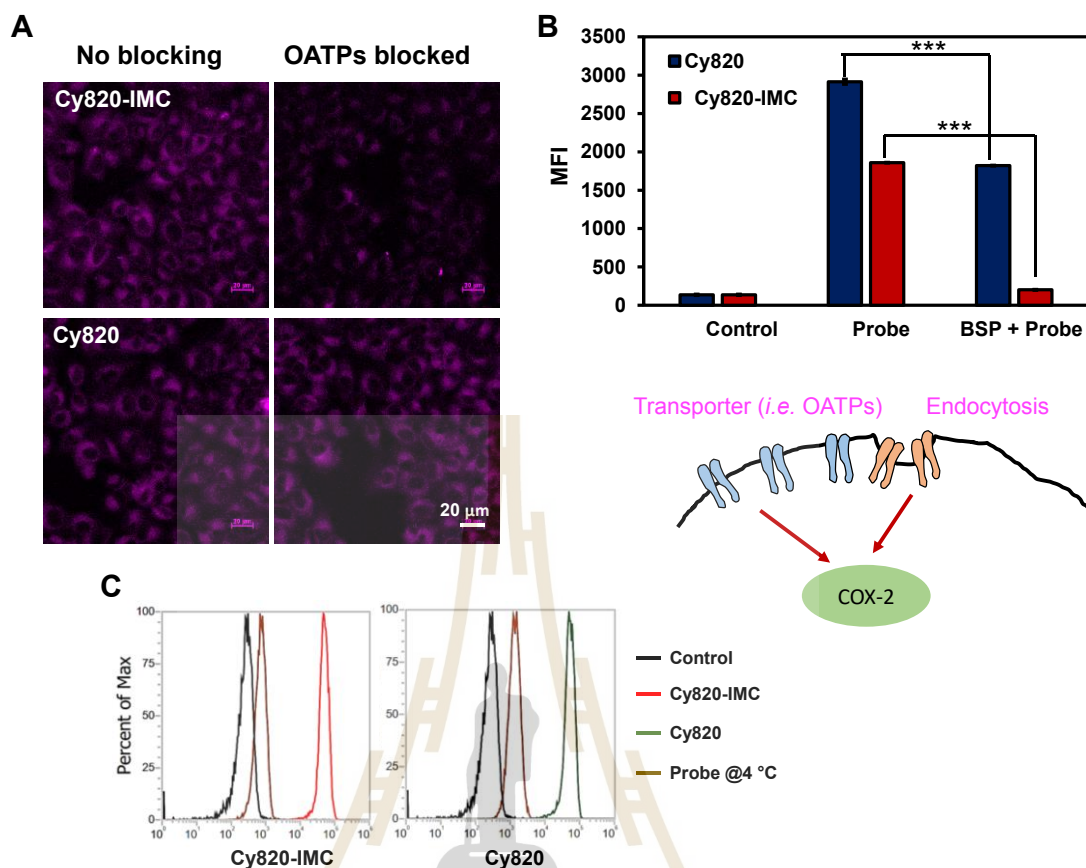


**Figure 4.17** A) confocal imaging of HepG2 cells, B) Mean fluorescence intensity (MFI), and Flow cytometry of HepG2 cells. HepG2 cells were pre-incubated with 250  $\mu$ M of BSP for 10 min and then treated with 5  $\mu$ M of **Cy820-IMC** and **Cy820** for 3 h. C) Flow cytometry of HepG2 cells that were treated with 5  $\mu$ M of **Cy820-IMC** and **Cy820** at 4  $^{\circ}$ C and 37  $^{\circ}$ C for 3 h. data are presented as means  $\pm$  SD (n = 3), \*P < 0.05, \*\*P < 0.01, or \*\*\*P < 0.001 are based on Student's T-test.

Interestingly, when **Cy820-IMC** exposed to the cells that were pre-treated with COX-2 inhibitors (Pewklang, Chansaenpak, Lai, Noisa, and Kamkaew, 2019), aceclofenac and celecoxib for 2 h, significant competitive binding behavior was observed (Figure 4.18A and C). In contrast, **Cy820** in the same condition showed no significant competitive binding behavior due to its structure does not contain indomethacin as part of the structure (Figure 4.18B and D). Therefore, when indomethacin conjugated with **Cy820** that leads to **Cy820-IMC** can be a promising probe that has significantly target COX-2.

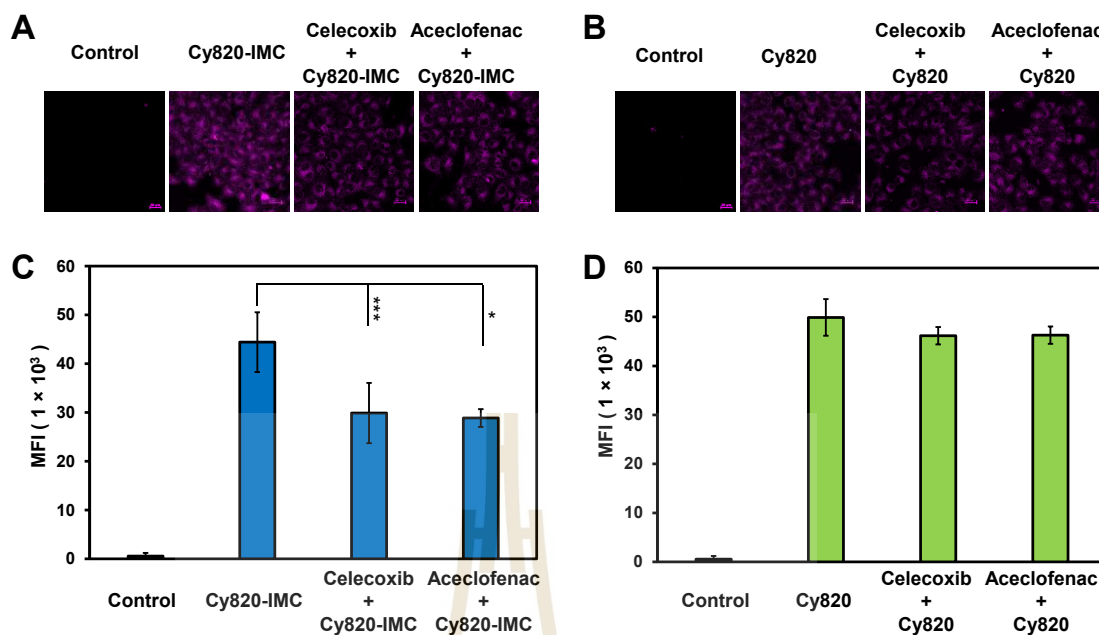


**Figure 4.18** A) and B) Confocal images of COX-2 inhibition. C) and D) Mean Fluorescence intensity (MFI) of HepG2 cells. HepG2 cells were incubated with COX-2 specific inhibitors (aceclofenac and celecoxib, 20  $\mu$ M) for 2 h, then incubated with 5  $\mu$ M of Cy820-IMC and Cy820 for 3 h. data are showed as means  $\pm$  SD (n = 3), \*P < 0.05, \*\*P < 0.01, or \*\*\*P < 0.001 are determined on Student's T-test.

#### 4.2.5 Intracellular localization

Golgi apparatus is an organelle that is a key structure for transporting and secreting some important enzymes which are overexpressed in cancer cells (Zhang et al., 2013). It has been reported that when the stress signaling threshold is exceeded, the Golgi apparatus is actively involved in the initiation and execution of the apoptotic process, which results in COX-2 accumulating in the Golgi apparatus (Wang et al., 2015; Zhang et al., 2013). Therefore, Cy820-IMC fluorescence signals from cancer cells were shown to be co-localized with several organelle trackers (Golgi, mitochondria, lysosomes, and endoplasmic reticulum [ER]) to investigate the dye location inside the cells. It was found that Cy820-IMC colocalized to some degree with Golgi, mitochondria lysosomes, and ER markers in HepG2 cells with Pearson's coefficients of 0.83, 0.80, 0.84, and 0.69, respectively (Figure 4.19). This shows that probe can

be localized inside and internalized cancer cells, and it could indicate that internalization is induced by Cy820-IMC binding.

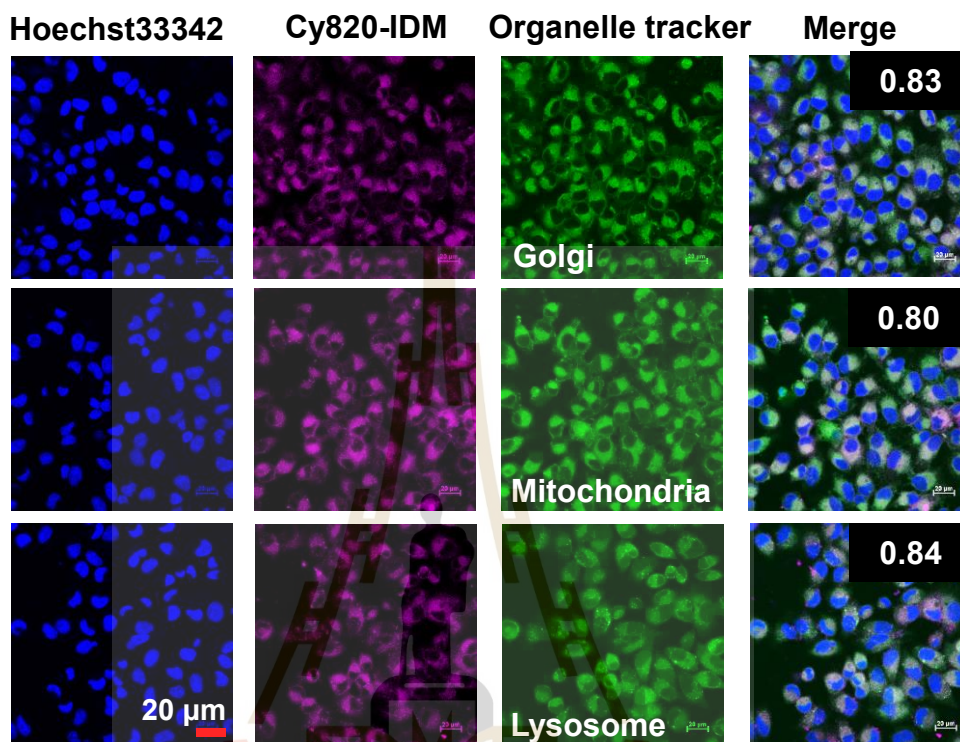


**Figure 4.19** HepG2 cells incubated with 5  $\mu\text{M}$  of Cy820-IMC for 6 h are shown in confocal pictures and colocalization of Cy820-IMC with NBD-C6-ceramide (Pearson's R value =0.83), MitoTracker Green (Pearson's R value =0.80), LysoTracker green (Pearson's R value =0.84) and ER-Tracker Green (Pearson's R value =0.69). Scale bars =20  $\mu\text{m}$ .

#### 4.2.6 Photocytotoxicity

From imaging experiments, it is apparent that Cy820 and Cy820-IMC accumulate in cancer cells. Therefore, a series of photodynamic therapy experiments were performed to ensure the efficiency of the probe. In a photocytotoxicity assay, HepG2 and HEK-293 cells were treated with various doses (0-20  $\mu\text{M}$ ) of Cy820 and Cy820-IMC for 6 h before 30 min light irradiation (780 nm, power density of 2.37  $\text{mW cm}^{-2}$ ) and then cells were then left to grow in the dark for another 24 h. As shown in Figure 4.20A and B, as the dose of Cy820-IMC increased from 1 to 10  $\mu\text{M}$ , the cancer

cell viability reduced considerably in a dose-dependent manner under light illumination, while the cells maintain full viability in the dark state. On the other hand, normal cells (HEK-293) did not show obvious photocytotoxicity until the dose of **Cy820-IMC** was over 5  $\mu\text{M}$  (Figure 4.20C). For the compound without IMC, cancer cell viability was reduced after exposure to **Cy820** at 1.25  $\mu\text{M}$  and gradually decreased as the dose increased under irradiation. However, this compound seemed to be toxic to the cells even without light illumination. However, **Cy820** did not show cytotoxicity to HEK-293 cells in both light and dark states (> 80% viability, Figure 4.20D)

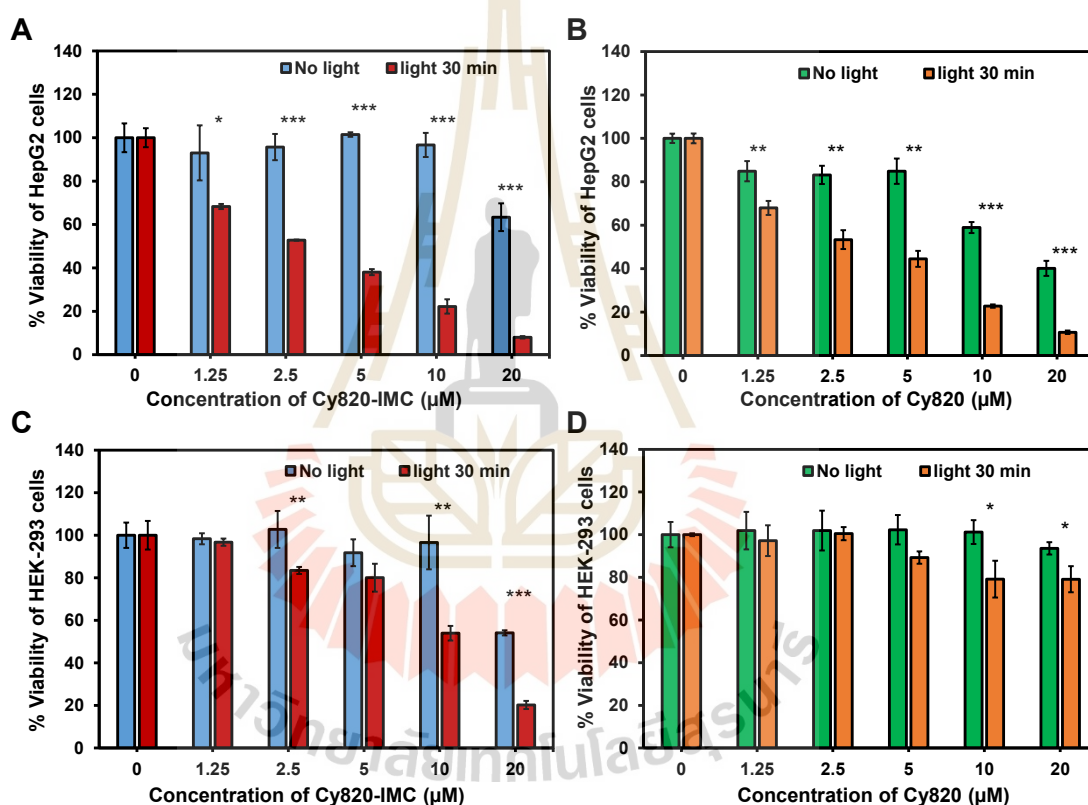


**Figure 4.20** The relative cell viability of HepG2 cells and Hek293 under irradiation (0, 30 min) after incubation with **Cy820-IMC** and **Cy820** (5  $\mu\text{M}$ ) for 6 h. data are showed as means  $\pm$  SD (n = 3), \*P < 0.05, \*\*P < 0.01, or \*\*\*P < 0.001 are determined on Student's T-test.

In addition, the half-maximal inhibitory concentration ( $\text{IC}_{50}$ ) of **Cy820** and **Cy820-IMC** in both cell lines with and without light irradiation was determined and presented in Table 4.2. In the case of cancer cells, **Cy820-IMC** displayed a better

photocytotoxicity index ( $IC_{50}$  dark/ $IC_{50}$  light) compared to **Cy820**. This implies that IMC conjugate could enhance photodynamic efficiency in cancer cells.

**Table 4.2**  $IC_{50}$  and photocytotoxicity index of **Cy820** and **Cy820-IMC**.

Cell line	$IC_{50}$ ( $\mu$ M)					
	Cy820- IMC (light)	Cy820- IMC (dark)	Photocytotoxicity index ( $IC_{50}$ dark/ $IC_{50}$ light)	Cy820 (light)	Cy820 (dark)	Photocytotoxicity index ( $IC_{50}$ dark/ $IC_{50}$ light)
HepG2	2.805	>20	>7.13	3.038	14.90	4.90
HEK-293	10.18	>20	>1.96	>20	>20	~1

#### 4.2.7 Intracellular singlet oxygen generation

Live/dead viability/cytotoxicity assays and internalized singlet oxygen detection assays were used to confirm that the cancer cells were killed by light activation to produce  $^1O_2$ . Calcein AM and propidium iodide (PI) were used to distinguish between viable and dead cells because calcein AM can reach live cells and be cleaved by intracellular esterase and then emit green fluorescence, while PI can only pass through the broken cell membrane and interact with the nuclei of dead cells, resulting in red fluorescence.

As shown in Figure 4.22, only HepG2 cells that were incubated with **Cy820** and **Cy820-IMC** followed by light irradiation exhibit a great red fluorescent signal, indicating the light triggered cell death in the presence of our probes. In contrast, the control cells (no light irradiation), cells under irradiation without the compound, and cells incubated with **Cy820** and **Cy820-IMC** (without light) mostly remained viable as indicated by the green fluorescence where the red signal is hardly detected. On the other hand, HEK-293 cells showed little to no red fluorescent signals from PI in all cases under the same experimental conditions as HepG2 (Figure 4.21).

Furthermore, 2',7'-dichlorofluorescein diacetate (DCFH-DA) was utilized to detect intracellular  $^1O_2$  because this non-fluorescent dye could be oxidized by  $^1O_2$

inside living cells to create 2',7'-dichlorofluorescein (DCF). DCF emits green fluorescence and can be seen under a fluorescence microscope with a 488 nm excitation wavelength. Bright green fluorescence is clearly visible only in HepG2 cells treated with Cy820-IMC followed by light irradiation, as shown in Figure 4.23, showing that  $^1\text{O}_2$  was created within the cells. No singlet oxygen was observed in control cells which only irradiated with light and only treated with the compound.

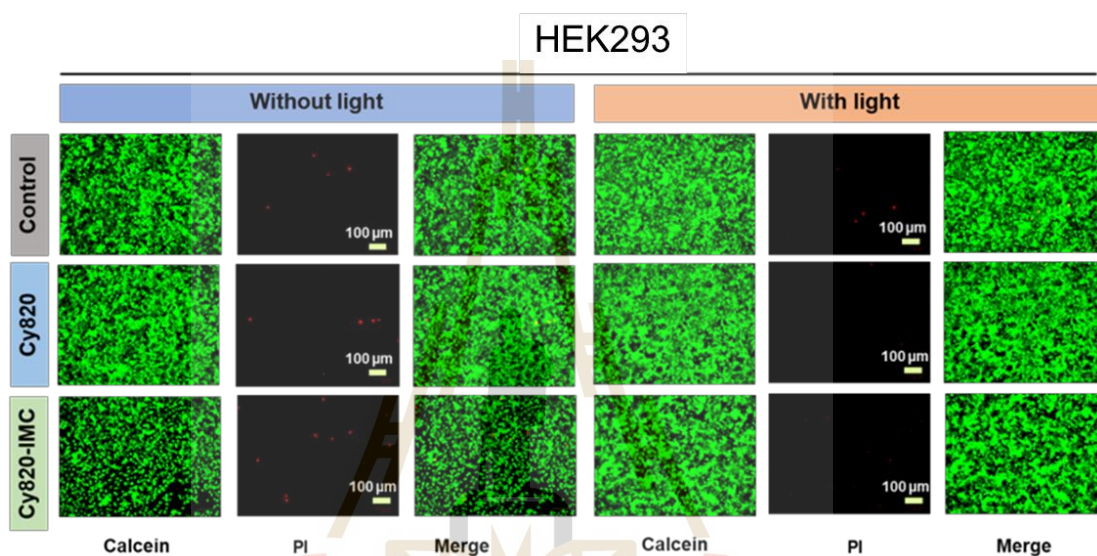


**Figure 4.21** Fluorescence pictures of calcein AM and PI of HEK293 cells after treatment with Cy820 and Cy820-IMC (5  $\mu\text{M}$ ) for 6 h Scale bars = 100  $\mu\text{m}$ .

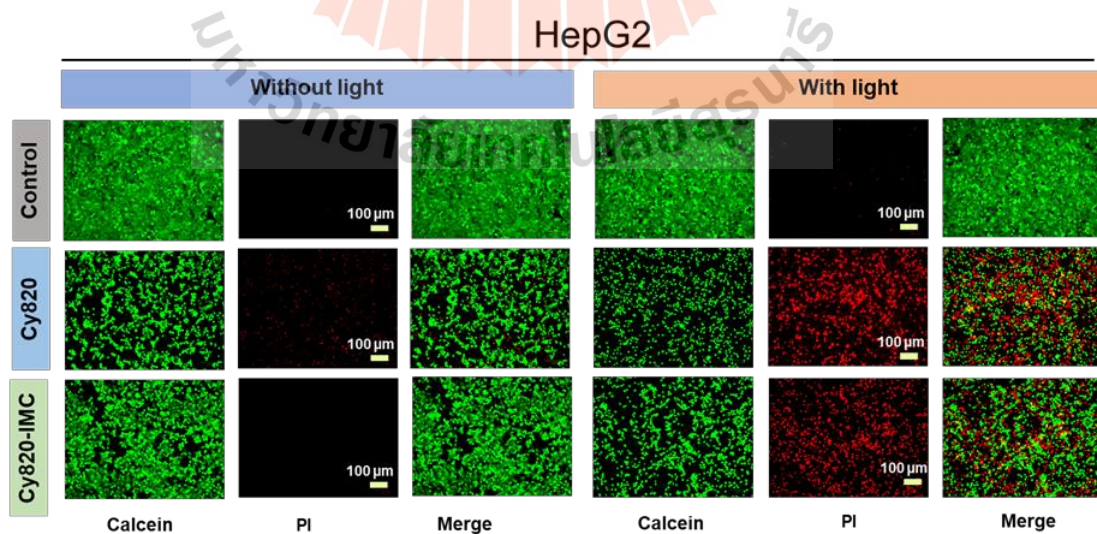


**Figure 4.22** Fluorescence pictures of calcein AM and PI of HepG2 cells after treatment with Cy820 and Cy820-IMC (5  $\mu\text{M}$ ) for 6 h Scale bars = 100  $\mu\text{m}$ .



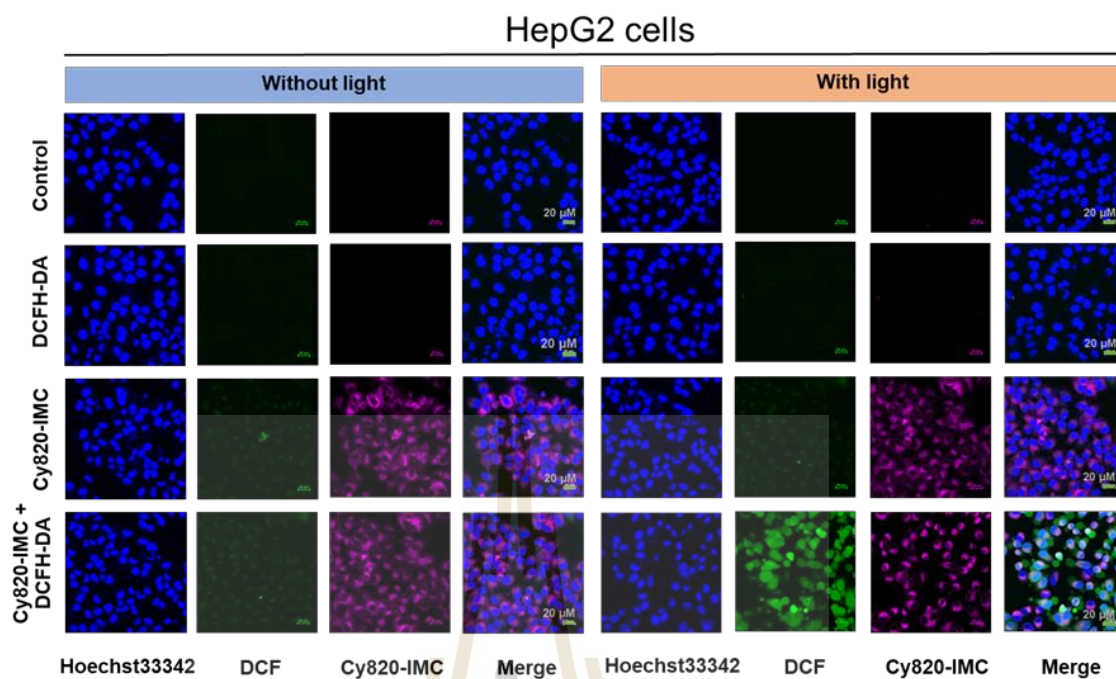


Figure 4.23 DCF relative fluorescence signal in HepG2 cells of incubated with Cy820-IMC (5  $\mu$ M) for 6 hours, DCFH-DA was used to evaluate intracellular singlet oxygen detection in HepG2 cells. Scale bars = 20  $\mu$ m.



## CHAPTER V

### CONCLUSION

In summary, we successfully developed two systems to target cancer. The first one is tumor environment targeting and another is enzyme targeting.

To target the tumor environment, a pH-sensitive theranostic compound, **I<sub>2</sub>-IR783-Mpip**, was synthesized for fluorescence imaging and photodynamic therapy (PDT). In acidic conditions, the Vis-NIR absorbance spectra of **I<sub>2</sub>-IR783-Mpip** were red-shifted, while in basic ones, they were blue-shifted. **I<sub>2</sub>-IR783-Mpip** produced more <sup>1</sup>O<sub>2</sub> in a more acidic environment after 30 minutes of exposure to 850nm LED light. **I<sub>2</sub>-IR783-Mpip** was also selectively internalized into cancer cells with time-dependent uptake. **I<sub>2</sub>-IR783-Mpip** produced light-induced cytotoxicity in HepG2 cells at concentrations as low as 20 μM, resulting in approximately 10% and 30% viability in acidic and neutral environments, respectively. In addition, **I<sub>2</sub>-IR783-Mpip** maintained its PDT efficacy against cancer cells in a simulated deep-tissue condition. In the acidic (pH 5.0) environment, **I<sub>2</sub>-IR783-Mpip** produced more reactive oxygen species than in the neutral condition (pH 7.4). Therefore, **I<sub>2</sub>-IR783-Mpip** could be a suitable option for a tumor environment targeting molecule for photodynamic treatment.

To target cyclooxygenase-2 (COX-2) enzyme that is overexpressed in tumor cells, heptamethine cyanine (**Cy820**) was demonstrated as intrinsic tumor targeting with photodynamic properties. When **Cy820** is combined with a non-specific COX2 inhibitor (indomethacin), a novel NIR sensitizer (**Cy820-IMC**) is obtained, which improves COX-2 specificities and PDT efficiency in cancer cells with a high photocytotoxicity index. Singlet oxygen has been shown to be an important species in the collapse of cancer cells.



REFERENCES

มหาวิทยาลัยเทคโนโลยีสุรนารี

## REFERENCES

- Ahlin, G., Hilgendorf, C., Karlsson, J., Szigyarto, C. A.-K., Uhlén, M., and Artursson, P. (2009). Endogenous gene and protein expression of drug-transporting proteins in cell lines routinely used in drug discovery programs. *Drug Metab. Dispos.* 37(12), 2275. doi:10.1124/dmd.109.028654.
- Atchison, J., Kamila, S., Nesbitt, H., Logan, K. A., Nicholas, D. M., Fowley, C., and Callan, J. F. (2017). Iodinated cyanine dyes: a new class of sensitizers for use in NIR activated photodynamic therapy (PDT). *Chem. Commun.* 53, 2009–2012. doi: 10.1039/c6cc09624g.
- Buxhofer-Ausch, V., Secky, L., Wlcek, K., Svoboda, M., Kounnis, V., Briasoulis, E., and Thalhammer, T. (2013). Tumor-specific expression of organic anion-transporting polypeptides: transporters as novel targets for cancer therapy. *J. Drug. Deliv.* 863539. doi: 10.1155/2013/863539.
- Calixto, GM., Bernegossi, J., de Freitas, LM., Fontana, CR., and Chorilli, M. (2016). Nanotechnology-based drug delivery systems for photodynamic therapy of cancer: A Review. *Molecules.* 21(3), 342. doi: 10.3390/molecules21030342.
- Castellone, M. D., Teramoto H., and Gutkind J. S. (2006). Cyclooxygenase-2 and colorectal cancer chemoprevention: The  $\beta$ -Catenin connection. *Cancer Res.* 66, 11085-11088. doi: 10.1158/0008-5472.CAN-06-2233.
- Dolmans, D. E., Fukumura, D., and Jain, R. K. (2003). Photodynamic therapy for cancer. *Nat. Rev. Cancer.* 3, 380–387. doi: 10.1038/nrc1071.
- Echizen, K., Hirose, O., Maeda, Y., and Oshima, M. (2016). Inflammation in gastric cancer: Interplay of the COX-2/prostaglandin E2 and Toll-like receptor/MyD88 pathways. *Cancer Sci.* 107, 391–397. doi: 10.1111/cas.12973.

- Edelman, M.J., Hodgson, L., Wang, X., Kratzke, R.A., and Vokes, E.E. (2012). Cyclooxygenase-2 (COX-2) as a predictive marker for the use of COX-2 inhibitors in advanced non-small-cell lung cancer. *J. Clin. Oncol.* 30(16), 2019–2020. doi: 10.1200/JCO.2011.41.4581.
- Evans, J. F., and Kargman S. L. (2004). Cancer and cyclooxygenase-2 (COX-2) inhibition. *Curr. Pharm. Des.* 10, 627-634. doi: 10.2174/1381612043453126.
- Feng, L. Z., Dong, Z. L., Tao, D. L., Zhang, Y. C., and Liu, Z. (2018). The acidic tumor microenvironment: a target for smart cancer nanotheranostics. *Nat. Sci. Rev.* 5, 269–286. doi: 10.1093/nsr/nwx062.
- Fitzpatrick, F. A. (2004). Cyclooxygenase enzymes: regulation and function. *Curr. Pharm. Des.* 10, 577-588. doi: 10.2174/1381612043453144.
- Flower, R. J. (2003). The development of COX2 inhibitors. *Nat. Rev. Drug. Discov.* 2(3), 179-191. doi: 10.1038/nrd1034.
- Goldenberg, M. M. (1999). Celecoxib is a selective cyclooxygenase-2 inhibitor for the treatment of rheumatoid arthritis and osteoarthritis. *Clin. Ther.* 21(9), 1497-513. doi: 10.1016/s0149-2918(00)80005-3.
- Goldsmith, H. S. (1969). Clinical advances in the treatment of cancer, *Am. J. Surg.* 118(3), 368-376. doi: 10.1016/0002-9610(69)90141-X.
- Hao, G. Y., Xu, Z. P., and Li, L. (2018). Manipulating extracellular tumor pH: an effective target for cancer therapy. *RSC Adv.* 8, 22182–22192. doi: 10.1039/c8ra02095g.
- Khalili, F., Henni, A., and East, A. L. L. (2009). pKa values of some piperazines at (298, 303, 313, and 323) K. *J. Chem. Eng. Data* 54, 2914–2917. doi: 10.1021/jc900005c.
- Kim, H. S., Park, T., Ren, W. X., Lim, J. Y., Won, M., Heo, J. S., Lee, S. G., and Kim, J. S. (2018). COX-2 targeting indomethacin conjugated fluorescent probe. *Dyes Pigment.* 150, 261-266. doi: 10.1016/j.dyepig.2017.11.053.

- Kim, H. S., Sharma, A., Ren, W. X., Han, J., and Kim, J. S. (2018). COX-2 Inhibition mediated anti-angiogenic activatable prodrug potentiates cancer therapy in preclinical models. *Biomaterials*. 185, 63-72. doi: 10.1016/j.biomaterials.2018.09.006.
- Kroemer, G., and Jaattela. (2005). Lysosomes and autophagy in cell death control. *Nat. Rev. Cancer*. 5, 886–897. doi: 10.1038/nrc1738.
- Kullak-Ublick, G. A., Beuers, U., and Paumgartner, G. (1996). Molecular and functional characterization of bile acid transport in human hepatoblastoma HepG2 cells. *Hepatology*. 23(5), 1053-1060. doi:10.1002/hep.510230518.
- Lin, J., and Alexander-Katz, A. (2013). Cell membranes open “Doors” for cationic nanoparticles/biomolecules: Insights into uptake kinetics. *ACS Nano*. 7, 10799–10808. doi: 10.1021/nn4040553.
- Liu, C., Xiang, J., Xiang, C., and Li, H. (2021). Enhancing the tumor cell selectivity of a rhodamine-decorated iridium(III) complex by conjugating with indomethacin for COX-2 targeted photodynamic therapy. *Bioorg Chem*. 114, 105142. doi:10.1016/j.bioorg.2021.105142.
- Liu, T. and Li, Q. (2014). Organic anion-transporting polypeptides: a novel approach for cancer therapy. *J. Drug. Target*. 22, 14–22. doi: 10.3109/1061186X.2013.832767.
- Luo, S., Zhang, E., Su, Y., Cheng, T., and Shi, C. (2011). A review of NIR dyes in cancer targeting and imaging. *Biomater*. 32, 7127–7138. doi: 10.1016/j.biomaterials.2011.06.024.
- Mao, Y., Wang, L., Xu, C., and Han, S. (2018). Effect of photodynamic therapy combined with Celecoxib on the expression of the cyclooxygenase-2 protein in HeLa cells. *Oncol. Lett*. 15(5), 6599–6603. doi: 10.3892/ol.2018.8163.
- Meng, X., Yang, Y., Zhou, L., Zhang, li, Lv, Y., Li, S., Wu, Y., Zheng, M., Li, W., Gao, G., Deng, G., Jiang, T., Ni, D., Gong, P., and Cai, L. (2017). Dual-responsive molecular

- probe for tumor targeted imaging and photodynamic therapy. *Theranostics*. 7, 1781–1794. doi: 10.7150/thno.18437.
- Mengle-Gaw, L. J., and Schwartz, B. D. (2002). Cyclooxygenase-2 inhibitors: promise or peril?. *Mediat. Inflamm*. 11(5), 275–286. doi: 10.1080/09629350290000041.
- Myochin, T., Kiyose, K., Hanaoka, K., Kojima, H., Terai, T., and Nagano, T. (2011). Rational design of ratiometric near-infrared fluorescent pH probes with various pKa values, based on aminocyanine. *J. Am. Chem. Soc.* 133, 3401–3409. doi: 10.1021/ja1063058.
- Persi, E., Duran-Frigola, M., Damaghi, M., Roush, W. R., Aloy, P., Cleveland, J. L., Gilies, R. J., and Ruppin, E. (2018). Systems analysis of intracellular pH vulnerabilities for cancer therapy. *Nat. Commun.* 9, 2997. doi: 10.1038/s41467-018-05261-x.
- Pewklang, T., Chansaenpak, K., Lai, R. Y., Noisa, P., and Kamkaew, A. (2019). Aza-BODIPY probe for selective visualization of cyclooxygenase-2 in cancer cells. *Rsc Adv.* 9, 13372–13377. doi: 10.1039/c9ra01948k.
- Sandell, J. L., and Zhu, T. C. (2011). A review of in-vivo optical properties of human tissues and its impact on PDT. *J. Biophotonics*. 4, 773–787. doi: 10.1002/jbio.201100062.
- Shi, C., Wu, J. B., and Pan, D. (2016). Review on near-infrared heptamethine cyanine dyes as theranostic agents for tumor imaging, targeting, and photodynamic therapy. *J. Biomed. Opt.* 21(5), 50901. doi: 10.1117/1.JBO.21.5.050901.
- Smith, A. M., Mancini, M. C., and Nie, S. (2009). Bioimaging: second window for in vivo imaging. *Nat. Nanotechnol.* 4, 710–711. doi: 10.1038/nnano.2009.326.
- Smith, F. G., Wade, A. W., Lewis, M. L., and Qi, W. (2012). Cyclooxygenase (COX) inhibitors and the newborn kidney. *Pharmaceuticals (Basel, Switzerland)*. 5(11), 1160–1176. doi: 10.3390/ph5111160.

- Sobolewski, C., Cerella, C., Dicato, M., Ghibelli, L., and Diederich, M. (2010). The role of cyclooxygenase-2 in cell proliferation and cell death in human malignancies. *Int. J. Cell Biol.* 215158. doi:10.1155/2010/215158.
- Song, F., Peng, X., Lu, E., Wang, Y., Zhou, W., and Fan, J. (2005). Tuning the photoinduced electron transfer in near-infrared heptamethine cyanine dyes. *Tetrahedron Lett.* 46, 4817–4820 doi:10.1016/j.tetlet.2005.04.089.
- Subbaramaiah, K., and Dannenberg, A. J. (2003). Cyclooxygenase 2: a molecular target for cancer prevention and treatment. *Trends Pharmacol Sci.* 24, 96-102. doi: 0.1016/S0165-6147(02)00043-3.
- Sun, W., Guo, S., Hu, C., Fan, J., and Peng, X. (2016). Recent development of chemosensors based on cyanine platforms. *Chem. Rev.* 116, 7768–7817. doi: 10.1021/acs.chemrev.6b00001.
- Suwannakham, P., Chaiwongwattana, S., and Sagarik, K. (2018). Mechanisms of photoexcitation and photoionization in small water clusters. *Rsc Adv.* 8, 36731–36744. doi: 10.1039/c8ra06095a.
- Tan, X., Luo, S., Wang, D., Su, Y., Cheng, T., and Shi, C. (2012). A NIR heptamethine dye with intrinsic cancer targeting, imaging, and photosensitizing properties. *Biomater.* 33, 2230–2239. doi: 10.1016/j.biomaterials.2011.11.081.
- Thakkar, N., Lockhart, A. C., and Lee, W. (2015). Role of Organic Anion-Transporting Polypeptides (OATPs) in Cancer Therapy. *AAPS J.* 17, 535–545. doi: 10.1208/s12248-015-9740-x.
- Trifan, O. C., and Hla, T. (2003). Cyclooxygenase-2 modulates cellular growth and promotes tumorigenesis. *J. Cell. Mol. Med.* 7(3), 207–222. doi: 10.1111/j.1582-4934.2003.tb00222.x.
- Usama, S. M., Lin, C. M., and Burgess, K. (2018). On the mechanisms of uptake of tumor-seeking cyanine dyes. *Bioconjugate Chem.* 29, 3886–3895. doi: acs.bioconjchem.8b00708.



- Vane, J. R., and Botting, R. M. (1998). Mechanism of action of nonsteroidal anti-inflammatory drugs. *Am. J. Mediat.* 104(3, Supplement 1), 2S-8S. doi: 10.1016/S0002-9343(97)00203-9.
- Warburg, O., Wind, F., and Negelein, E. (1927). The metabolism of tumors in the body. *J. Gen. Physiol.* 8(6), 519–530. doi: 10.1085/jgp.8.6.519.
- Wang, B., Fan, J., Wang, X., Zhu, H., Wang, J., Mu, H., and Peng, X. (2015). A Nile blue based infrared fluorescent probe: imaging tumors that over-express cyclooxygenase-2. *Chem. Commun. (Camb)*. 51(4), 792-795. doi:10.1039/c4cc08915d.
- Wang, D., and Dubois, R. N. (2010). The role of COX-2 in intestinal inflammation and colorectal cancer. *Oncogene*. 29(6), 781–788. doi: 10.1038/onc.2009.421.
- Wang, Y., Liu, T., Zhang, E., Luo, S., Tan, X., and Shi, C. (2014). Preferential accumulation of the near infrared heptamethine dye IR-780 in the mitochondria of drug-resistant lung cancer cells. *Biomaterials*. 35, 4116-4124. doi: 10.1016/j.biomaterials.2014.01.061.
- Weissleder, R. (2001). A clearer vision for in vivo imaging. *Nat. Biotechnol.* 19, 316–317. doi: 10.1038/86684.
- WHO. (2017). Cancer fact sheet.
- Williams, C. S., Mann, M., and DuBois, R. N. (1999). The role of cyclooxygenases in inflammation, cancer, and development. *Oncogene*. 18(55), 7908-16. doi: 10.1038/sj.onc.1203286.
- Xu, S., Uddin, M. J., Banerjee, S., Duggan, K., Musee, J., Kiefer, J. R., Ghebreselasie, K., Rouzer, C. A., and Marnett, L. J. (2019). Fluorescent indomethacin-dansyl conjugates utilize the membrane-binding domain of cyclooxygenase-2 to block the opening to the active site. *J. Biol. Chem.* 294(22), 8690-8698. doi:10.1074/jbc.RA119.007405.

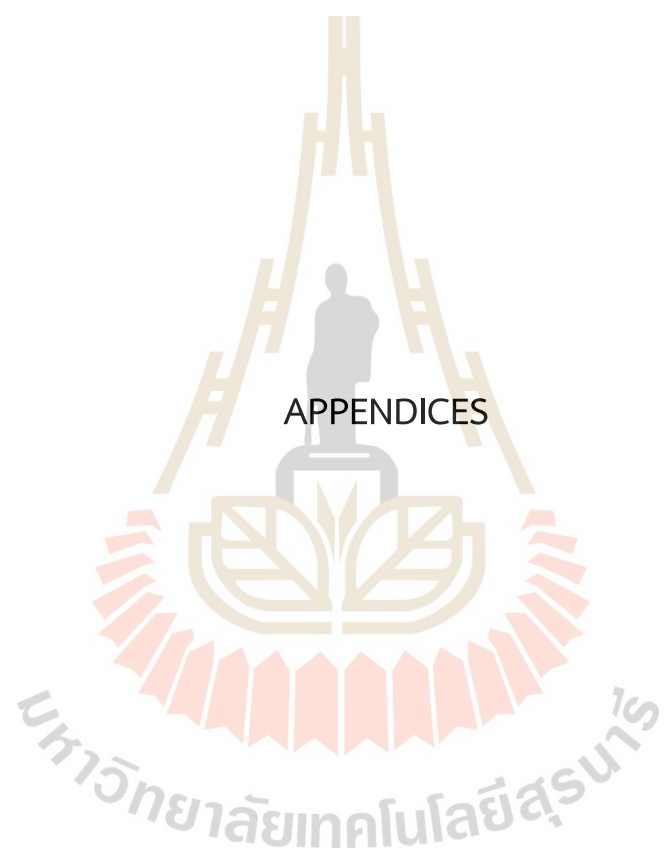
- Xue, F., Wen, Y., Wei, P., Gao, Y., Zhou, Z., Xiao, S., and Yi, T. (2017). A smart drug: a pH-responsive photothermal ablation agent for Golgi apparatus activated cancer therapy. *Chem. Commun.* 53, 6424–6427. doi: 10.1039/c7cc03168h.
- Zarghi, A., and Arfaei, S. (2011). Selective COX-2 Inhibitors: A Review of their structure-activity relationships. *Iran J Pharm Res.: IJPR.* 10(4), 655–683. doi: 10.22037/IJPR.2011.1047.
- Zhang, H., Fan, J., Wang, J., Dou, B., Zhou, F., Cao, J., Qu, J., Cao, Z., Zhao, W., and Peng, X. (2013). Fluorescence discrimination of cancer from inflammation by molecular response to COX-2 enzymes. *J. Am. Chem. Soc.* 135(46), 17469–17475. doi:10.1021/ja4085308.
- Zhang, H., Fan, J., Wang, J., Zhang, S., Dou, B., and Peng, X. (2013). An off-on COX-2-specific fluorescent probe: targeting the Golgi apparatus of cancer cells. *J. Am. Chem. Soc.* 135(31), 11663–11669. doi:10.1021/ja4056905.
- Zhang, H., Fan, J., Wang, K., Li, J., Wang, C., Nie, Y., Jiang, T., Mu, H., Peng, X., and Jiang, K. (2014). Highly sensitive naphthalene-based two-photon fluorescent probe for in situ real-time bioimaging of ultratrace cyclooxygenase-2 in living biosystems. *Anal. Chem.* 86(18), 9131–9138. doi:10.1021/ac501944y.
- Zhang, J., Liu, Z., Lian, P., Qian, J., Li, X., Wang, L., Fu, W., Chen, L., Wei, X., and Li, C. (2016). Selective imaging and cancer cell death via pH switchable near-infrared fluorescence and photothermal effects. *Chem. Sci.* 7, 5995–6005. doi: 10.1039/c6sc00221h.
- Zhang, J., Yang, M., Li, C., Dorh, N., Xie, F., Luo, F.-T., Tiwari, A., and Liu, H. (2015). Near-infrared fluorescent probes based on piperazine-functionalized BODIPY dyes for sensitive detection of lysosomal pH. *J. Mater. Chem. B.* 3(10), 2173–2184. doi: 10.1039/c4tb01878h.
- Zhang, J. Y., Liu, Z. N., Lian, P., J. Qian, Li, X. W., Wang, L., Fu, W., Chen, L., Wei, X. B. and Li, C. (2016). Selective imaging and cancer cell death via pH switchable

near-infrared fluorescence and photothermal effects. *Chem. Sci.* 7, 5995-6005. doi: 10.1039/C6SC00221H.

Zhang, Q., Han, Z., Tao, J., Zhang, W., Li, P., Tang, L., and Gu, Y. (2018). A novel near-infrared fluorescent probe for monitoring cyclooxygenase-2 in inflammation and tumor. *J. Biophotonics*. 11, e2017003. doi: 10.1002/jbio.201700339.

Zhou, X., Lee, S., Xu, Z., and Yoon, J. (2015). Recent progress on the development of chemosensors for gases, *Chem. Rev.* 115(15), 7944-8000. doi: 10.1021/cr500567r.





APPENDIX A  
SUPPORTING INFORMATION

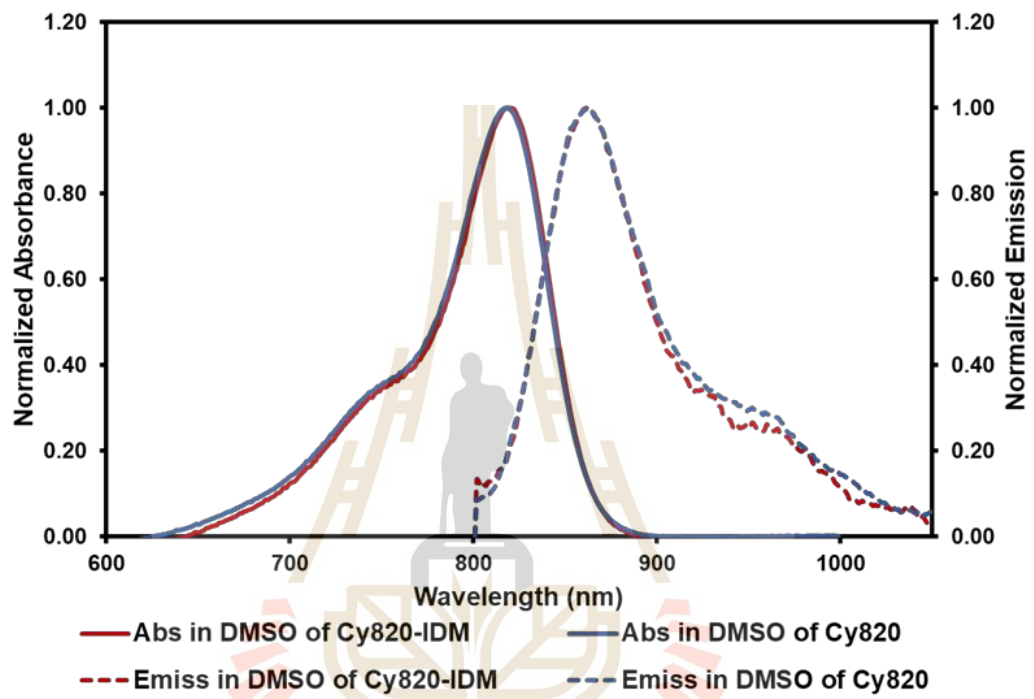


Figure S1 UV-Vis-NIR and fluorescence spectra of Cy820 and Cy820-IMC in DMSO.

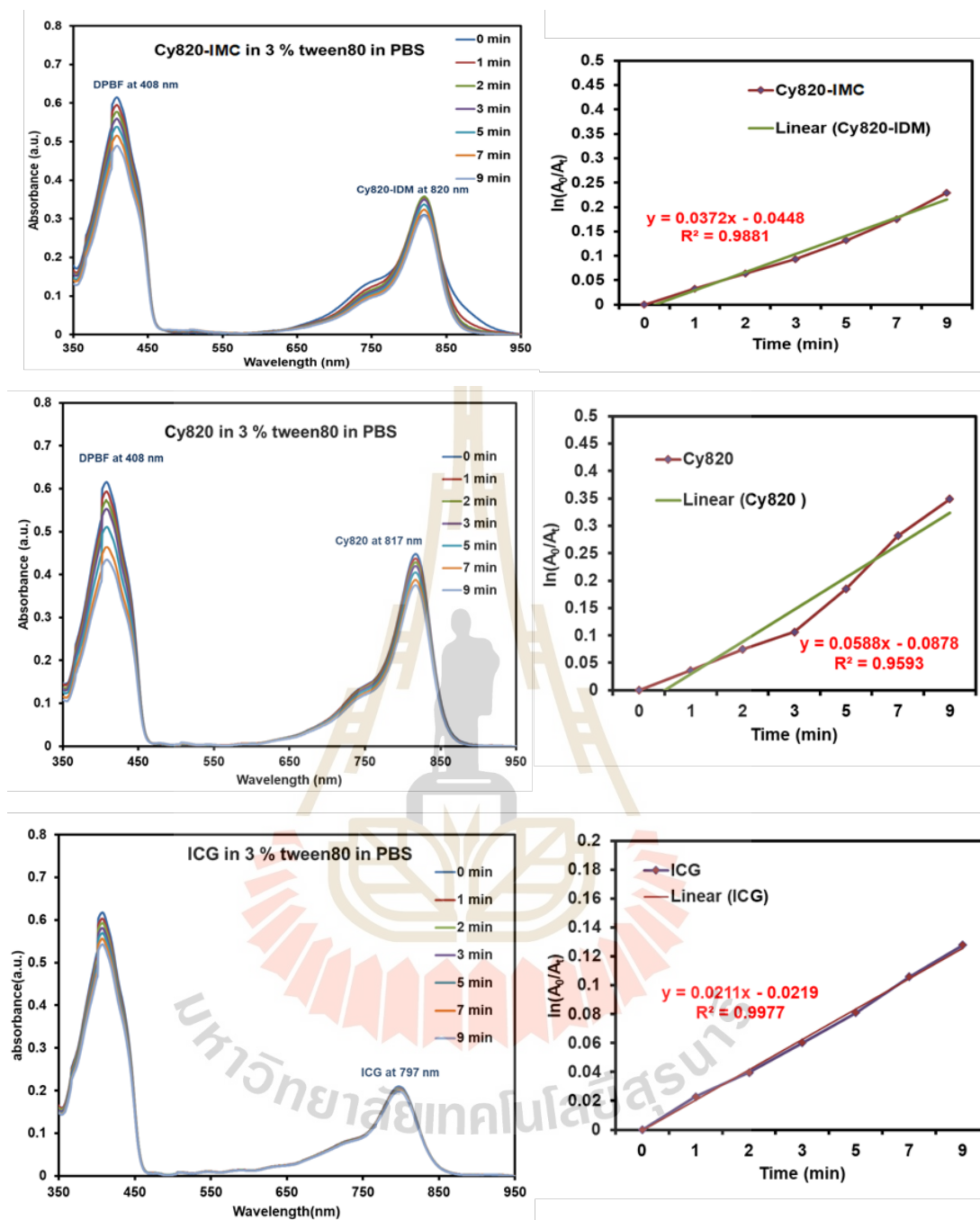


Figure S2 (a) Singlet oxygen generation of 2  $\mu$ M of Cy820-IMC, Cy820, and ICG in PBS.

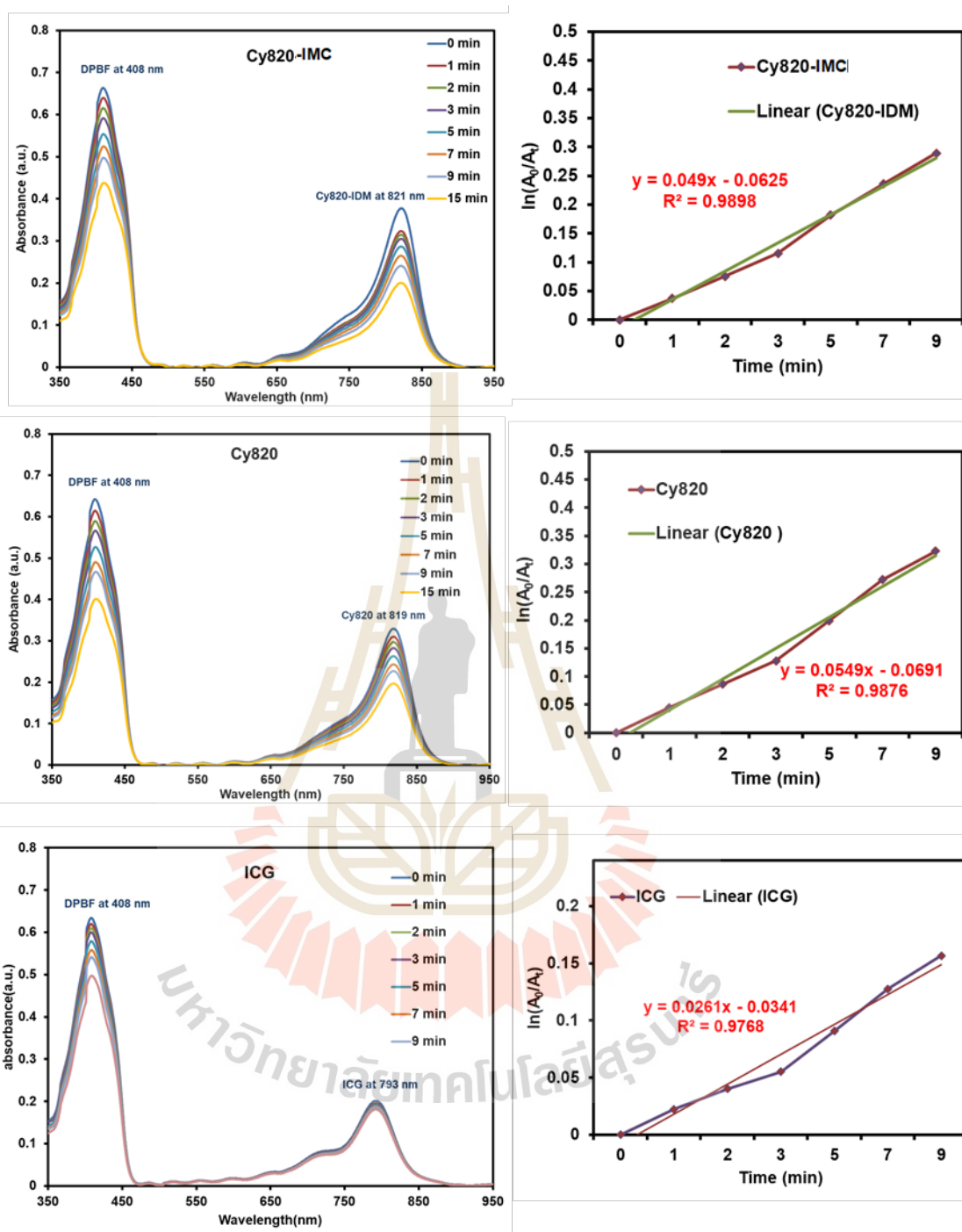


Figure S3 (a) Singlet oxygen generation of 2  $\mu$ M of Cy820-IMC, Cy820, and ICG in DMSO.

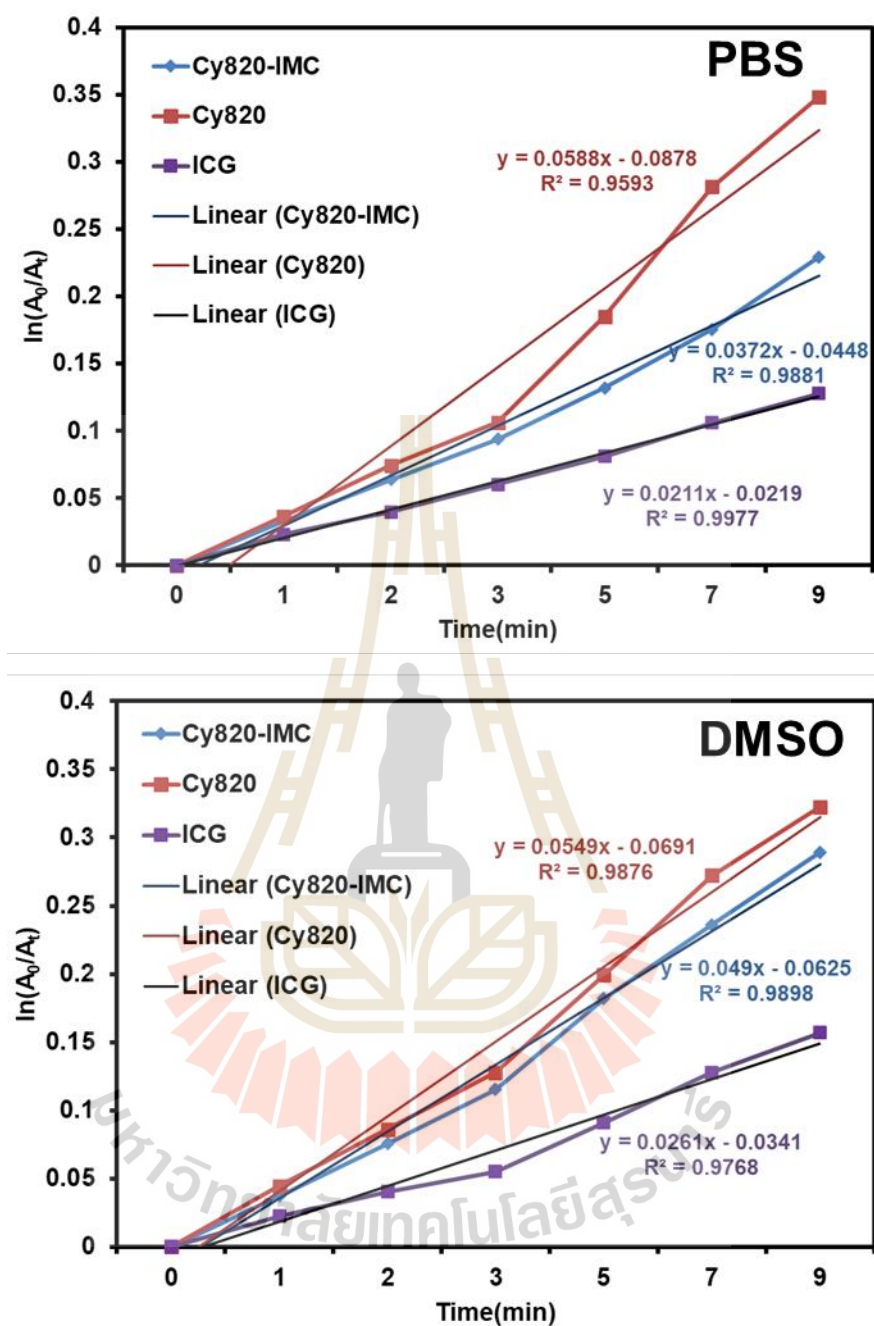


Figure S4 Singlet oxygen generation of 2  $\mu\text{M}$  of Cy820-IMC and Cy820 in PBS and DMSO compared to standard (ICG).



## APPENDIX B

### THESIS OUTPUT

#### Publication

**Siriwibool, S.**, Kaekratoke, N., Chansaenpak, K. Siwawannapong, K.,S., Panajapo, P., Sagarik, K., Noisa, P., Lai, R-Y., and Kamkaew, A. (2020). Near Infrared Fluorescent pH Responsive Probe for Targeted Photodynamic Cancer Therapy. **Sci. Rep.** 10(1283): doi.org/10.1038/s41598-020-58239-5.

#### Conferences

Kaekratoke, N., Siriwibool, S., Kamkaew, A.,(2018). Near-Infrared Fluorescent pH Responsive Probe for Targeted Photodynamic Cancer Therapy, **Pure and Applied Chemistry International Conference 2018 (PACCON 2018, poster)**. February 7-9, 2018, The 60th Anniversary of his Majesty the king's Accession to the Throne International Convention Center (ICC Hat Yai), Hat Yai, Songkhla, Thailand.

Siriwibool, S., Kaekratoke, N., Kamkaew, A.,(2019). Near-Infrared Fluorescent pH Responsive Probe for Targeted Photodynamic Cancer Therapy, **Pure and Applied Chemistry International Conference 2019 (PACCON 2019, poster)**. February 7-8, 2019, BITEC, Bangkok, Thailand.

## CURRICULUM VITAE

**Name** Siriwalee Siriwibool

**Date of Birth** April 23<sup>th</sup>, 1997 at Bangkok, Thailand

### Education

2019–Present M.Sc. in Master of Science Program in Cellular and Molecular Science for Biomedical Applications , Suranaree University of Technology, Thailand ( At present)

2015-2019 B.Sc. in Chemistry, Suranaree University of Technology, Thailand (First class Honors)

### Scholarships

2019–Present Thailand Graduate Institute of Science and Technology – TGIST

2015-2018 The Auspicious Occasion of His Majesty the King’s 84th Birthday

### Research Experience

December 1, 2018–February 28, 2019: Chulabhorn Research Institute, Bangkok, under the supervision of Dr. Sakunchai Khumsubdee on title of “Synthesis of organometallic iridium(III) complexes for studying anticancer activity”

May 15, 2021–December 15, 2021: Texas A&M University, Texas, USA, under the supervision of Prof. Dr. Kevin Burgess on title of “Discovery of Compact Inhibitors of SPSB2 Protein Using IBM”

### Publications

**Siriwibool, S.**, Kaekratoke, N., Chansaenpak, K. Siwawannapong, K., S., Panajapo, P., Sagarik, K., Noisa, P., Lai, R-Y., and Kamkaew, A. (2020). Near Infrared Fluorescent pH Responsive Probe for Targeted Photodynamic Cancer Therapy. *Sci. Rep.* 10(1283). doi.org/10.1038/s41598-020-58239-5.

**Siriwibool, S.**, Wangngae, S., Chansaenpak, K., Wet-osot, S., Lai, R.-Y., Noisa, P., Sukwattanasinitt, M., and Kamkaew, A. (2022). Indomethacin-based near-infrared photosensitizer for targeted photodynamic cancer therapy. *Bioorg. Chem.*, 122, 105758. doi.org/10.1016/j.bioorg.2022.105758.